Assessing the potential of iron oxide nanoparticles to treat cancer through magnetic hyperthermia

A thesis submitted to The University of Dublin, Trinity College for the degree of Doctor of Philosophy

2020

Submitted by

Gary Hannon, M. Sc.

Declaration

I declare that this thesis has not been submitted as an exercise for a degree at this or any other university and is entirely my own work (published or unpublished), except where duly acknowledged.

I agree to deposit this thesis in the University's open access institutional repository or allow the library to do so on my behalf, subject to Irish Copyright Legislation and Trinity College Library conditions of use and acknowledgement.

Gary Hannon

Summary

This thesis begins with an introduction to pancreatic ductal adenocarcinoma (PDAC), its clinical burden and issues involved with treating such an aggressive cancer. Following this, potential novel treatments that have shown promise in treating PDAC are described, one of which is iron oxide nanoparticles (IONP), and their ability to treat cancer with heat when exposed to alternating magnetic fields. Expanding on IONP, their biocompatibility is discussed, with particular emphasis placed on their potential to induce hypersensitive effects. Finally, a brief overview of Trinity College's experience in magnetic hyperthermia research and nanomedicine translation is provided which leads into the aims of the project.

After the introduction, the thesis is divided into four chapters: the first has been submitted to a peer-reviewed journal, and the other three are currently in writing with many internal and external collaborators involved. In chapter 1, the efficacy of IONP to treat PDAC *in vitro* through magnetic hyperthermia is confirmed. One key conclusion from this chapter is that intracellular nanoparticles played no role in the efficacy of the treatment, whereas extracellular nanoparticles could induce significant levels of necrosis in the cells. Chapter 2 assessed the nanoparticles used in chapter 1 for endotoxin contamination and found there to be high levels which would prevent this nanoparticle continuing into preclinical assessment. Additionally, chapter 2 finds the source of the endotoxin in this nanoparticle, and also summarizes a subsequent screen of 21 nanoparticles that were also tested for endotoxin. Chapter 3 takes the IONP with the lowest endotoxin levels from the screen and assesses its potential to activate the complement system in humans as this is one of the contributing reasons to why IONP have failed in the clinic. In the final chapter, the lead nanoparticle is tested *in vivo* to determine the dose at which it induces acute infusion reactions. This study was undertaken with consideration to publications by the European Medicines Agency and the Food and Drug Administration highlighting the risk associated with intravenous iron and allergic reactions.

Following the four chapters is an overall conclusion which describes the lessons learned from each and how they led to the selection of the lead nanoparticle for the project. Finally, a section on future work explains the experiments that will follow-on from this research.

Acknowledgements

I would firstly like to thank my supervisor Adriele Prina-Mello, who has been hugely supportive of my research and has always encouraged my thoughts and ideas being implemented into this project. At many points during this project, Adriele has provided great advice and introduced me to many contacts which helped me get the best out of this wonderfully challenging journey. Ciaran Maguire, a former post doctorate researcher in our laboratory, for selflessly giving up his time at the beginning of my journey to train me in many of the techniques I needed to begin my research. Yuri, for his supervision and guidance throughout the project. Additionally, Anna, Melissa, Dania and Oli for being a joy to work with, and making the office and lab a fun and enjoyable place to be part of!

There are many external institutions and individuals I would also like to thank for their services, support, and supplies for this project. I would like to thank BioKeralty, Chemicell, and Resonance Circuits Limited for providing the IONP essential to my research; the advanced microscopy laboratory (AML) for providing training on the transmission electron microscope; the chemistry department in Trinity College, Dublin for allowing me continued use of the dynamic light scattering and spectrometer facilities; Prof. John Cassidy of Dublin Institute of Technology for training me on the optical emission spectrometer and atomic absorption spectrometer; Dr. Caterina Dell'Aquila at London's Metallomics Facility in Kings College London for analysing our *in vivo* samples with inductively coupled plasma mass spectrometry; Prof. Kevin Conlon for the clinical advice associated with this treatment and the members of NoCanTher and the EUNCL, which are European projects in which our laboratory is currently involved for providing their expertise and advice on my project.

I would also like to thank my family and Alex, who have always managed to put me in a good mood no matter what the circumstances. Without you, I wouldn't be where I am today.

Finally, I would also like to give a huge thanks to the Irish Research Council for believing in me, and funding this project.

Achievements

Publications

Hannon G, Tutty M, and Prina-Mello A, Immunotoxicity and Safety Considerations for Iron Oxide Nanoparticles, Chapter 14, Clinical Applications or Magnetic Nanoparticles: From Fabrication to Clinical Applications, 2019, ISBN 9781138051553.

Hannon G, Lysaght J, Liptrott N, and Prina-Mello A, Immunotoxicity Considerations for Next Generation Cancer Nanomedicines, *Adv. Sci.* 2019, DOI:10.1002/advs.201900133.

Submitted papers

Hannon G, Bogdanska A, Volkov Y and Prina-Mello A, Comparing the effects of intracellular and extracellular magnetic hyperthermia on the viability of BxPC-3 cells.

Papers in writing

Hannon G, Elena De Calatrava, Giulia Coradello, Yuri Volkov, and Adriele Prina-Mello, The hurdle of endotoxin contamination to the early pre-clinical evaluation of nanomedicines.

Hannon G, Curley P, Liptrott N and Prina-Mello A, Haemocompatibility assessment of iron oxide nanoparticles.

Hannon G, Bogdanska A, Gobbo O, Volkov Y and Prina- Mello A, Acute toxicities associated with single, high exposure injections of iron oxide nanoparticles in rats.

Presentations

Poster
Trinity Cancer Conference, 21st October 2018, Trinity College, Dublin, Ireland.
Poster title: Superparamagnetic Iron Oxide Nanoparticles to Diagnose and Treat Cancer.

Irish Biological Inorganic Chemistry Society Conference, 3rd November 2017, Maynooth University, Kildare, Ireland.
Poster title: A Preclinical Screening Model for the Translation of Iron Oxide Nanoparticles for the treatment of Pancreatic Cancer by Magnetic Hyperthermia.

Oral

12th International Conference on the Scientific and Clinical Applications of Magnetic Carriers, 22-26th May 2018, Copenhagen, Denmark.
Presentation title: A Systematic Approach to Endotoxin Contamination Assessment of Iron Oxide Nanoparticles.

Annual Congress of the Italian Society of Photobiology, 19-21st June 2019, Bologna, Italy.
Keynote speech title: Challenges in translating a physically- triggered therapy to the clinic.

Trinity Translational Medicine Institute Seminar Series, 25th June 2019, Dublin, Ireland.
Presentation title: Magnetic Hyperthermia applied to Cancer: Challenges and Translational requirements

Scholarships

Summer School of Molecular Medicine, University Hospital of Jena, Germany, 15th August – 15th September 2016.

Eurolife Summer School on the Molecular Mechanisms of Cancer, Leiden University Medical Center, Netherlands, 8th – 13th July 2018.

LERU Doctoral Summer School on Building Research Capacity and Collaborative Global Community, University of Edinburgh, Scotland, 15th- 19th July 2019.

Credits

Postgraduate Certificate in Innovation and Entrepreneurship, 2017-2018, Trinity College, Dublin, Ireland. (30 ECT's)

Abstract

5-year survival for pancreatic cancer is about 10% worldwide. A subset of this cancer, pancreatic ductal adenocarcinoma (PDAC), is estimated to become the second leading cause of cancer-related deaths in the US by 2030. This cancer is commonly diagnosed late, so by the time the patient presents with symptoms, current treatments are ineffective against PDAC in its advanced stage. Research into novel therapies is therefore necessary to tackle this aggressive malignancy. Iron oxide nanoparticles (IONP) are small, magnetic materials with a variety of interesting properties that make them promising candidates for treating and diagnosing cancer. Upon exposure to external alternating magnetic fields, these materials can heat up and treat tumours through a procedure called magnetic hyperthermia. Moreover, this magnetic hyperthermia treatment can be incorporated into current treatment regimens for PDAC patients, where it has shown to enhance the effects of chemotherapy and radiation. Currently, an IONP called Nanotherm® is clinically approved to treat glioblastoma, an aggressive brain cancer, with magnetic hyperthermia. It has also shown promising results in trials for prostate cancer.

This project follows the testing of new IONP to treat PDAC with magnetic hyperthermia. The nanoparticles were characterized, tested for their heating capabilities, assessed for endotoxin contamination and their potential to induce immunotoxicities *in vitro* and *in vivo*. This work was run in parallel to the work of collaborators with the hopes of contributing to a dossier for a clinical trial for these nanoparticles.

Table of Contents

List of Figures

List of Tables

Abbreviations

7-AAD: 7-Aminoactinomycin D

AAS: Atomic absorption spectroscopy

AMF: Alternating magnetic field

APC: Allophycocyanin

ATP: Adenosine triphosphate

BCA: Bicinchoninic acid assay

BER: Base excision repair

C1-9: Complement protein 1-9

CAF: Cancer associated fibroblasts

CARPA: Complement activation-related pseudoallergy

CFU: Colony forming units

CSE: Control standard endotoxin

CSF: Colony-stimulating factor

CT: Computed tomography

CTLA-4: Cytotoxic T-lymphocyte-associated protein 4

CV: Coefficient of variation

DC: Dendritic cell

DLS: Dynamic light scattering

DMSO: Dimethyl sulfoxide

DNA: Deoxyribonucleic acid

DNA-PK: Deoxyribonucleic acid- Protein kinase

DSB: Double strand breaks

ECM: Extracellular matrix

EL: Endotoxin limit

ELISA: Enzyme-linked immunosorbent assay

EMA: European Medicines Agency

EPR: Enhanced permeability and retention

EU: Endotoxin units

EUNCL: European Union Nanoparticle Characterization Laboratory

EV: Extracellular vesicle

FDA: Food and Drug Administration

FOLFIRINOX: Fluorouracil [5-FU], leucovorin, irinotecan and oxaliplatin

GNP: Gold nanoparticle

HCl: Hydrochloric acid

HCS: High content screening

HPRA: Health Products Regulatory Authority

HR: Homologous recombination

HSP: Heat shock protein

ICP-MS: Inductively coupled plasma mass spectrometry

ICP-OES: Inductively coupled plasma optical emission spectrometry

IEC: Inhibition enhancement control

IL: Interleuken

ILP: Intrinsic loss power

IONP: Iron oxide nanoparticles

ISO: International Organization for Standardization

kDa: kiloDaltons

LAL: Limulus amebocyte lysate

LDH: Lactate dehydrogenase

LPS: Lipopolysaccharide

MCP: Methyl-accepting chemotaxis protein

MDSC: Myeloid-derived suppressor cells

MHC: Major histocompatibility complex

MIP: Macrophage inflammatory protein

MMP-2/9: Matrix Metalloproteinase-2/9

MNP: Magnetic nanoparticle

MTT: 3-(4,5-dimethylthiazol-2-yl)-2,5-diphenyl tetrazolium bromide

MultiFun: Multifunctional nanotechnology for selective detection and Treatment of cancer

MVD: Maximum valid dilution

NaOH: Sodium hydroxide

NHEJ: Non-homologous end joining

NK: Natural killer

NoCanTher: Nanomedicine upscaling for early clinical phases of multimodal cancer therapy

NTA: Nanoparticle tracking analysis

OGG1: 8-oxoguanine DNA glycosylase

PBS: Phosphate buffered saline

PDAC: Pancreatic ductal adenocarcinoma

PD-L1: Programmed death-ligand 1

PEG: Polyethylene glycol

PEGPH20: Pegvorhyaluronidase alfa

PS: Phosphatidylserine

ROS: Reactive oxygen species

RPT: Rabbit pyrogen test

SAR: Specific absorbance rate

SCID: Severe combined immunodeficient

SHH: Sonic hedgehog protein

siRNA: Small interfering ribonucleic acid

SPION: Superparamagnetic iron oxide nanoparticles

SSB: Single strand breaks

TEM: Transmission electron microscopy

TNF: Tumour necrosis factor

Treg: Regulatory T cells

USNCL: United States Nanoparticle Characterization Laboratory

1. Chapter 1: Introduction

1.1. Pancreatic ductal adenocarcinoma

Pancreatic ductal adenocarcinoma (PDAC) comprises 90% of pancreatic cancers and develops within the lining of the ducts in the pancreas. Carrying a 20% 1-year survival post-diagnosis, and about 6% survival after 5 years, PDAC is one of the world's most deadly malignancies [1-3]. There are many reasons that contribute to this poor survival rate, but the underlying issue behind each of these is the fact that 80% of PDAC patients present with locally advanced or metastatic disease that is inoperable and therefore the majority of patients can only receive palliative care [4]. Symptoms of this cancer display late, so by the time a patient presents, the tumour is too progressed and conventional treatments (chemotherapy and radiation) are minimally effective. This is emphasised by the fact that the overall survival for PDAC has barely increased in the last 40 years (<4%) [5-7]. Additionally, PDAC is epidemiologically projected to be the second leading cause of cancer-related deaths in the United States by 2030 [8]. Clearly, there is a huge unmet need for novel treatment options with this malignancy.

1.1.1. The PDAC microenvironment as a hurdle for conventional treatments

Chemotherapy struggles with the dense desmoplastic stroma and low blood perfusion rates characteristic of pancreatic tumours. An extensive stroma is a defining feature of PDAC, which can comprise up to 90% of the tumour volume [9, 10]. This desmoplastic reaction, or desmoplasia, refers to significant upregulations in activated pancreatic stellate cells and immune cell infiltrate within the tumour microenvironment, along with significant increases in extracellular protein deposition, which cumulatively increase interstitial fluid pressure and thereby inhibit drug accumulation into the tumour [11, 12]. Moreover, the gene signature of the stroma alone has been shown to have prognostic value in PDAC [13]. The acellular component of this microenvironment is the extracellular matrix (ECM), which contains a cocktail of structural fibres, adhesion proteins, pro-metastatic enzymes, growth factors, and glycoproteins – to name but a few - that act in unison to aid in tumour proliferation, resistance and metastasis [14, 15]. Pairing this with an abundance of cancer-associated fibroblasts and pro-tumour immune cell infiltrate, this creates an environment that enables the cancer to thrive while

simultaneously acting as a mechanical barrier for chemotherapeutic drugs [16] (Figure 1.1). Likewise, the notably poor blood flow into these tumours creates an extremely hypoxic environment which inhibits the efficacy of chemotherapy and radiation [17, 18]. The current standard-of-care for locally advanced PDAC – FOLFIRINOX with gemcitabine or Abraxane® with gemcitabine – has brought the median overall survival time for these patients closer to the 1 year mark in comparison to gemcitabine alone (6-8 months) [19]. With regards to radiation, the benefits at this stage are questionable due to the variability in delivery methods used in trials along with the various study endpoints measured (overall survival versus time to progression versus quality of life). The overall consensus is that currently, the benefits of radiation may not outweigh its associated toxic effects [20-22]. Stratifying patients most likely to respond to radiation, optimizing its delivery and standardizing trial endpoints will shine light into the true benefits of this avenue in the future. Currently, conventional treatments such as chemotherapy and radiation are yet to make an impressionable impact in the overall survival of PDAC patients.
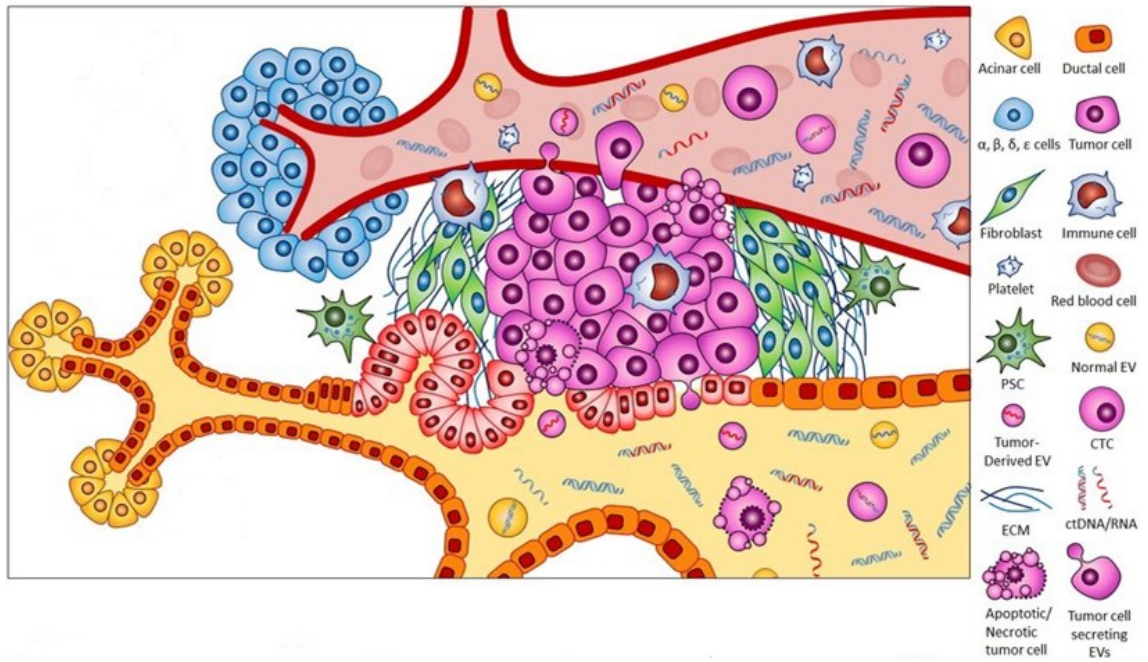
Figure 1.1. Illustration of the PDAC microenvironment.

The PDAC tumour develops on the lining of the duct in the pancreas. A dense desmoplastic stroma consisting of fibroblasts, immune cells and the ECM aid in tumour progression and can also act as a mechanical barrier for therapies entering the tumour. Once large enough, the tumour can generate its own vascular system enabling metastasis and the secretion of extracellular vesicles and genetic material. Image adapted from [23]. Abbreviations: PSC, pancreatic stellate cell; EV, extracellular vesicle; CTC, circulating tumour cell; ECM, extracellular matrix; ctDNA/RNA, circulating tumour DNA/RNA.

1.1.2. Novel treatment approaches for PDAC

Because of the poor survival statistics related to conventional treatments, a large amount of research has gone into novel mechanisms to treat this cancer. Many of these aim at either improving the current standard-of-care through alleviating the chemoresistant mechanisms common to PDAC, re-wiring the immunosuppressive pathways in the cancer to boost the anti-tumour immune response, or utilising the novel therapeutic properties of nanomaterials in an effort to treat PDAC through alternative approaches [24]. Some of the most promising of these are described below.

1.1.2.1. Stoma-targeting agents

A vast number of targeted therapies acting on the various markers of PDAC and its microenvironment are currently in preclinical and clinical evaluation. One such avenue currently in clinical trials involves targeting the stromal microenvironment in combination with chemotherapy for PDAC [25].

Cancer- associated fibroblasts (CAF's)- which can even outnumber the cancer cells in a pancreatic cancer tumour [26, 27]- have been shown to progress PDAC through the secretion of growth factors, inflammatory cytokines, structural proteins, and metabolites. Importantly, CAF's rely on the sonic hedgehog (SHH) ligand produced by PDAC cells to generate ECM proteins which develops the stroma and invasive potential of these tumours [28, 29]. This ligand is overexpressed in PDAC, where it binds to its receptor Ptch (or Patched) on CAF's and leads to an activation of the hedgehog pathway resulting in an increased proliferative and metastatic potential of cancer cells [30]. Various inhibitors of SHH have been developed and tested preclinically and clinically in combination with chemotherapy with the hope of improving penetration into the tumour [31]. However, despite showing promise preclinically [32, 33], overall response, progression-free survival, and overall survival was not significantly increased in phase II trials using Vismodegib (SHH inhibitor) in combination with gemcitabine (NCT01064622) [34].

The ECM contains a vast array of potential targets for novel therapies. Many of these targets have been explored with limited success. Notably, a structural polysaccharide called hyaluronan was found to be expressed 12 times more in PDAC tissue versus healthy pancreas [35]. Hyaluronan is an adhesion molecule with multiple roles in healthy tissue including cell motility. In PDAC xenograph models, high levels of

hyaluronan has been shown to accelerate tumour growth and promote metastasis [36, 37]. Similarly, preclinical data has created optimism by inhibiting hyaluronan in combination with chemotherapy to improve efficacy [38]. This has resulted in clinical trials which evaluated PEGPH20 – an inhibitor of hyaluronan – in combination with Abraxane® and gemcitabine (NCT01839487 and NCT02715804 respectively) or FOLFIRINOX (NCT 01959139). Despite phase II trials of PEGPH20 in combination with Abraxane® and gemcitabine showing an improved progression-free survival, questions remain on the safety of this treatment with adverse effects to the musculoskeletal system and thromboembolic events commonly observed [39].

1.1.2.2.   Immunotherapy

As with most malignancies, the microenvironment of PDAC is strongly immunosuppressive. Studies suggest PDAC escapes immune control early on in its development, with myeloid-derived suppressor cells (MDSC) and regulatory T cells (Tregs) seemingly the major mediators of this immune suppression [40, 41]. Moreover, levels of Tregs and PD-L1 (programmed cell death protein- 1) have shown prognostic value for PDAC [42-45]. Efforts have been made to target the immunosuppressive mechanisms of MDSCs, Tregs, and PD-L1 in a number of clinical trials [46]. Although these therapies have been largely unsuccessful as monotherapies, there are a number of phase I and II trials ongoing using checkpoint inhibitors (anti-PD-L1 and anti-CTLA-4) in combination with various inhibitors and chemotherapeutics [47]. During activation, T cells upregulate the receptors PD-1 and CTLA-4 (cytotoxic T-lymphocyte-associated protein 4) as a method of controlling the over stimulation of the immune system. When these receptors bind to their respective ligands (PD-L1 and CD80/86), the activated T cell can lose its proliferative and effector ability, dampening the immune response. In cancer, this process is hijacked by the tumour to evade the immune system, with immunotherapies aiming to counteract this suppression [48, 49]. It remains to be seen whether immunotherapies hold true promise in the treatment of PDAC. Until now, PDAC has remained resistant to such treatments, however, results from these ongoing trials with combination therapies will shed light on their potential in the near future [46].

1.1.2.3.   Nanoparticle- based therapies

As noted in section 1.1.1., the desmoplastic stroma and poor blood supply characteristic of PDAC tumours creates an extremely hypoxic microenvironment that is high in interstitial pressure and can strongly hinder the efficacy of chemotherapies for this cancer.

Moreover, issues with solubility, off-target effects and poor circulation time are additional challenges commonly observed with chemotherapeutics. Nanotechnology has subsequently been suggested as a promising approach to potentially circumvent the obstacles arising with the use of conventional treatments [50]. The unique physiochemical characteristics (PCC) of nanotechnology (e.g. size, charge and surface area) means they can be loaded with chemotherapies noted for their poor tumour accumulation and/or safety profile in order to improve their pharmacokinetics and toxic effects within the patient. This is possible due to the various biocompatible coatings around the nanoparticle which shield the carried drug until its timely release in the tumour, and the nanoparticles ability to utilise the enhanced permeability and retention (EPR) effect to preferentially accumulate in tumours. The EPR effect enables nanoparticles to capitalise on the porous vasculature and irregular lymphatic drainage of the tumour to selectively accumulate and be retained at this site [51, 52]. A systematic review in 2016 analysed the results of clinical trials using nanoparticles as delivery systems for various therapeutics (chemotherapy, cytokines and gene therapies) in pancreatic cancer and found that the overall safety and efficacy of these treatments were improved via this mechanism [53]. This has resulted in the clinical approval of two nanomedicines to treat PDAC: Albumin-bound paclitaxel (Abraxane®) and liposomal irinotecan (Onivyde®) in 2013 and 2015 respectively [54]. Although the improvements in median overall survival with these treatments were modest (<2 months against their respective control groups [55]), both displayed improved safety profiles and increased tumour accumulation against their carried chemotherapeutic alone [56-61]. The success of these treatments subsequently opened the floodgates to a massive amount of work in the space of nanomedicines to treat PDAC [54].

In addition to the large amount of work testing nanocarriers of chemotherapeutics against PDAC, novel methods of treating these tumours through the unique properties of nanoparticles have surfaced. One such promising treatment is hyperthermia – an elevation in temperature within the tumour – which relies on an external trigger (mainly light or magnetic fields) to generate a thermal response via stimuli-responsive nanoparticles residing in tumours [62-64]. Although gold nanoparticles have shown promise in this area as photothermal agents that generate heat in response to light [65], the most successful of these thermal treatments so far has been magnetic hyperthermia. This treatment approach uses external alternating magnetic fields (AMF) to stimulate iron oxide nanoparticles (IONP) localised in tissue, resulting in elevations of heat [66]. Magnetic hyperthermia

has been tested in many solid malignancies and has even achieved clinical approval to treat Glioblastoma and Prostate cancer [67-69].

1.2. Hyperthermia and magnetic hyperthermia in cancer

The use of heat to treat cancer is not a novel idea. In fact, there are reports of the Egyptians and Greek philosophers using such treatments as early as 2000- 3000 BC and 300- 500 BC respectively for various solid tumours [62, 70]. Albeit, in these cases, the treatment was not very controlled and usually consisted of hot blades pressed against tissue in order to thermally ablate the tumour. It was not until the 19th century, however, where greater advances were made after the connection between cancer and fever was first identified. In these cases, cancer patients that subsequently contracted infections (intentional or not) were noted to have a better outcome than those that did not [71]. This newfound knowledge is famous for laying the foundations of cancer immunotherapy as we know it today; however, it also worth noting that temperature elevations were also a determinant in the success of these treatments [72, 73].

1.2.1. The origins of magnetic hyperthermia

The first published record of the use of magnetic particles and magnetic fields to generate temperature elevations in tumours comes from Gilchrist *et al* in 1957 [74]. In this paper, 20 – 100 nm maghemite nanoparticles were injected directly into the lymphatic system of canines. Subsequent AMF were then applied with the aim of treating lymph node metastasis not identified during surgical resection. This basic procedure of using IONP exposed to AMF as a form of controlled hyperthermia has remained popular ever since. Following this, significant advances were made in the early 2000's, where IONP of various designs that would allow for improved tumour targeting and a more controlled application of heat to cancer were explored [75-77]. Additionally, a large amount of *in vivo* efficacy studies began to emerge [78-82]. It was through this work that the now well-recognised clinical procedure of magnetic hyperthermia emerged which relies on the intratumoural injection of the nanoparticles to ensure the temperatures achieved within the tumour are controlled and off-target heating was limited [83-86].

1.2.2. The effects of hyperthermia on cancer: benefits, drawbacks and considerations

1.2.2.1. Hyperthermia and vasculature

It is well recognised that cancer cells are more sensitive to elevated temperatures than healthy cells [87, 88]. The irregular vasculature characteristic of tumours makes them less efficient at thermoregulation than healthy tissue, and so vascular stasis occurs in a tumour at temperatures of approximately 43°C, whereas this effect manifests closer to 47°C in healthy tissue [89]. The mechanisms behind this stasis include endothelial cell damage, platelet and leukocyte adhesion and capillary thrombosis [90, 91]. Following this circulatory disruption, the tumour becomes nutrient deprived and increasingly hypoxic which in turn leads to elevated levels of acidosis [92, 93].

Another dimension to this hyperthermia/vascular effect, however, is that at slightly lower temperatures (41-43°C), blood perfusion can actually increase in tumours [89, 93, 94]. An increase in blood perfusion can enhance the chemosensitivity of tumours through a number of mechanisms such as increasing levels of chemotherapy reaching the tumour [95], increasing tumour cell proliferation thereby enabling chemotherapies to induce their cytotoxic effect [96] and a restoration of the augmented resistant mechanisms associated with hypoxic tumours (i.e. upregulation of multidrug resistant genes and inhibitions to p53 signalling) [97, 98]. Additionally, oxygenation of a tumour can also improve the efficacy of radiotherapy through increases in reactive oxygen species (ROS) and subsequent DNA damage following radiation treatment [99]. Therefore, a slight change in temperature could have large implications on the efficacy of combination treatments such as chemotherapy and radiation [93].

1.2.2.2. Hyperthermia and cytotoxicity

With regards to the direct cytotoxic effects of magnetic hyperthermia in cancer, temperatures of 42°C and above have been shown to damage cellular architecture through protein denaturation, leading to cell membrane and mitochondrial damage as well as disruption to many signalling pathways [100, 101]. Additionally, magnetic hyperthermia has been shown to upregulate ROS by both hyperthermia and as a by-product of IONP natural metabolism which in itself can induce apoptosis [102, 103]. Interestingly, depending on the temperatures generated, apoptosis or necrosis can be induced. Temperatures of approximately 42-43°C have shown to induce apoptosis in cells, whereas temperatures of 45°C or more induce cell death primarily through necrosis [104-106].

This is an important consideration as inducing high levels of necrosis in a tumour will result in an inflammatory response that could harm healthy tissue if not properly controlled and isolated to the desired location. Likewise, unintentionally heating healthy tissue to these higher temperatures will induce off-target side-effects.

1.2.2.3. Hyperthermia and DNA repair

As described, heat can damage proteins and disrupt intracellular signalling so it is possible that an elevation in heat could interfere with DNA repair processes in cells. Reviews by Oei A. L. *et al* (2015) and Kampinga H. H. *et al* (2004) describe the evidence associated with hyperthermia and its ability to inhibit various DNA repair pathways [107, 108]. Much of the research described, however, is based on indirect effects of repair inhibition, such as increased cell sensitivity to chemotherapy or radiation following hyperthermia as an indicator for DNA repair inhibition [109, 110]. The molecular mechanisms behind these inhibitions remain elusive in most cases. Below is a description of a number of papers that hint at molecular events associated with DNA repair inhibition.

Fantini D. *et al* showed that heating HeLa cells to 42°C for four hours could inhibit 8-oxoguanine DNA glycosylase (OGG1) signalling, resulting in its ubiquitination and proteasomal degradation [111]. OGG1 recognises the purine lesion 8-oxo-7,8-dihydroguanine (8-oxoG) and initiates base excision repair (BER) signalling [112]. Additionally, a number of studies have shown reduced activity of DNA polymerase β in cells following exposure to temperatures between 40- 46°C – lending weight to the potential inhibition of BER [113, 114]. Otherwise, little literature is available on the alterations to nucleotide excision repair and miss-match repair systems following heat and so further investigation is required for these pathways.

The majority of research in this space, however, derives from double strand break (DSB) repair signalling [115]. DNA-dependant protein kinase (DNA-PK) and its subunits p470 and Ku were isolated from human leukaemia cells through column chromatography and centrifugation and exposed to 44°C for 30 minutes. A strong suppression of kinase activity was identified following treatment [116]. This result complemented *in vitro* experiments hinting at an aggregation of Ku80 in the nucleus of melanoma cells following heat treatment at 45.5°C for 15- 30 minutes [117] and a reduction in DNA-PK activity in hybrid (DNA-PK expressing) severe combined immunodeficient (SCID) cells heated to 44°C for 15 minutes [118]- all pointing towards a potential inhibition of the non-homologous end-joining (NHEJ) pathway of DSB repair. One study published in 2014

took these same cells and treated them with 44°C for various timepoints to measure the degree of DSB repair inhibition and radiosensitization [119]. Heating the hybrid cells to 44°C for 15 minutes could reduce Ku80 and Ku70 levels, resulting in a reduction in DNA-PK activity and increased radiosensitization. Interestingly, cells negative for DNA-PK also exhibited an enhanced radiosensitization following heat treatment. The paper additionally showed a slight reduction in BRCA1 and 53BP1 (76% and 83% of their control levels respectively) following heat treatment of the hybrid cells so it could be theorized that both NHEJ and homologous recombination (HR) is inhibited in these cells thus eliminating any compensatory effects from alternative pathways following DNA damage.

A reduction in BRCA2 signalling following hyperthermia has been well reported in the literature and has been discussed as a potential mechanism involved in the inhibition of the HR pathway [120]. One comprehensive study by Krawczyk P. M. *et al* assessed the potential of hyperthermia (41- 42.5°C for various durations) to mitigate HR *in vitro* and *in vivo* [121]. Treating multiple cell lines and a cervix tumour biopsy with hyperthermia resulted in a reduction in BRCA2 and HR efficiency. Moreover, two different *in vivo* cancer models were shown to be highly sensitive to hyperthermia combined with poly (ADP-ribose) polymerase-1 inhibitors (inducing synthetic lethality of the HR repair pathway) and hyperthermia combined with heat shock protein- 90 inhibitors (inhibiting regulation of BRCA2 signalling), prolonging survival in both systems, particularly when all three treatments were used together.

There are a number of points to acknowledge when considering the potential of heat to inhibit DNA repair as an adjuvant to chemotherapy and/ or radiation. It is important to note that although a number of studies can point to the molecular events associated with inhibitions of various DNA repair pathways in cells, there are also papers that determine otherwise. For example, many studies have shown that cells deficient in the repair pathway inhibited by hyperthermia in the wild type cells still experience the same sensitization to chemotherapy and/ or radiation following treatment, potentially nullifying results from the molecular studies discussed here [108]. Reasons suggested for this include the transient nature of this inhibition (literature consistently shows that the levels of the repair mechanism of interest normalizes after a varied period of time following exposure to heat), the ability of the DNA repair system to compensate with an alternative pathway when one is compromised and the ability of chemotherapy and radiation to induce both SSB and DSB in DNA, thus not relying on one pathway for repair

[107, 119, 122]. Hence, it is clear that heat can disrupt DNA repair processes in cells, but in order to take advantage of this potential therapeutic enhancement, it must be assessed in a case-by-case basis for each cancer to determine whether the elevated repair signalling characteristic of the cancer is sensitive to heat, and whether the potential inhibition observed complements the combination treatment of interest. Finally, comparing these hyperthermia effects to magnetic hyperthermia treatment is also essential to see if they occur regardless of the heating source as there is limited literature in this regard [123, 124].

1.2.2.4.   Hyperthermia and tumour mechanics

Recent studies have demonstrated the ability of nanoparticle- generated heat to alter mechanical properties of tumours [125, 126]. As discussed in section 1.1.1., the desmoplastic stroma of PDAC is a major barrier for chemotherapies which has led to a surge of research into treatments aiming to normalize the stroma in an effort to enhance penetration of drugs. Heat has been shown to alter the mechanical properties of tumours at both the micro and macroscopic scale. Photodynamic therapy and magnetic hyperthermia have both been shown to denature collagen fibres locally, with multiple treatments allowing for increased nanoparticle penetration that in turn enables a larger area of the tumour to be heated in the following runs (43°C and above) [127]. This paper also evaluated tumour stiffness following photothermal therapy and noted a significant reduction in comparison to untreated controls days after treatment. Importantly, a significant increase of drug and nanoparticle penetration into the tumour was observed following magnetic hyperthermia treatment (Figure 1.2.). Similar results have also been reported elsewhere at 42-43°C [128, 129].
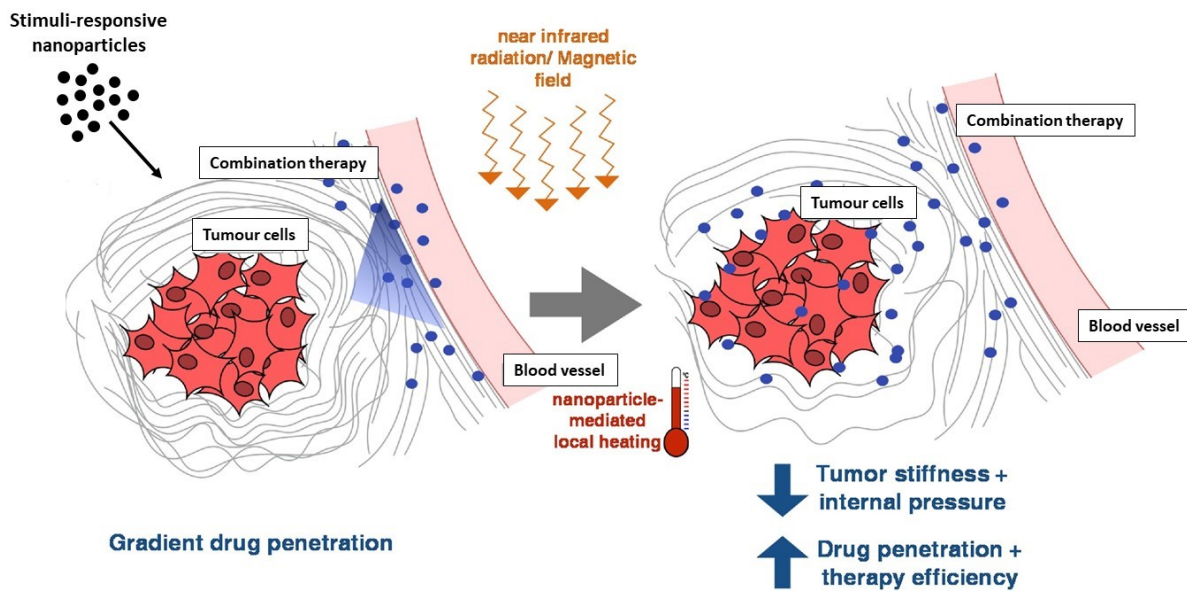
Figure 1.2. Utilising stimuli-responsive nanoparticles to improve penetration of therapies into tumours.

Nanoparticles residing in tumours can generate heat in response to various stimuli (infrared radiation and magnetic fields). This heat treatment has been shown to alter the mechanical properties of the tumour microenvironment, enabling combination therapies to accumulate further into the tumour and at higher concentrations. Image adapted from Kolosnjaj-Tabi J. *et al* [126].

1.2.2.5. Hyperthermia and the immune system

As fever is a by-product of an immune reaction, it makes sense that hyperthermia would induce an immunomodulatory effect. A review by Peer A. J. *et al* 2010 looks at the diverse effects to the immune system following various thermal treatments [130]. The literature regarding heat and the immune system is varied and complex, and depending on temperatures generated and duration of treatment, contrasting responses can be observed. What is well known, however, is the fact that controlled, localised hyperthermia can stimulate an anti-tumour immune response. Many mechanisms of anti-tumour immunity have been suggested in the literature including induction of dendritic cell (DC) maturation and antigen presentation to $CD8^+$ T cells, heightened cytotoxic profile of natural killer (NK) cells and a sensitization of cancer cells to these and a decrease in regulatory T cells levels in tumours [131]. One interesting *in vivo* study took rats with rat glioma tumours generated on both their left and right femurs. Liposomes encapsulating IONP were then injected into the left femur tumours only and the rats were treated with 3 cycles (24 hours apart) of magnetic hyperthermia that lasted 30 minutes and reached temperatures between 42- 45°C. Remarkably, after 28 days, both tumours had disappeared in the animals and did not regrow after 3 months, achieving complete regression [132]. Immunohistological analysis revealed that NK cells, $CD8^+$ and $CD4^+$ cells were present in both tumours and so it was determined that an anti-tumour immune response was induced following the heat treatment.

Following temperature elevations in cells, heat-shock proteins (HSP) are upregulated as a form of thermotolerance. Mathematical modelling has suggested that temperatures of 43°C for 100 minutes are optimum to achieve the maximum extracellular concentration of HSP [133]. HSP main role in cells are to act as molecular chaperones to prevent protein aggregating and misfolding [134]. It is now believed that following hyperthermia treatment in a tumour, some cells will undergo necrosis, some will become apoptotic, and some will be spared from any cytotoxic effects. For the necrotic and apoptotic cells, HSP will be upregulated as a response to this heat which will in turn chaperone tumour antigens. Necrotic cells will release these antigens into the tumour microenvironment, while apoptotic cells will have elevated expression of these on the surface of their cells. Antigens released into the tumour microenvironment can be recognised and processed by DC that in turn present these antigens to T cells which elicits an adaptive immune response through cytotoxic T cells, killing the remaining cells that were spared from the heat treatment. For the apoptotic tumour cells, the elevated

expression of tumour antigens on their surface will increase their chances of recognition and elimination by cytotoxic T cells (Figure 1.3.) [133, 135, 136].

While the immune stimulatory effects of HSP are well reported and considered beneficial to hyperthermia treatment of cancers, the thermotolerance role of HSP can also protect cells from temperature- associated effects, and so some groups have sought to inhibit HSP as a combination therapy to hyperthermia [137, 138]. In these cases, inhibition of HSP70 in combination with hyperthermia (43°C for two hours) significantly benefited the treatment and even acted synergistically with magnetic hyperthermia (41°C / 43°C for 30 minutes) in *in vitro* and *in vivo* studies. In these cases, both gene silencing and inhibitors of HSP70 function were used to successfully achieve the desired response.

Therefore, depending on the desired endpoint for a study (treating metastatic disease versus a localised tumour), magnetic hyperthermia treatment could be tailored to suit a particular scenario. An important consideration in this regard is that most *in vivo* studies testing the efficacy of magnetic hyperthermia are conducted in immunocompromised mice, which may not portray the true efficacy of the treatment as the immune system could play a key role in its response. Noteworthy, hyperthermia generated through IONP may also elicit an inherent inflammatory response through the upregulation of ROS associated with their metabolism which has been shown to polarise macrophages in tumours and induce an anti-tumour immune response [139].
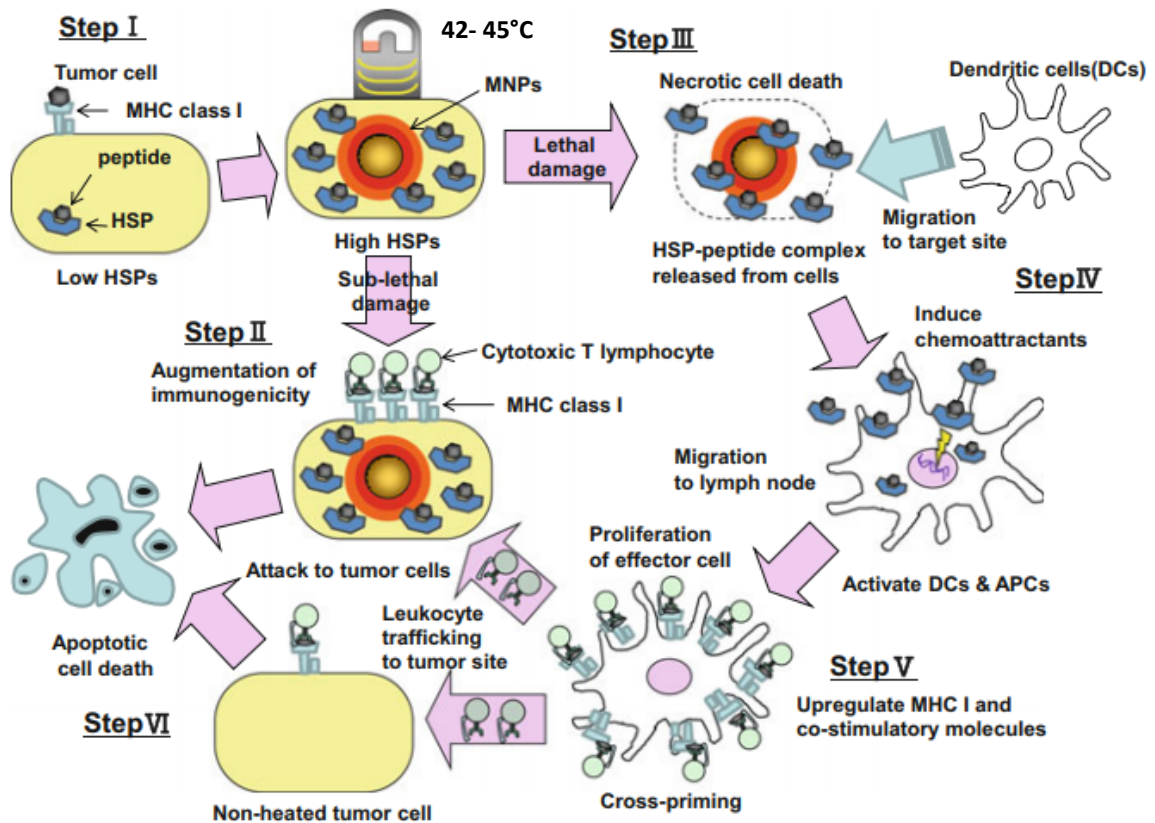
Figure 1.3. Suggested mechanism for the stimulation of an anti-tumour immune response following magnetic hyperthermia treatment.

Step I. The basal levels of heat shock protein (HSP) in tumour cells is relatively low. Nanoparticle-mediated hyperthermia at temperatures between 42- 45°C results in an increased expression of HSP in the successfully treated cells which chaperone endogenous antigens. Step II. The HSP-antigen complexes can be processed and expressed on the cells surface enabling immune recognition. Step III. Cells undergoing necrosis as a result of the heat treatment release the HSP-antigen complexes into the local microenvironment which act as danger signals for the immune system. Step IV. Dendritic cells recognise the danger signals and activate local monocytes which recruit more antigen presenting cells to the tumour. Step V. The dendritic cells internalise and process the HSP-antigen complexes and present them to T lymphocytes through MHC class I or MHC class II signalling. Step VI. The cytotoxic T lymphocytes specific for the presented tumour antigens can induce apoptotic cell death on the remaining cells left following heat treatment. Image adapted from [135]. Abbreviations: MHC, major histocompatibility complex; MNP, magnetic nanoparticles; HSP, heat shock proteins; DC, dendritic cells; APC, antigen presenting cells.

1.2.2.6. Hyperthermia and metabolism

There are few reports on the effects of heat on cancer cell metabolism, particularly with Seahorse[TM] extracellular flux technology. One study published in 2007 compared base line oxygen consumption rates in PANC-1 and AsPC-1 pancreatic cancer cell lines following five minutes treatment at 46°C and found a significant reduction in both cases 24 hours post treatment. A healthy pancreatic epithelial cell control on the other hand showed a significant increase in oxygen consumption following treatment [140]. These results were not normalised for cell count or protein concentration, however. A more recent study measured changes in glycolysis and mitochondrial function following heat treatment of colorectal cancer cells. Heat treatment at 42°C for 60 minutes could induce significant increases in all measures of glycolysis (non-glycolytic acidification, glycolysis, glycolytic reserve and glycolytic capacity) during the glycolytic stress test, while a significant increase in proton leakage was observed in the mitochondrial stress test [141]. As no other changes were observed during the mitochondrial test, it could be surmised that heat treatment may damage the mitochondrial membrane without having any influence on adenosine triphosphate (ATP) synthase functional capacity. Other than these two relatively recent studies, most of the research published on heat and metabolism was undertaken in the mid-to-late 1900's. This work was reviewed by Streffer C. in 1985 and 1988 [142, 143] and led to the conclusions that metabolic activity is overall increased when cells are treated with hyperthermia, however, conflicting results make it difficult to decipher which metabolic mechanism becomes favourable following treatment, and whether this could be cell dependant.

It is clear that hyperthermia alters the metabolic activity of cancer cells. Despite this, many questions remain unanswered with regards to this response. Much of the early research in this space is *in vivo* work which does not consider the potential changes in blood perfusion to different tumours following heat treatment which would certainly affect metabolism in itself and give varied results. Additionally, most of this *in vivo* work treated the tumours through whole body hyperthermia and not the localised treatment associated with magnetic hyperthermia. Therefore, it is difficult to draw comparisons in this regard. Identifying which metabolic processes are dominant following heat treatments is essential to determine whether the tumour microenvironment is becoming more acidic and which molecular processes are active. This, in turn, will aid in decisions as to what combination therapies would be most appropriate for each individual case.

1.2.2.7. Hyperthermia and metastasis

A number of studies have shown the potential of heat (whole body or localised through magnetic or light stimulation of nanoparticles) to inhibit the invasive potential of cancer [144-146]. Heating melanoma and breast cancer cells in a water bath to 43, 45 and 47°C for 30 minutes was shown to significantly inhibit cell invasiveness (via Matrigel invasion assay) and expression of MMP-2, MMP-9 and TGF-β1 in a temperature dependant manner [144, 145]. Likewise, photothermal therapy using IONP to generate temperatures of 42, 45 and 48°C for 10-20 minutes could selectively kill triple-negative breast cancer stem cells *in vitro*, while also inhibiting secondary mammosphere formation in these cells in a temperature-dependent manner. This treatment was additionally shown to significantly inhibit lymph node and lung metastasis in mouse models of this cancer [146]. Many papers have described this ability of nanoparticle-mediated hyperthermia to kill cancer stem cells and/or inhibit their renewal capacity [147-149]. In a similar study, Jia D. *et al* aimed to inhibit lung metastasis in a mouse melanoma model following whole body hyperthermia [150]. Treating with 40°C for 30 minutes proved more efficient at reducing the number of lung metastatic colonies against chemotherapy alone. Moreover, there was a negligible difference in metastasis between a combination of hyperthermia and chemotherapy versus hyperthermia alone.

Despite these results, some reports do exist which show that heat alone has no effect (or even detrimental effect) on cancer spread. Wang C. *et al* showed that photothermal therapy with carbon nanotubes alone (45-55°C for 10 minutes) was ineffective at suppressing lung metastasis but required the addition of anti-CTLA-4 therapy to achieve this desired response [151]. Strikingly, a similar paper by Bear A. S. *et al* noted photothermal therapy (treatment lasted 3 minutes; temperatures not provided) significantly increased lung metastasis in a mice melanoma model [152]. This increased metastasis was associated with a dramatic rise in proinflammatory cytokines and an expansion and recruitment of myeloid-derived suppressor cells into the tumour microenvironment. When this heat treatment is combined with adoptive T cell transfer, however, a significant reduction in tumour mass and near complete reduction in metastasis is observed. This worrying response has also been reported in the clinic in a small number of patients (4 out of 96) receiving laser hyperthermia for liver metastasis with colorectal cancer [153].

It is apparent that in the majority of cases, hyperthermia can elicit an anti-metastatic response in cancer. The mechanisms behind this effect vary but can include a

downregulation in metastatic protein expression, as well as a cytotoxic response to cancer stem cells. It is important to note, however, that in rare cases, heat treatments have been shown to accelerate metastasis in cancer. Although literature in this regard is limited, available data would suggest that this is due to a stimulation of the immune system which may aid in angiogenesis and hence cancer invasion.

1.2.2.8. Hyperthermia and DNA damage

There is an abundance of literature describing heat-induced DNA damage. This damage may occur directly (heat alone) or indirectly (ROS associated or inhibition of DNA repair pathways – see section 1.2.2.3.) [154, 155]. As magnetic hyperthermia has been shown to upregulate ROS more than hyperthermia alone (either as a by-product of IONP metabolism or through more localised heating) [85, 156, 157], it may exacerbate the DNA damage observed in hyperthermia studies [158].

Until recent times there has been conflicting evidence as to whether heat could induce DSB in DNA. Some papers used levels of phosphorylated H2AX (γH2AX) as a marker for DSB following heat treatment (40-47°C for multiple durations) [159, 160]. Following DSB, H2AX becomes phosphorylated close to the damage site and plays a major role in DSB repair [161]. However, heat alone (43°C for 30 minutes) has been shown to phosphorylate H2AX independent of DNA damage [162]. On the other hand, Nueda A. *et al* could show that cells negative in DNA-PK signalling (pathway involved in DSB repair – see section 1.2.2.3.) are highly sensitive to heat treatment [163]. A study published in 2012 treated MCF-7 breast cancer cell line with 42, 44 and 45.5°C in a water bath for 30 minutes. This paper found that heat could induce DSB in G1 and G2 phase cells (measured by γH2AX levels, neutral comet assay and terminal deoxynucleotidyl transferase incorporation assay), but not S phase cells, where it causes an attenuation in the progression of replication forks that occurs in a temperature dependant manner [164]. It has been well established that cells in S phase of cell cycle are most thermosensitive and so identifying potential mechanisms involved in this sensitization is essential for advancing this treatment [165-167]. Subsequently, another paper by this group probed further the molecular mechanisms associated with heat-induced SSB observed with cells in S phase of cell cycle [168]. HeLa and human fibroblast cells in early S phase were shown to be most vulnerable to heat shock at 45.5°C (but not 41°C or 43°C) for 30 minutes which resulted in a senescence-like state marked by nuclear enlargement, elevated expression of β-galactosidase and p21$^{\text{CIP1}}$ and persistent DNA damage initiated

by SSB generated through inhibitions to topoisomerase-1. It is thought that these SSB are subsequently converted to DSB during DNA replication which triggers this senescence-like phenotype. Moreover, inhibiting DNA replication in these cells could prevent the generation of these senescent-like cells. Following this, the group showed that the heat-induced senescent-like state in HeLa cells can be transient, and the cells could progress to mitosis four days after heat treatment. However, these cells have amplified centromeres resulting in a multipolar mitosis [165].

Interestingly, Bewicke-Copley F. *et al* (2017) identified a potential bystander effect with MCF-7 cells treated with heat. Here, the cells were heated to 45°C for one hour in an incubator. After 24 hours, extracellular vesicles (EV) were isolated from their medium and added to the medium of untreated cells. Both the heat treated and EV treated cells experienced a significant increase in DNA damage via the alkaline comet assay, along with a significant decrease in viability against cells treated with EV's derived from untreated cells. Moreover, these cells were also more resilient to subsequent heat treatment [169].

It is clear that heat is capable of inducing DNA damage in cells. Both DSB and SSB have been generated following heat treatment, with the literature suggesting that the response is cell cycle dependent. Interestingly, cells in S phase have been shown to be most thermosensitive, making radiation an ideal combination therapy as S phase cells are most resistant in this case [100]. The mechanisms behind SSB have recently been determined and associated with an inhibition of topoisomerase-1 activity in S phase cells. This can also indirectly lead to DSB following DNA replication. DSB have also been shown to be selective to cells in G1 and G2 phase of cell cycle, however the mechanisms behind this are yet to be elucidated [107, 155]. It is important to note that this work must be repeated in multiple cell lines from multiple cancers to determine if this is a universal response that can be hijacked to enhance the effects of combination therapies.
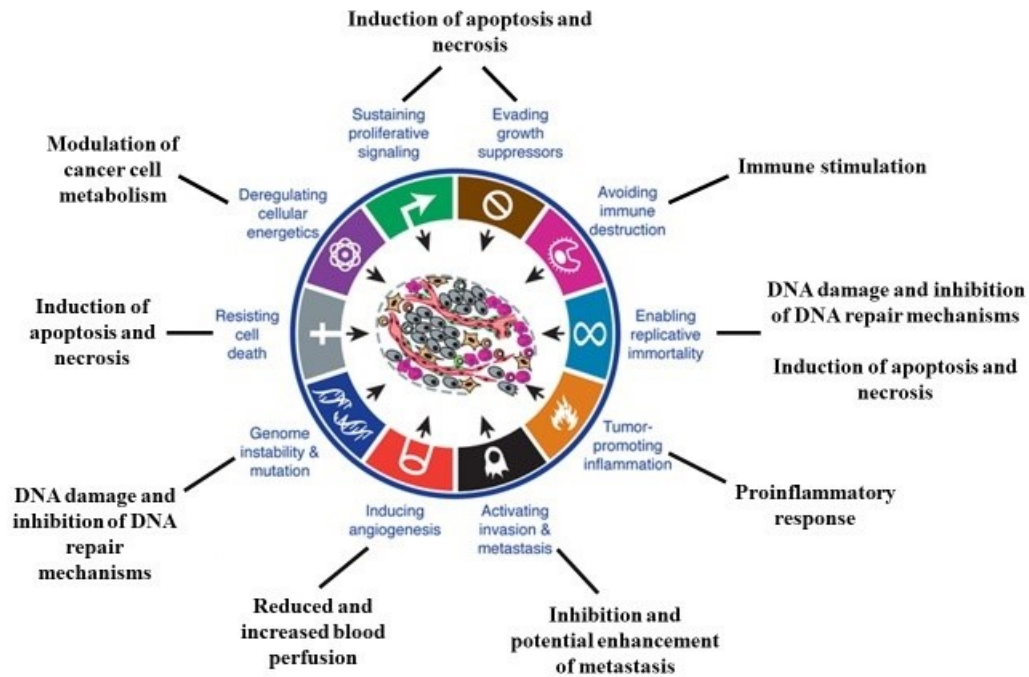
Figure 1.4. Effects of hyperthermia on the hallmarks of cancer.

Based on the literature detailed above, the effects of hyperthermia on the hallmarks of cancer are described here. Hyperthermia has been shown to both inhibit and augment various cancer hallmarks. Image adapted from [170].

1.2.2.9. Considerations to the application of magnetic hyperthermia in cancer

It is therefore clear that there is no 'one size fits all' approach to hyperthermia treatment of cancer. The variety of different preferential responses that can occur at different temperatures and durations make this treatment very complex and so it is important to explore all scenarios to ensure the most effective response is achieved (Figure 1.4.). For example, if the aim is to combine magnetic hyperthermia with a chemotherapy, it might be detrimental to use temperatures of 43°C and above as this may induce vascular stasis and inhibit drug accumulation in the tumour. On the other hand, temperatures of 43°C and above can reduce tumour stiffness and enable increased concentration of chemotherapeutic drugs into the tumour. To complicate things further, the inhibition of DNA repair mechanisms at various temperatures are a further consideration that could enhance the effects of chemotherapy. Likewise, aiming to improve blood perfusion into a tumour to enhance the efficacy of radiotherapy at temperatures of 42°C may benefit this therapy alone, but increasing this to 43°C may increase the expression of HSP further and elicit a stronger anti-tumour immune response (Figure 1.5).

It is therefore necessary to explore multiple temperatures and durations when combining magnetic hyperthermia with conventional treatments. Importantly, different cancers may also respond to temperatures differently (for example, PDAC has a notably tough stroma and low blood perfusion therefore heat treatment may alleviate one or both of these) and so it is not expected that one temperature will fit all cancers.
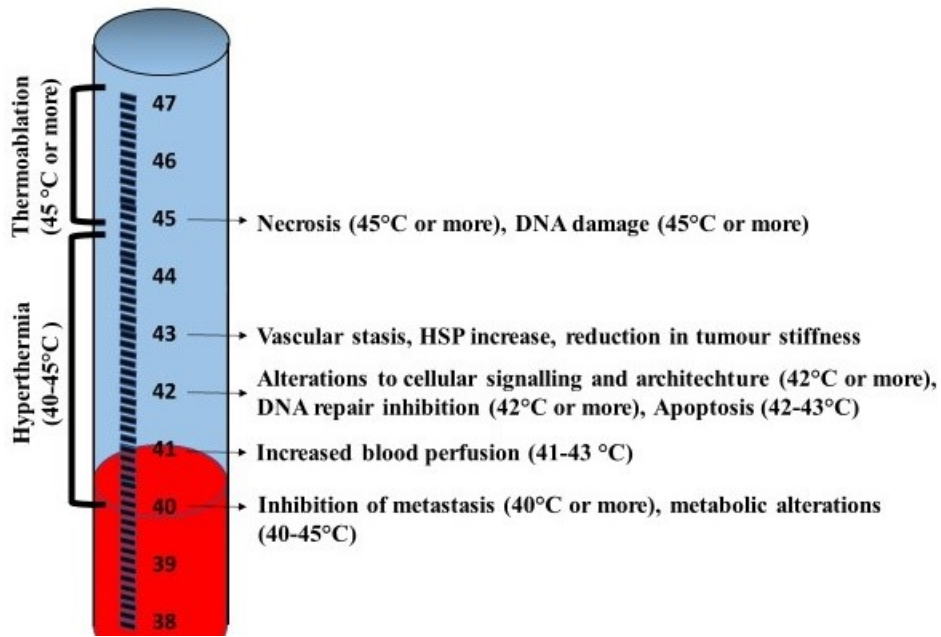
Figure 1.5. Summary of the various effects of heat on tumours.

This summary is based on the literature described in section 1.2. For the purposes of simplicity in this figure, durations of time related to these temperatures were not included but play a contributing factor. This image combines the effects of both hyperthermia and magnetic hyperthermia data. Numbers mentioned are in degrees Celsius.

1.3. IONP and magnetic hyperthermia

IONP used in biomedical applications consist of an iron oxide core - mainly magnetite (Fe_3O_4) or maghemite (Fe_2O_3) - which is coated in a biocompatible polymer such as polyethylene glycol (PEG) or dextran to provide stability and prevent aggregation to the system as well as limiting potential toxic effects [171, 172]. This basic design has been successful in the clinic for a range of applications including magnetic resonance imaging of various diseases, iron supplementation for iron-deficiency anaemia, and magnetic hyperthermia for various cancers [173, 174].

1.3.1. Superparamagnetism with IONP

Below sizes of approximately 50 nm, it becomes energetically favourable for IONP to become single domain structures. Domains in this case refer to the orientation of the atomic magnetic moments within the nanoparticle. When these magnetic moments line up uniformly in one direction within the nanoparticle, this is defined as a single domain IONP. Larger IONP have multiple domains due to magnetic moments orientated in many different directions [175].

Single domain IONP can experience spontaneous reversals or 'flips' in magnetic moments as a result of thermal fluctuations in the system which overcome the energy barrier for magnetisation reversal; the time between two of these flips is known as Néel relaxation time. When the time required to measure magnetisation is greater than the Néel relaxation time, the overall average of magnetic moments in the absence of a magnetic field equals zero. These nanoparticles are defined as superparamagnetic [175-177]. Superparamagnetic IONP are ideal materials for inducing hyperthermia in tumours as they have a high net magnetisation when subjected to an external magnetic field and retain no remnant magnetisation after a magnetic field is removed, thus eliminating potential for aggregation (Figure 1.6.). Therefore superparamagnetic IONP can provide a very controlled method of inducing temperature elevations in tumours with minimal side effects to healthy tissue [178].
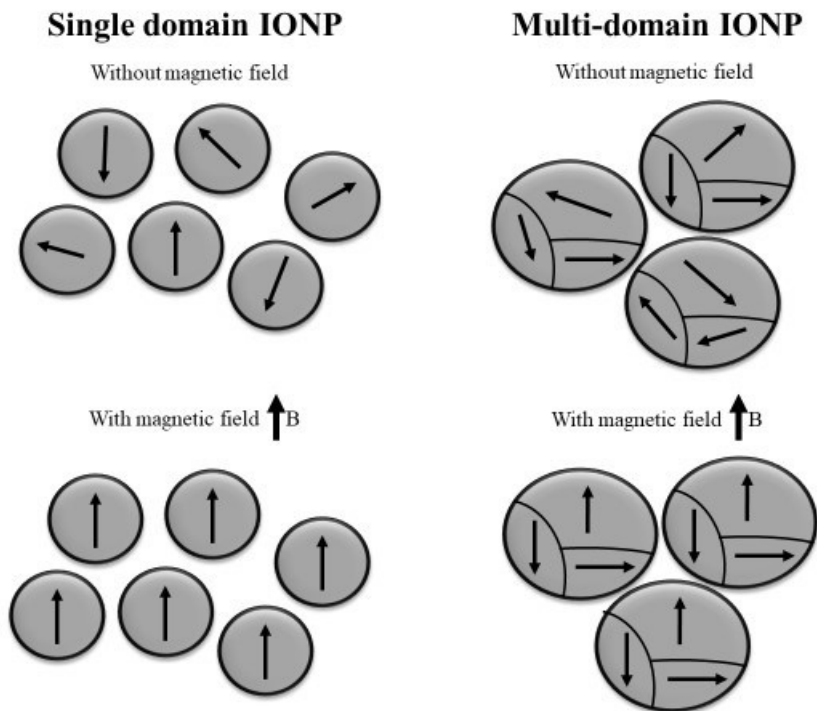
Figure 1.6. Effects of external magnetic fields on single domain and multi-domain IONP.

At sufficiently small sizes (<50nm) IONP exist in single magnetic domains. This allows the nanoparticles to act uniformly in response to an externally applied magnetic field, *B*, and retain no remnant magnetisation following field removal. This is not the case with multi-domain nanoparticles and so single domain are the predominant nanoparticles used for the magnetic hyperthermia.

1.3.2. Using IONP to generate heat in tumours

Upon exposure to an external AMF, both single and multi-domain IONP can generate heat. In multi-domain nanoparticles, these temperature elevations are mainly a result of domain wall reorganization known as hysteresis losses. In superparamagnetic IONP, however, heat is generated predominantly through Néel and Brownian relaxation. Néel relaxation refers to the change in direction to the magnetic moment of a nanoparticle in response to a magnetic field, whereas Brownian relaxation refers to the physical rotation of the nanoparticle in suspension (Figure 1.7.) [176, 179, 180]. When these nanoparticles are localised in tissue, Brownian motion is inhibited and so Néel relaxation becomes the predominant mechanism of heat generation in tumours [86].
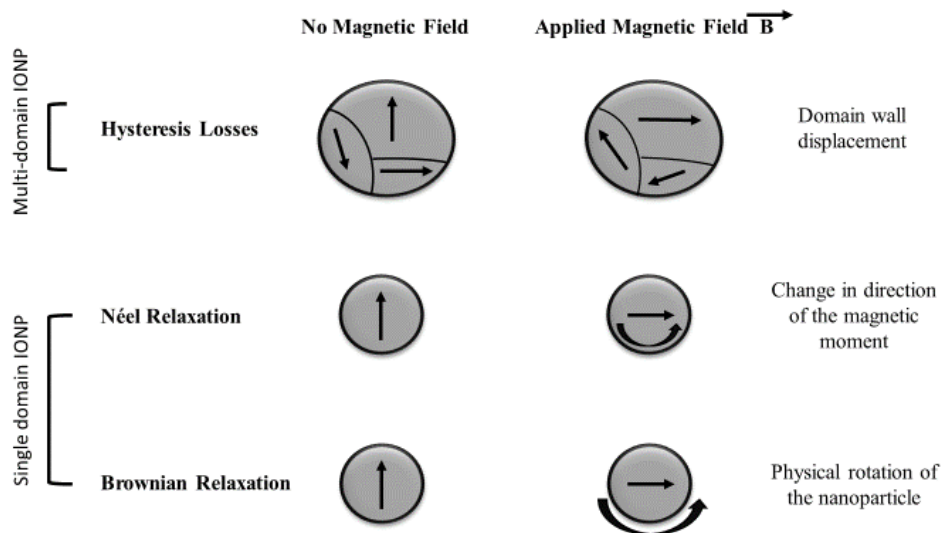
Figure 1.7. Mechanism of heat generation of IONP exposed to AMF.

Single domain IONP generate heat through Néel and Brownian relaxation when exposed to AMF. By contrast, multi-domain IONP achieve this temperature elevation principally through hysteresis losses. *B* refers to the direction of the applied magnetic field.

1.3.3. Measuring the heating efficiency of IONP

In order to measure and compare the heating efficacy of various IONP, two parameters are commonly measured – specific absorbance rate and intrinsic loss power. Specific absorbance rate, or SAR, is a measure of the heating potential of IONP per unit mass of iron, and defined as:

$$SAR = c * \frac{mF}{mP} * \frac{\Delta T}{\Delta t},$$

where c is the specific heat capacity of the solution, mF and mP are the mass of the fluid and mass of the nanoparticles respectively, and $\frac{\Delta T}{\Delta t}$ is the initial slope of the heating curve after the AMF is applied to the IONP [181-183]. In order to account for the variability in field strengths and frequencies used in these measurements in the literature, intrinsic loss power (ILP) can be calculated as follows:

$$ILP = \frac{SAR}{H^2 f},$$

where H is the applied field and f is the frequency, which enables direct comparisons to be made between different experiments [184]. An ideal IONP used for magnetic hyperthermia would have a high ILP value as less material would be required to induce a desirable thermal effect, limiting potential toxic effects.

1.3.4. Application of IONP and magnetic hyperthermia in the clinic

Magforce AG (Germany) successfully achieved regulatory approval from the European Medicines Association (EMA) in 2011, and the United States Food and Drug Administration (FDA) in 2018 for the use of their IONP (Nanotherm®) and AMF generator (NanoActivator®) to treat glioblastoma multiforme and prostate cancer respectively. Additional trials are also ongoing for the use of this therapy in various cancers such as pancreatic, breast, and oesophageal cancer [68]. Their treatment uses aminosaline-coated magnetite nanoparticles approximately 12 nm in diameter that are injected intratumorally and imaged using computed tomography scans to develop a treatment plan. For patients with glioblastoma, they receive six hour-long therapy sessions (aiming to generate no more than 43°C) in conjunction with standard radiation treatment for their disease [185, 186]. Magforce AG has reported survival benefits with the use of their therapy on primary and recurrent glioblastoma multiforme [68, 186]. Since Magforce AG achieved approval for glioblastoma, many clinical trials are now ongoing using magnetic hyperthermia to treat a range of cancers [187].

1.4. Biocompatibility of IONP

IONP are generally considered as biocompatible due to the fact that iron occurs naturally in high levels in the body and that IONP can be naturally metabolised and utilised for subsequent cellular processes [188-190]. Despite this, four clinically approved IONP have been subsequently discontinued (Combidex® in 2007, Feridex® in 2008, Resovist® in 2009, and Gastromark® in 2012) which has led to the EMA and FDA publishing reports regarding their safety [191-193]. In these reports, hypersensitive reactions were highlighted as major risks when administering these nanoparticles intravenously and recommendations were provided to tackle these. To limit these potentially fatal allergic reactions upon treatment, particular attention should be given during and at least 30 min after infusion, with appropriate treatment administered if reactions do occur.

1.4.1. Role of the complement system in allergic reactions to nanomedicines

Upon reaching the bloodstream, nanoparticles are immediately covered with proteins from the serum. This surface covering can occur in a dynamic manner referred to as the "Vroman effect," which explains the competitive adsorption of proteins with respect to their concentration, affinity and incubation time [194]. Once bound, these proteins may decide the nanoparticles fate *in vivo*, acting as markers for phagocytic uptake and clearance of nanoparticles [195, 196]. One such family of proteins that play a major role in these reactions are the complement system [197]. This system acts as a rapid response to pathogens, enabling their recognition, destruction and opsonization through a stimulation of the immune system [198]. More than 30 plasma proteins comprise the complement system, which can become activated through three independent mechanisms: the classical, alternative, and lectin pathways. Each of these mechanisms converges at the point of complement alternative 3 (C3) convertase with cleavage into its active subunits C3a and C3b, the defining step in complement activation [198, 199] (Figure 1.8.).
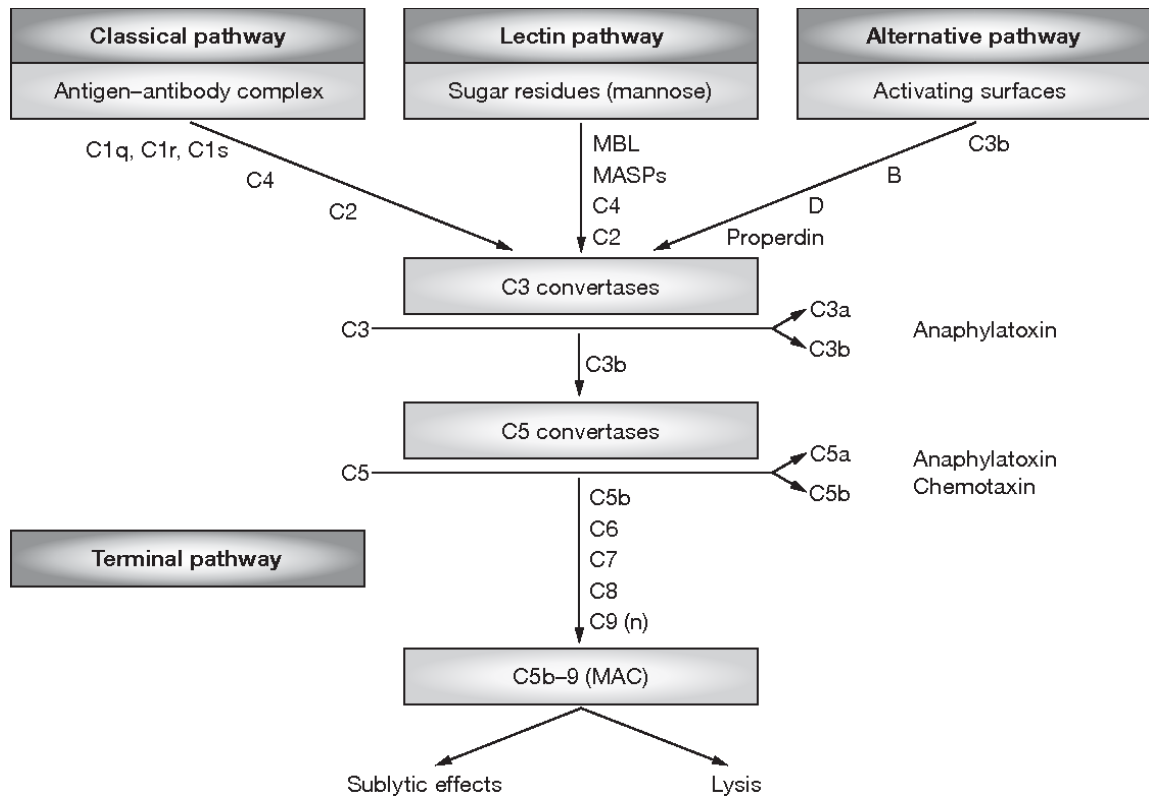
Figure 1.8. Graphical illustration of the complement system.

Three individual pathways (classical, lectin and alternative) become activated by distinctive events: the classical pathway becomes activated following IgG or IgM-antigen binding, the lectin pathway requires mannose-binding lectin to associate to carbohydrate residues on pathogens and the alternative pathway begins with the activation of C3 following pathogen binding. Regardless of the pathway activated, each converge at the point of C3 cleavage into its subunits C3a and C3b. From here, downstream proteolytic events lead to the formation of C5b-9 (membrane attack complex) which lodges into cellular membranes and induces cell lysis. Abbreviations: MAC, membrane attack complex; C1-9, complement proteins; MBL, mannose-binding lectin; MASPs, mannose-binding-lectin-associated serine proteases. Reproduced with permission from Cook H. T. *et al* (2006) [200]. Copyright 2019, Springer Nature.

Uncontrollable complement activation, however, can lead to overstimulation of the immune system, resulting in acute allergic reactions that can be fatal in some instances [197]. These IgE independent reactions are referred to as CARPA (or complement activation- related pseudoallergy), which is a common dose-limiting infusion reaction that occurs with many medicinal products, including nanomedicines [201]. CARPA involves a complex network of cells including white blood cells, platelets, endothelial cells, masts cells, basophils and macrophages which manifests in a variety of symptoms involving many organ systems that can be mild or severe depending on the individual (Figure 1.9.) [202]. Reviewed by Szebeni in 2014, CARPA is not sufficiently evaluated at the preclinical stage of nanomedicine development [197, 203], potentially leading to hypersensitivity reactions occurring in patients during clinical trials resulting in implications for time, money and potentially lives [204].
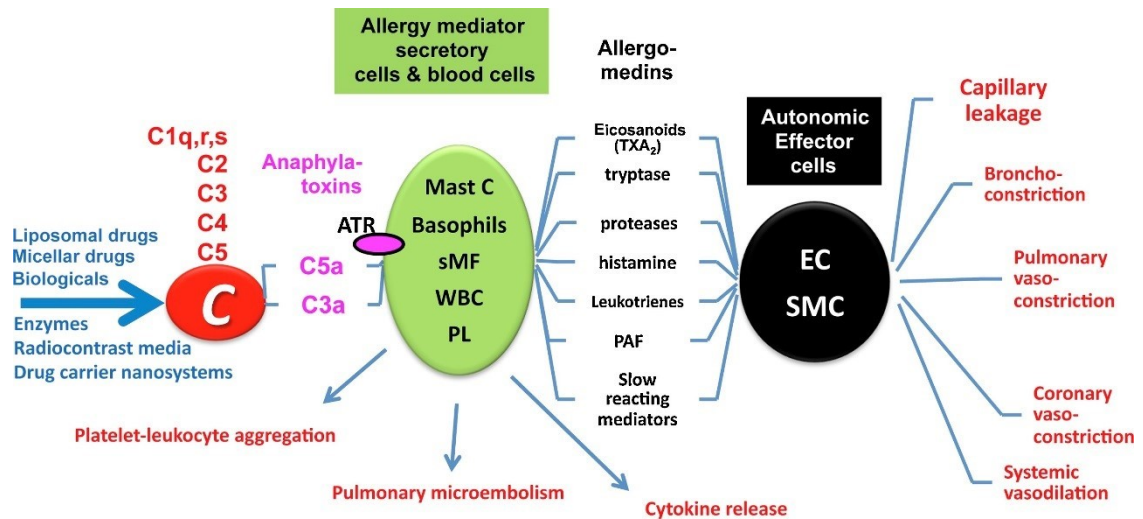
Figure 1.9. Graphical illustration of the "CARPA cascade" and its associative effects.

Many different nanomaterials have been shown to activate complement and induce CARPA effects in the clinic. These effects can vary hugely from pulmonary microembolisms and cytokine storm, to systemic vasodilation and capillary leakage. Abbreviations: C, complement; ATR, anaphylatoxin receptor; Mast C, mast cells; sMF, secretory macrophages; WBC, white blood cells; PL, platelets; EC, endothelial cells and SMC, smooth muscle cells. Reproduced with permission from Szebeni J. (2014) [197]. Copyright 2019, Elsevier.

1.4.2. Evidence for IONP activating the complement system

There is an abundance of literature published on the effects of IONP on the complement system [205-207]. Negatively-charged, 10 nm maghemite nanoparticles coated in an amphiphilic polymer were shown to increase C3a, C5a and C5b-9 in human whole blood (at 10 µg/ml) which also resulted in a pro-inflammatory response (significant upregulation of IL-6, IL-1β, TNF-α). This inflammatory response could be neutralised using inhibitors for C3 and C5 [205]. Likewise, Escamilla-Rivera V. *et al* (2019) came to a similar conclusion with negatively-charged polyethylene glycol (PEG)-coated magnetite nanoparticles of a similar size in human plasma (1 mg/ml) and BALB/c mice (5 mg/kg) following intravenous injection. This same study also found that bare magnetite nanoparticles and polyvinylpyrrolidone-coated magnetite nanoparticles (also negatively charged and of similar size) did not induce this response in either system. The complement activation observed with the PEG-IONP was proposed to be a result of selective complement-activating proteins deposited on the surface of these nanoparticles [207]. Taking this a step further, Banda N. K. *et al* (2014) investigated which pathway was activated between human and mouse serum with dextran-coated iron oxide nanoworms (IONW). The nanoworms (hydrodynamic diameter of 169 ± 77.43 nm and zeta potential of -6.05 ± 8.29 mV) could activate the lectin pathway and alternative pathway (indirectly) in mouse serum (100 µg/ml), whereas the alternative pathway was found to be activated directly in addition to the lectin pathway in human serum (200 µg/ml) [206]. Two years later, this same group investigated whether this complement activation with IONW was related to the iron/ dextran ratio of the nanoparticles, and whether modification of its surface chemistry could dampen this response. It was found that complement activation occurred primarily via the alternative route regardless of the dextran ratio, and modifications to the dextran surface (neutralising hydroxyl groups or anionic charge) could not hamper this activation [208]. A further publication with these IONW showed that this complement activation resulted in the uptake of these nanoworms by monocytes, lymphocytes and neutrophils of healthy and tumour-bearing mice and humans. Interestingly, when C3 is depleted in mice, and the alternative complement pathway is inhibited in humans, leukocyte uptake is dramatically reduced. Moreover, this study could also significantly dampen this leukocyte uptake in mice and humans through hydrogelation (via epichlorohydrin) of the dextran surface coating [209]. Finally, a recent publication in Nature could pinpoint the role of the protein corona (the protein covering

that develops on nanoparticles when they reach the blood) and subsequent immunoglobulin deposition on nanoparticles (including the IONW and the clinically-approved Feraheme®) to be significant steps in the activation of complement [210]. Pairing the evidence in the literature with the reports for hypersensitive effects in the clinic suggests that the complement system is a significant hurdle to overcome when advancing an IONP to the clinic [204, 211]. It is therefore essential that these effects are evaluated early into preclinical assessment of these nanoparticles.

1.5. Trinity College's experience with magnetic hyperthermia research and nanomedicine translation

As described previously, magnetic hyperthermia is certainly not a straight-forward treatment approach for cancer and requires expertise from many specialist areas to ensure efficient translation. Over the last decade, the Nanomedicine and Molecular Imaging Group at Trinity College Dublin – led by Professors Yuri Volkov and Adriele Prina-Mello- has been involved in large, multinational collaborations aiming to translate nanomedicines to the clinic for cancer. These collaborations brought together experts from many different areas which proved hugely beneficial for advancing knowledge in the areas of nanomedicine translation and magnetic hyperthermia. A description of some of these projects is provided next.

1.5.1.   MultiFun Project

MultiFun- or MultiFunctional nanotechnology for selective detection and treatment of cancer- was the first major project involving magnetic hyperthermia research to be awarded, in part, to Trinity College's Nanomedicine and Molecular Imaging Group. This project was funded by the European Commission's 7th Framework Programme and lasted from 2011 to 2015, with a budget of more than €13 million. The overall aim of this project was to develop and validate multifunctional magnetic nanoparticles to diagnose and target pancreatic and breast cancer. This project brought 13 universities and 3 industrial partners from a variety of disciplines all across Europe together to achieve this goal (Figure 1.10.).

Figure 1.10. The MultiFun consortium.

7 countries were brought together for this collaboration. This included Trinity College, Dublin; University College, Cork; University of Manchester; Queen Mary University of London; Kings College, London; University Hospital, Jena; University of Paris; National Institute of Applied Sciences, Toulouse; Institute of Physics of the Czech Academy of Sciences; Pepric, Leuven; PharmaMar, Madrid; IMDEA, Madrid (Project Coordinator). Image adapted from https://cordis.europa.eu/project/rcn/99273/factsheet/en.

MultiFun proved hugely successful with over 50 peer-reviewed papers published, which eventually led to the selection of two lead candidate multifunctional nanoparticles capable of treating pancreatic cancer and breast cancer tumours with magnetic hyperthermia, and also capable of acting as magnetic resonance imaging contrast agents [86, 212, 213]. These lead nanoparticle designs were subsequently patented (Patent number: WO2016150521A1).

1.5.2. NoCanTher Project

Following the success of MultiFun, a follow-up project was also funded by the European Commission's Horizon 2020 Programme: NoCanTher (Nanomedicine upscaling for early clinical phases of multimodal Cancer Therapy). This project also brought together a large collaboration of 6 universities and 5 industrial partners (Figure 1.11.)- many retained from the MultiFun project- with an overall budget of more than €10 million spanning 5 years (2016-2021).
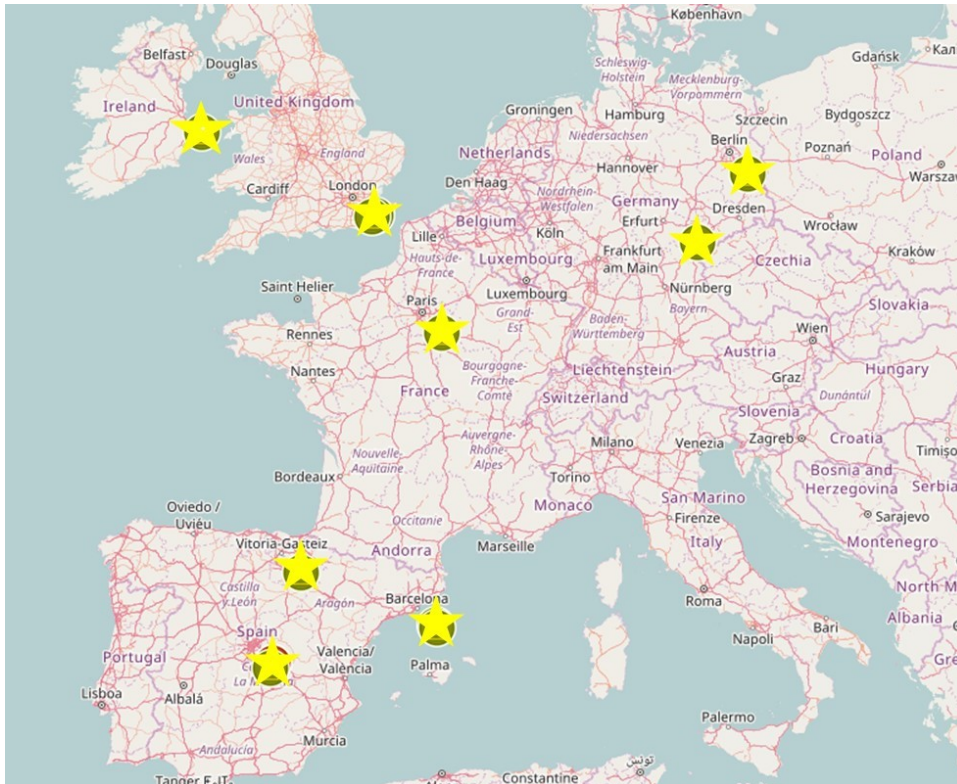
Figure 1.11. The NoCanTher Consortium.

6 countries are participating in this project, many of which were involved in MultiFun. These partners include Trinity College, Dublin; University Hospital, Jena; University of Paris; Institute of Research, Vall d'Hebron; Institute of Oncology, Vall d'Hebron; ImmuPharma, London; Resonant Circuits, London; Chemicell, Berlin; BioKeralty, Minano; IMDEA, Madrid (Project coordinator). Image adapted from https://cordis.europa.eu/project/rcn/200812/factsheet/en.

The overall aim of this project is narrowed with respect to MultiFun. NoCanTher aims to scale-up the patented nanoparticle design from MultiFun and generate enough safety and efficacy data to initiate a clinical trial for patients with pancreatic ductal adenocarcinoma. Work with this project is ongoing, but some key publications so far include [127, 214-218].

1.5.3. European Union Nanoparticle Characterization Laboratory (EUNCL)

In addition to experience in magnetic hyperthermia to treat cancer, the Nanomedicine and Molecular Imaging group at Trinity College Dublin is also a core member of the EUNCL. The EUNCL was set up in 2015 (through funding from Horizon 2020) following the establishment of the USNCL in 2004, with the aim of providing pre-clinical characterization and assessment to promising nanomedicines. Because the characterization of nanomaterials can be very complex, large scale cooperation is required to adhere to regulatory requirements for approval. The EUNCL has brought together many research institutions within the EU with the aim of 'combining diverse core competences in one unique service center', providing data for promising nanomedicines to seek clinical approval, free of charge [219] (Figure 1.12.). The Nanomedicine and Molecular Imaging Groups role as part of the EUNCL is to provide characterization, endotoxin and sterility testing and *in vivo* safety assessments of selected nanoparticles.

EUNCL Core Expert Team
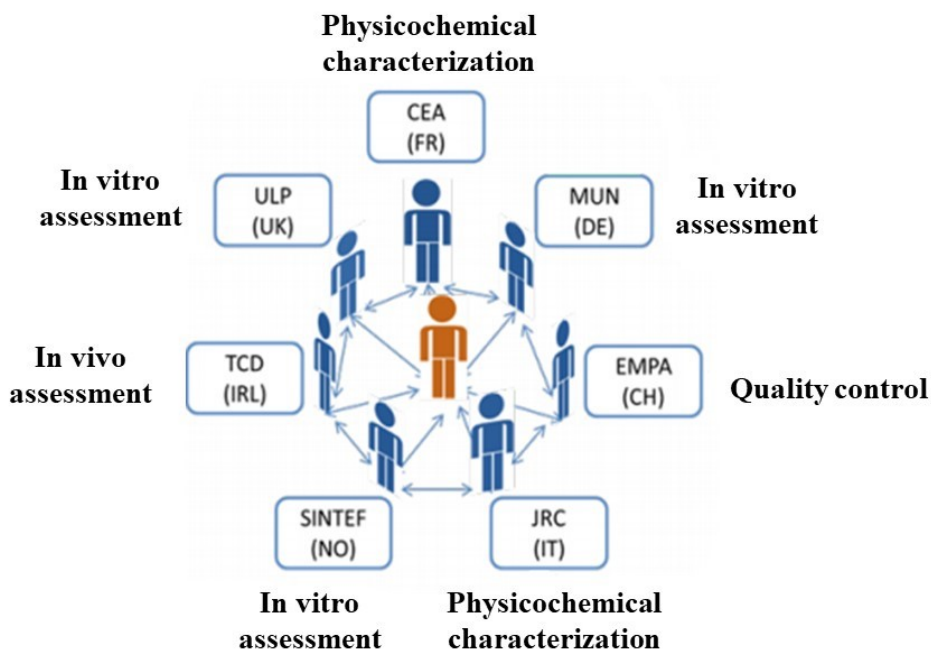
Figure 1.12. The members that make up the core expert team of the EUNCL.

7 countries make up the EUNCL core expert team, contributing different skills required to fully assess nanomedicines towards clinical evaluation. Abbreviations: CEA, French Alternative Energies and Atomic energy Commission; FR, France; ULP, University of Liverpool; UK, United Kingdom; TCD, Trinity College Dublin; IRL, Ireland; SINTEF, Stiftelsen Sintef; NO, Norway; JRC, Joint Research Centre; IT, Italy; EMPA, Eidgenössische Material- und Prüfungs-Anstalt; CH, Switzerland; MUN, Bioanalytik-Muenster; DE, Germany. Image adapted from http://www.euncl.eu/.

1.5.4. The importance of collaboration to nanoparticle translation

The most important lesson learned from these experiences so far is the fact that large-scale collaboration is essential for translational research with nanomaterials [220] (Figure 1.13.). The fact that the European Commission granted more than €5 million for the formation of the EUNCL is telling. Projects like MultiFun and NoCanTher with specific and novel objectives show that a large array of expertise is required for specialised nanoparticle research. Specialists in nanoparticle synthesis and functionalization, characterization, magnetic field testing, stability, sterility and endotoxin contamination, *in vitro* cytotoxicity, biocompatibility assessment and *in vivo* safety and efficacy testing were needed for these projects. Therefore, these consortiums included pharmaceutical and bioscience companies, engineering companies, hospitals, physicist, biologists, chemists and oncologists which were required to ensure smooth transition between disciplines when needed.

Translational Considerations for Nanomaterials
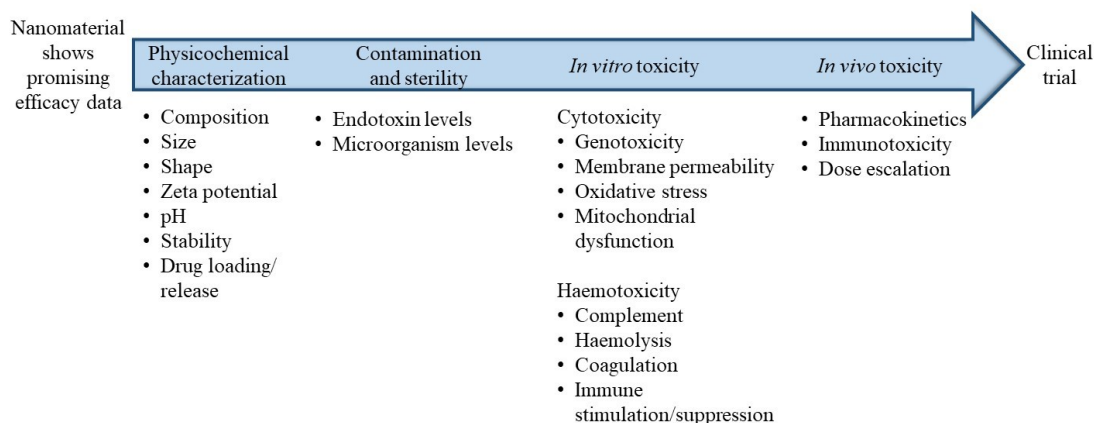
Figure 1.13. The scale of testing required for the translation of nanomaterials.

A vast amount of expertise is required to translate a nanomaterial towards a clinical trial. If a nanoparticle shows desirable efficacy, extensive physicochemical characterization, contamination assessment and *in vitro* and *in vivo* toxicity evaluations are required before a dossier can be submitted for clinical evaluation. This will likely require the work of a large network of institutions to be fulfilled.

1.6. Project hypothesis and aims

The overall goal of this Ph. D. project is to contribute data to a clinical trial dossier for a new superparamagnetic IONP to treat PDAC through magnetic hyperthermia. This is described in the project hypothesis and four separate aims, which are detailed below.

1.6.1.   Project hypothesis
Iron oxide nanoparticles are promising candidates for treating cancer.

1.6.2.   Project aims

1. Evaluate magnetic hyperthermia efficacy *in vitro*

Sub-aims:
*   Analyse the physicochemical characteristics of the IONP
*   Assess their heating capabilities under an AMF
*   Measure cytotoxicity of the IONP alone in PDAC cells
*   Measure cytotoxicity following magnetic hyperthermia treatment in PDAC cells

2. Determine levels of endotoxin contamination in the IONP

Sub-aims:
*   Identify suitable assay to test IONP for endotoxin contamination
*   Test for nanoparticle interference with the assay
*   Test nanoparticle for endotoxin contamination

3. Assess complement activation with the IONP

Sub-aims:
*   Determine suitable test in which the nanoparticles do not interfere
*   Use this test to assess for complement activation at clinically relevant doses

4. Assess *in vivo* toxicity of the IONP

Sub-aims:
*   Determine suitable doses of IONP to test *in vivo*
*   Carry out an acute toxicity study of IONP to identify the limiting effects of the nanoparticles *in vivo*

2. Chapter 2: Evaluating magnetic hyperthermia efficacy *in vitro*

2.1. Background to chapter

Superparamagnetic IONP supplied by Chemicell GmbH (Berlin, Germany) were analysed for their physicochemical characteristics by various techniques and assessed for their heating potential in response to AMF. Following this, the cytotoxic effects and cellular internalisation of the nanoparticles was determined with BxPC-3 (PDAC) cells. Finally, BxPC-3 cells were effectively treated with *in vitro* magnetic hyperthermia using extracellular IONP, but not intracellular IONP. This led to the conclusion that intracellular IONP may play a limited role in the overall efficacy of magnetic hyperthermia. This work has been submitted to a peer-reviewed journal and is currently undergoing review.

2.2. Introduction

As introduced previously in section 1.3.3., magnetic hyperthermia has made significant clinical advances in the last decade which has resulted in its clinical approval and testing in multiple cancers. Despite this, many fundamental questions related to the underlying mechanisms of this therapy remain. One such question is the role that intracellular and extracellular IONP play in this therapy, and whether one or both are necessary for successful magnetic hyperthermia treatment. In this chapter, the efficacy of magnetic hyperthermia is assessed *in vitro* with BxPC-3 cells, and the role that intracellular and extracellular IONP play in this treatment is compared. Extracellular magnetic hyperthermia was shown to effectively kill cells whereas intracellular magnetic hyperthermia showed no therapeutic effect, leading to a discussion on its true relevance to overall treatment efficacy.

2.3. Materials

Unless stated otherwise, all materials related to this chapter were purchased from Sigma Aldrich, Ireland. The superparamagnetic IONP used in this study were fluidMAG/C11-D magnetite nanoparticles coated in a starch matrix. Sterilisation was ensured through autoclaving. This material was produced and generously provided by Chemicell, GmbH (Berlin, Germany) as part of the NoCanTher project (Grant agreement #685795).

2.4. Methods

2.4.1. Characterization

The hydrodynamic diameter of the nanoparticles was assessed using nanoparticle tracking analysis (NS500 Nanosight, Malvern-Panalytical, UK; Software version 3.2) according to protocols published by our group previously [221, 222] and now established as a validated protocol for nanoparticle characterisation under the EUNCL (EU Nanomedicine Characterisation Laboratory) [223]. These results were confirmed with dynamic light scattering (DLS) measurements (Malvern Nano- ZS, Malvern-Panalytical, UK), following the EUNCL protocol for DLS size analysis [224]. Zeta potential data was provided by the nanoparticle supplier (at pH 7), Chemicell. For determining the dry diameter of the nanoparticles, transmission electron microscopy was used. Here, nanoparticles were diluted 1 in 1000 from the stock (100 mg/ml) in double distilled water (ddH$_2$0) and adhered to Lacey carbon grids (AGAR Scientific, UK). Images were taken using the JOEL 2100 (JOEL, Japan) at an acceleration of 200 kV and a beam current of 100-110 µA. The longest diameter of 200 individual nanoparticles is measured using ImageJ software to generate a size distribution (for hydrodynamic size, zeta potential and dry size analysis, see Supplementary Figure 1). Iron concentration was determined by atomic absorption spectroscopy (SpectraAA-200, Varian, US). Here the nanoparticles were dissolved in 1 ml 67-69 % trace-element nitric acid (Fisher, UK) at a concentration of 125 µg/ml and heated to 60 °C for four hours. The nanoparticles were then diluted in trace-elemental water (Fisher, UK) for analysis. A standard curve between 0 – 2.5 mg/L of iron was generated, and the concentration of the nanoparticles was determined from the average of 3 readings.

2.4.2. Heating performance

The thermal efficiency of these nanoparticles in response to an AMF was measured using a Five Celes inductor system (Five Celes, France). This system uses a six- turn, moulded solenoid coil with an internal diameter of 71 mm. In these experiments, 100 µl of the magnetic nanoparticles were dispersed in ddH$_2$0 and exposed to 35 mT, at a frequency of 92 kHz for 60 seconds. Temperature changes were monitored using fiber optic temperature sensors (Optocon, Germany) with an accuracy of ±0.2 °C. From these temperature changes, specific absorbance rate (SAR) and intrinsic loss power (ILP) were calculated at a frequency of 92 kHz, and a field of 35 mT, as reported in [184] and described in section 1.3.3.

2.4.3. *In vitro* cytotoxicity

BxPC-3 cells (ATCC, CRL- 1687; Pancreatic adenocarcinoma of a female human aged 61) were cultured at 37°C and 5% CO_2 in RPMI 1640 media supplemented with 10% FBS and 1% penicillin-streptomycin (Invitrogen) at 10,000 U/ml and 10,000 µg/ml respectively. Cells were seeded at 10,000 cells/ well in a 96 well plate for 24 hours. The cells were then washed with PBS and treated with either nanoparticles (12.5, 25, 50, 100 and 200 µg/ml; 200 µg/ml of nanoparticle corresponded to 147 µg Fe/ml), tacrine at 100 µM (positive control for organelle damage [225]), valinomycin at 120 µM (positive control for membrane damage [226, 227]), or media alone (untreated) for 72 hours. Following treatment, the cells were washed three times with PBS and stained with 50 µl of Lysotracker® red (acidic organelle stain) and YO- PRO®-1 (membrane permeability stain) at 3.5 µl and 0.35 µl per ml of media respectively for 30 minutes at room temperature (stains originate from Thermoscientific, UK and are summarized in Table 1). Lysotracker® red stains acidic organelles, with increases in intensity corresponding to pH, and indicative of nanoparticle localisation into lysosomes. Decreases in intensity, however, is a marker for lysosomal damage [222, 228]. YO- PRO®- 1 is a green dye that measures cell membrane permeability; it's localisation into the nucleus is a measure of cytotoxicity [222]. After staining for 30 minutes, the dyes are removed, and the cells fixed with 100 µl of 3.7% formaldehyde for 20 minutes at room temperature. Following fixation, 0.5 µl of Hoechst 33342/ ml in wash buffer is added to each well at 100 µl for 10 minutes. After two subsequent washes, the cells could be imaged. Images were taken using the Cytell Imaging System (GE Healthcare, UK), with 7 fixed fields acquired from each well. These images were recoded and analysed through the InCell Investigator software (GE Healthcare, UK) and intensity and morphology values for cell count, nuclear intensity, and organelle intensity were obtained and compared against untreated cells as measures of cytotoxicity.

Table 1: A description of each stain used for high content screening analysis.

Summary of excitation and emission wavelengths along with the stock concentrations for each dye used in the multiparametric analysis.

Stain	Excitation/Emission (nm)	Stock Concentration
Lysotracker® red	577/590	1 mM
YO-PRO®-1	491/509	1 mM
Hoechst 33342	350/461	16.2 mM

2.4.4. Cell uptake and Prussian blue staining

To measure the levels of nanoparticle internalised into the cells, 1×10^5 cells/ well were seeded for 24 hours in a 12 well plate. The cells were then treated with 200 μg/ml of nanoparticles for 24 hours before being washed with PBS, detached with trypLE, and washed a further two times with PBS (centrifugation at 1000 rpm -at 94 RCF- for 5 minutes could effectively separate the cells from most of the nanoparticles in media). Finally, the cells were counted using trypan blue staining and eventually dissolved in 67-69%, trace-element nitric acid (Fisher, UK) overnight at room temperature for subsequent inductively coupled plasma - optical emission spectrometry (ICP-OES) analysis (Liberty 150, Varian, US). For this measurement, each treatment group is pooled within each experiment (five experiments in triplicate) and the volume is made up to 5 ml in pure, trace-element water (Fisher, UK). ICP-OES was performed on these pooled samples as well as six iron standards in duplicate (from 0 – 2.5 mg/L). To complement this data, Prussian blue staining (iron- specific stain) was performed on three experiments in triplicate to provide representative images of this iron uptake and identify where the nanoparticles were localised. The experiment was performed as before except, following 24 hours treatment, the cells were washed three times with PBS, fixed with 4% formaldehyde for 20 minutes at room temperature, washed again as before, stained 1:1 with 4% HCl and 4% potassium ferrocyanide, and finally washed three times with PBS again. Bright field images were taken using Lionheart FX microscope (BIOTEK, Germany) at 10x magnification.

2.4.5. *In vitro* magnetic hyperthermia

For this experiment, intracellular hyperthermia was compared against extracellular hyperthermia and a combination of intracellular and extracellular hyperthermia. Intracellular hyperthermia involves the exposure of intracellular IONP to AMF (IONP allowed to internalise 24 hours) while extracellular hyperthermia only exposes extracellular IONP (IONP added to the media directly before) to AMF. Intracellular and extracellular hyperthermia contains both. A summary of this experiment is illustrated in Figure 2.1. below. BxPC-3 cells were seeded at 1×10^5 cells/ well in a 12 well plate. After 24 hours, cells to be treated with intracellular nanoparticles alone, intracellular hyperthermia, intracellular and extracellular nanoparticles alone, or intracellular and extracellular hyperthermia were treated with 200 μg/ml of nanoparticles (corresponding to 147 μg Fe/ml). At 48 hours, cells are treated with magnetic hyperthermia. Here, the

cells are washed with PBS and detached with trypLE into 1.5 ml Eppendorf tubes. They are then washed again in PBS and redispersed in 100 µl of either media (for intracellular hyperthermia or magnetic field alone), or 500 µg of nanoparticle (368 µg Fe) in 100 µl media (for extracellular nanoparticles alone, extracellular hyperthermia, intracellular and extracellular nanoparticles alone, or intracellular and extracellular hyperthermia). For the cells exposed to 500 µg of nanoparticle alone, they are kept at 37 °C for 30 minutes. For the cells exposed to the magnetic field, the Eppendorf's are wrapped in parafilm and a sterile fibre optic temperature probe (washed in 70% ethanol) is pierced through the film into the cells and media. A water bath keeps the cells at 37 ± 1.0 °C before the AMF is applied. The cells are then exposed to a field of 35 mT at a frequency of 92 kHz. Once the temperature in the media of the cells treated with extracellular nanoparticles reaches 40 °C (within 60- 120 seconds), the timer is started and the cells are exposed to temperatures of 40-42.5 °C, or 'mild hyperthermia' [101, 229] for a total of 30 minutes. Following AMF exposure, the cells are washed three times with their original RPMI media (1000 rpm -at 94 RCF- for 5 minutes could effectively separate cells from most of the nanoparticles in media) and placed back into a 12 well plate. After 24±1 hour, the cells are analysed by flow cytometry to identify populations or apoptotic and necrotic cells. As reported in Blanco-Andujar *et al* [230] and Ludwig *et al* [85] the effects of magnetic hyperthermia on viability are the most reflective in the first 24 hours, with changes in viability between 24 and 48 hours proving to be negligible.
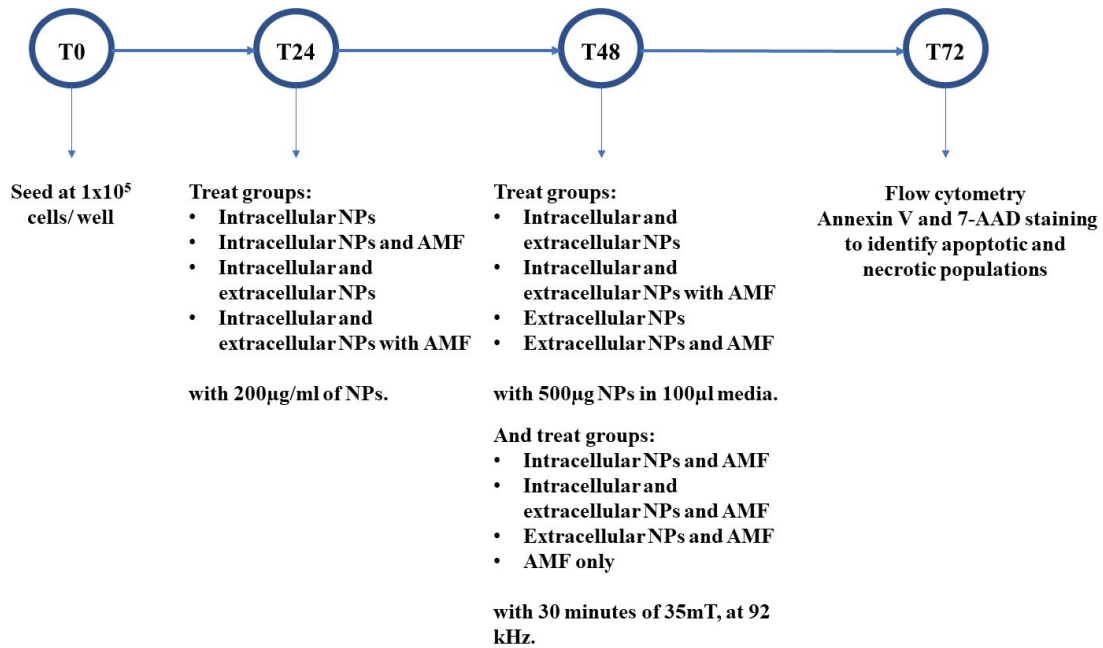
Figure 2.1. Summary of *in vitro* magnetic hyperthermia protocol.

BxPC-3 cells are seeded at time zero (T0). Cells to contain intracellular nanoparticles are treated with 200 µg/ml (147 µg Fe/ml) at 24 hours (T24). At 48 hours (T48), cells exposed to extracellular nanoparticles are treated with 500 µg of nanoparticles (368 µg Fe) in 100 µl media, and cells to be treated with magnetic fields, are exposed to 35 mT at 92 kHz for 30 minutes. Finally, at 72 hours (T72), all treatment groups are stained with annexin V and 7- AAD and analysed by flow cytometry for detection of apoptotic and necrotic cells. Abbreviations: NPs, nanoparticles; AMF, alternating magnetic field.

2.4.6. Apoptosis/ Necrosis detection

To detect levels of apoptosis and necrosis in the BxPC-3 cells after treatment, APC-Annexin V and 7-AAD stains (BioLegend, UK) were used as the nanoparticles were shown not to interfere in these channels (Supplementary Figure 2). 24 hours after the exposure to the AMF, the media and detached cells (trypLE) were pooled and washed twice with staining buffer and stained with 50 µl of APC- Annexin V (2.5 µl/ ml of Annexin binding buffer) for 30 minutes. After such staining, the cells were washed three times with Annexin binding buffer and redispersed in 2.5 µl/ ml of 7-AAD in staining buffer. The cells were then analysed with the FACSCanto II flow cytometer from BD Biosciences (10,000 recorded events per treatment) and the data was subsequently analysed via FlowJo 10 and Prism7 software (gating strategy: Supplementary Figure 3). Positive stain controls for APC- Annexin V were cisplatin treated cells at 50 µM for 24 hours and for 7-AAD was 10% DMSO treated cells for 1 hour.

2.4.7. Caspase 3 activity

Following apoptosis/ necrosis detection by flow cytometry, caspase 3 activity was measured colorimetrically at 405 nm according to manufacturer's protocol (Abcam ab39401, UK) to distinguish whether the main mechanism of cell death was apoptosis or necrosis. For this analysis, *in vitro* magnetic hyperthermia was repeated as before in four more experiments. In order to get enough protein for the analysis, each treatment group from two experiments had to be pooled together. For each experiment, BxPC-3 cells were also treated with 50 µM of cisplatin for 24 hours as a positive control. 1 µg/ µl of protein from each treatment group was tested in the assay and results were corrected for total protein concentration (BCA kit, Thermoscientific). Caspase activity was presented as levels of absorbance at 405 nm in each treatment group against the untreated.

2.4.8. Statistical analysis

All statistical analysis was done using GraphPad Prism7 software. Results are reported as mean± standard deviation. High content screening data was analysed via one-way ANOVA followed by Dunnett's test. Apoptosis/Necrosis data was analysed by two-way ANOVA followed by Tukey's test for multiple comparisons. Caspase activation was measured with one-way ANOVA followed by Dunnett's test. Significance was represented by $*p < 0.05$; $**p < 0.01$; $***p < 0.001$; $****p < 0.0001$.

2.5. Results

2.5.1. Nanoparticle characterization and heating performance

NTA reported a mean size of 100 nm, which closely resembled the DLS measurements of 91.2 nm. DLS measured an average zeta potential of -21 mV at pH 7, while TEM images were analysed on ImageJ to determine a mean diameter of 11 nm (based on 200 individual measurements of the largest diameter of each nanoparticle; see Supplementary Figure 1). Upon exposure to 35 mT at 92 kHz for 60 seconds, the nanoparticles displayed a SAR of 98 W/g $_{Fe}$ in water, corresponding to an ILP of 1.4 nHm^{2}kg^{-1} (Table 2 and Figure 2.2).

Table 2. Summary of fluidMAG/C11-D characterization.

Summary of characterization data by NTA, DLS, AAS, TEM and heating capability assessment through SAR and ILP values. Zeta potential was provided by the supplier: Chemicell, GmbH. Values represented as mean ± standard deviation.

Measured Parameter	Value
Mean hydrodynamic size	100.0 ± 2.6 nm (NTA) 91.2 nm (DLS)
Polydispersity index	0.145 (DLS)
Zeta potential	-21.0 ± 5.86 mV (DLS)
Mean dry size	11 ± 3 nm (TEM)
Specific absorbance rate	98 W/g_{Fe}
Intrinsic loss power	1.4 nHm^2kg^{-1}
Fe content	0.736 mg Fe/ mg NP (AAS)
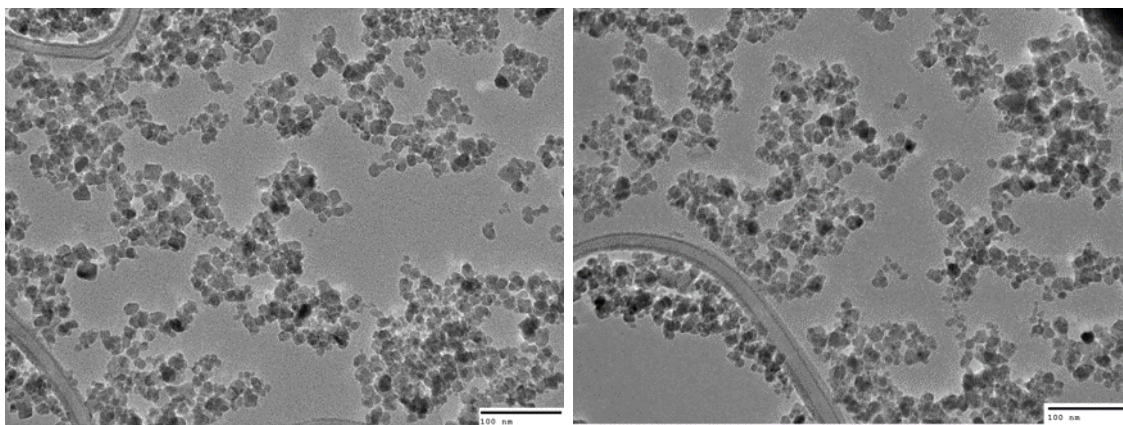
Figure 2.2. Representative TEM images of fluidMAG/C11-D nanoparticles.

Scale bar = 100 nm. Captured with the JOEL 2100 (JOEL, Japan) at an acceleration of 200 kV and a beam current of 100-110 µA.

2.5.2.   *In vitro* cytotoxicity

High content screening analysis showed no significant changes to cell count, nuclear membrane permeability, or lysosomal permeability after 72 hours treatment of up to 200 µg/ml of nanoparticles against the untreated negative control, while positive controls (valinomycin and tacrine) quantitatively and visibly reduced cell count and lysosomal mass, while increasing nuclear permeability (Figure 2.3.).

A.

Cell count

B.

Nuclear Membrane Permability

C.

Lysosomal permeability
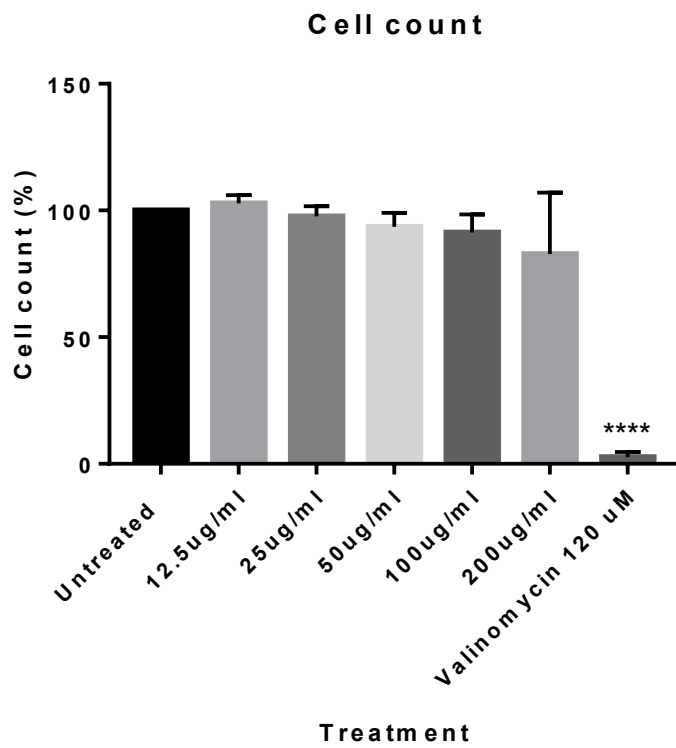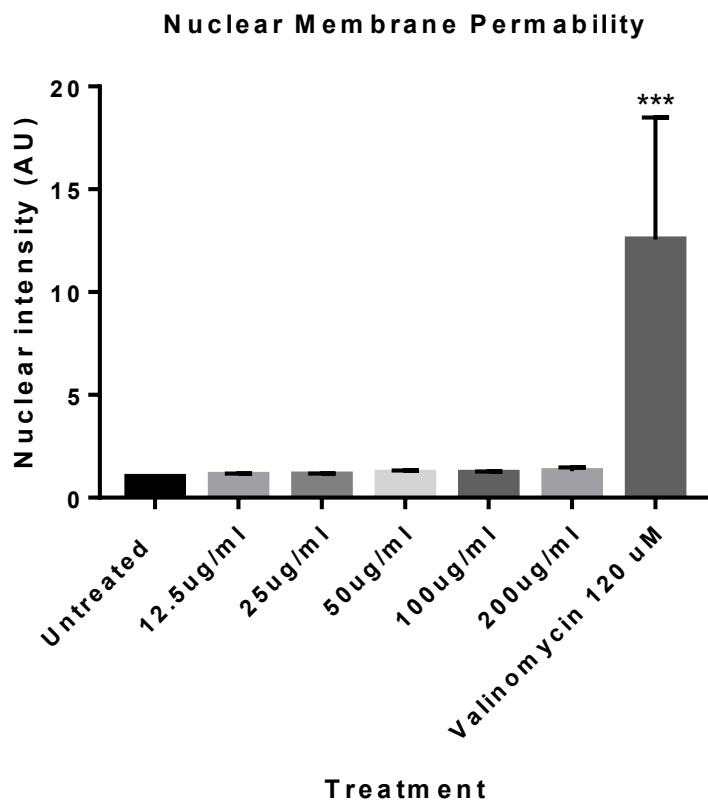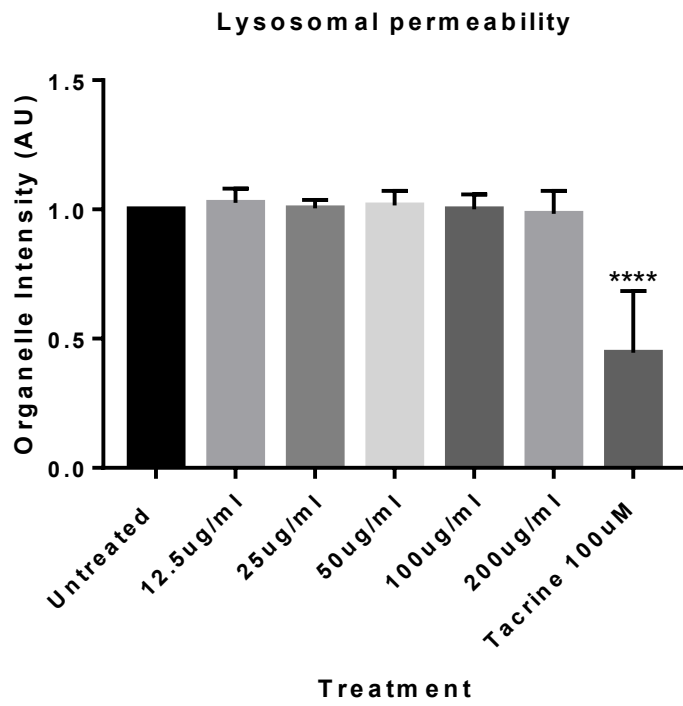
D.
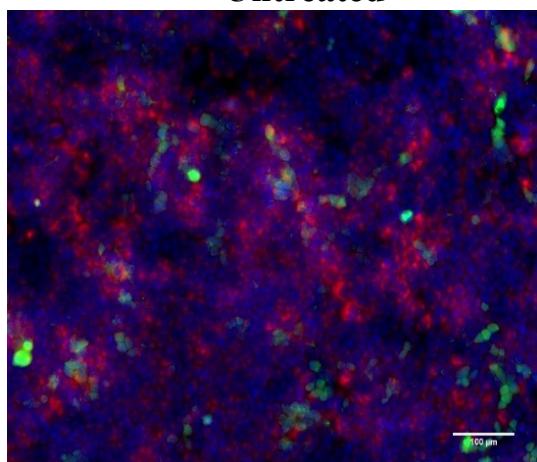
Untreated

E.

200 µg/ml
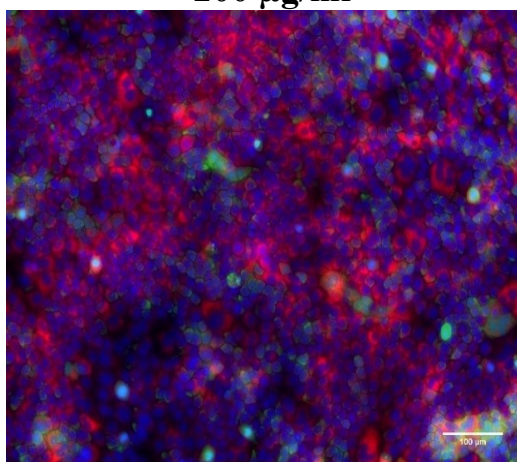
F.

Tacrine 100 µM
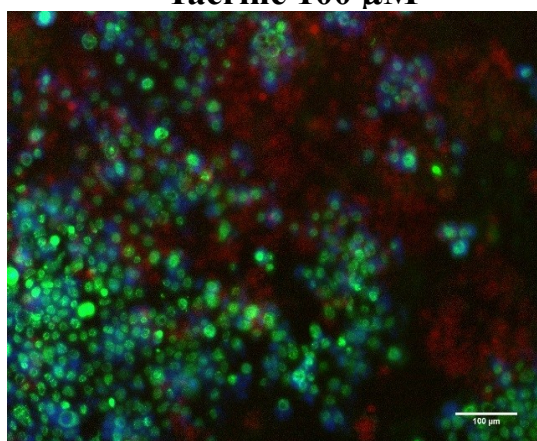
G.

Valinomycin 120 µM
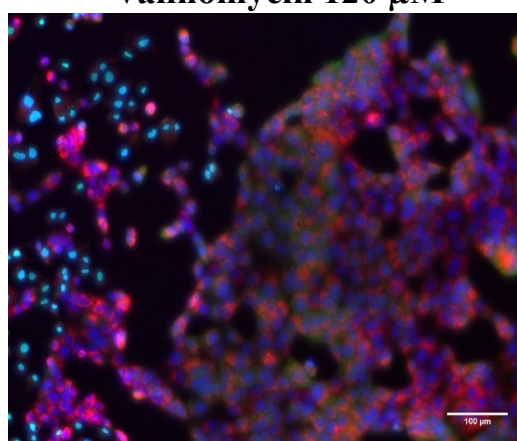
Figure 2.3. High content screening analysis of BxPC-3 cells treated with fluidMAG nanoparticles.

Graphs representing cell count (A), nuclear membrane permeability (B) and lysosomal permeability (C) of BxPC-3 cells after treatment with nanoparticles, tacrine and valinomycin. Results are normalised against the untreated and represent 3 experiments in triplicate. Significance was against the untreated and tested via one-way ANOVA followed by Dunnett's test. Error bars = standard deviation. ***$P<0.001$. ****$P<0.0001$. Moreover, representative merged images of untreated BxPC-3 cells (D), cells treated with 200 µg/ml of nanoparticles (E), cells treated with tacrine (F) and cells treated with valinomycin (G) are provided. Scale bar: 100 µm.

2.5.3. Cell uptake and Prussian blue staining

Cellular uptake of the nanoparticles was assessed through qualitative and quantitative measures. ICP- OES identified an average uptake of 12.8 ± 3.6 pg Fe/cell (12.8 pg Fe corresponds to 16,487 nanoparticles, measured by NTA) after 24 hours. Prussian blue staining confirmed this internalisation and an accumulation of the nanoparticles around the nuclear membrane was consistently observed (Figure 2.4.).

Untreated
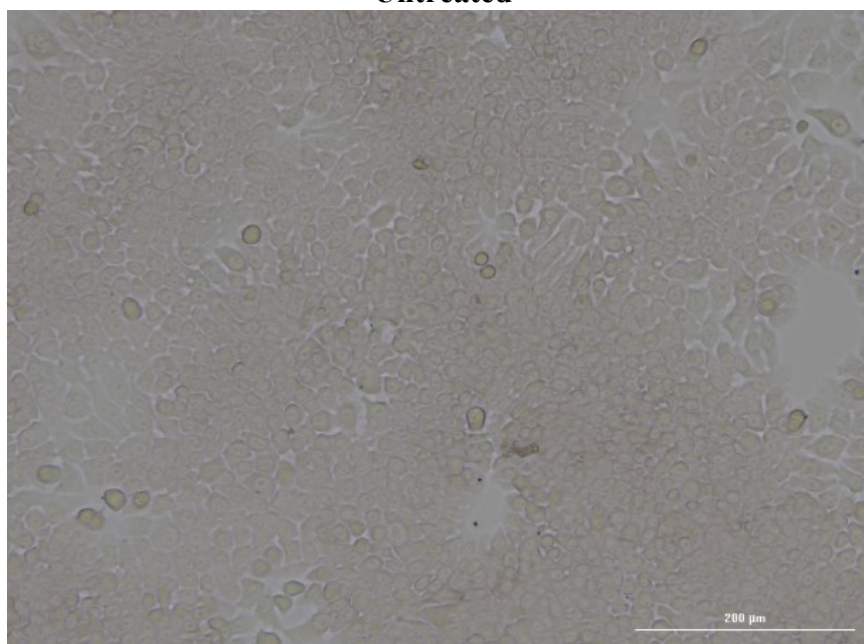
200μg/ml
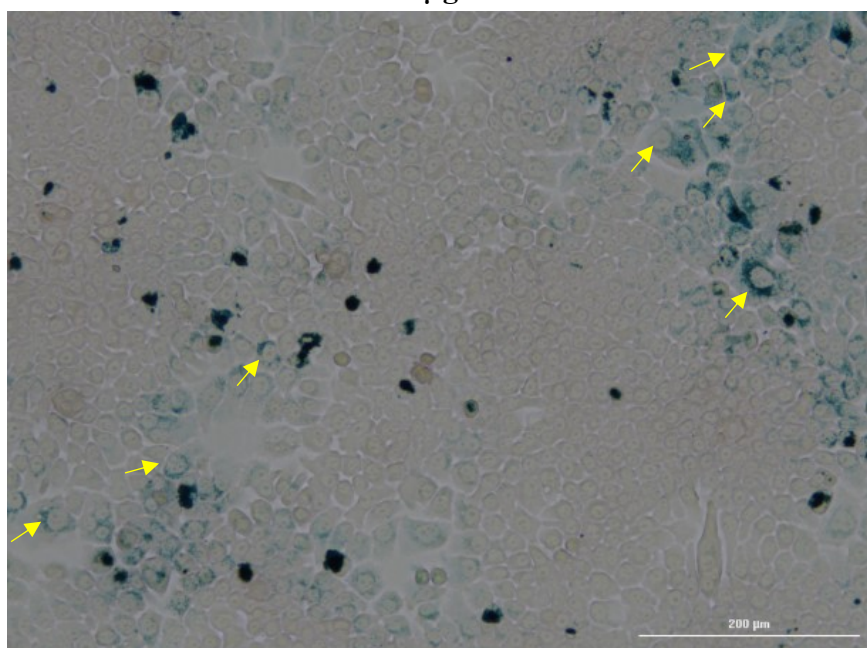
Figure 2.4. Prussian blue staining of untreated and treated BxPC-3 cells.

Blue staining for iron indicates the nanoparticles become internalised, complementing the results from ICP-OES. Moreover, the nanoparticles show a tendency to accumulate around the nucleus of the BxPC-3 cells, as highlighted by the yellow arrows. Results show representative images of three experiments in triplicate. Scale bar: 200 μm.

2.5.4. *In vitro* magnetic hyperthermia

Temperature graphs below show successful, controlled heating of the nanoparticles when used for extracellular hyperthermia (500 µg IONP – 368 µg Fe- in 100 µl media) and intracellular and extracellular hyperthermia with temperatures of 41.2±0.6 °C being achieved across all experiments. No changes in media temperature were seen with intracellular nanoparticles in comparison to cells treated with the magnetic field and media alone. Noteworthy, cells exposed to AMF alone never reached temperatures above 38 °C (Figure 2.5.).

A.

Intra + Extracellular MH

B.

Extracellular MH

C.
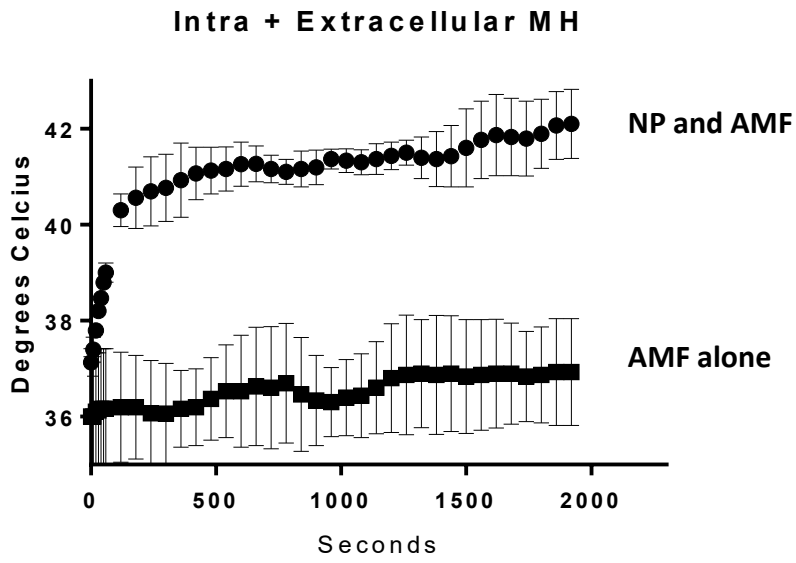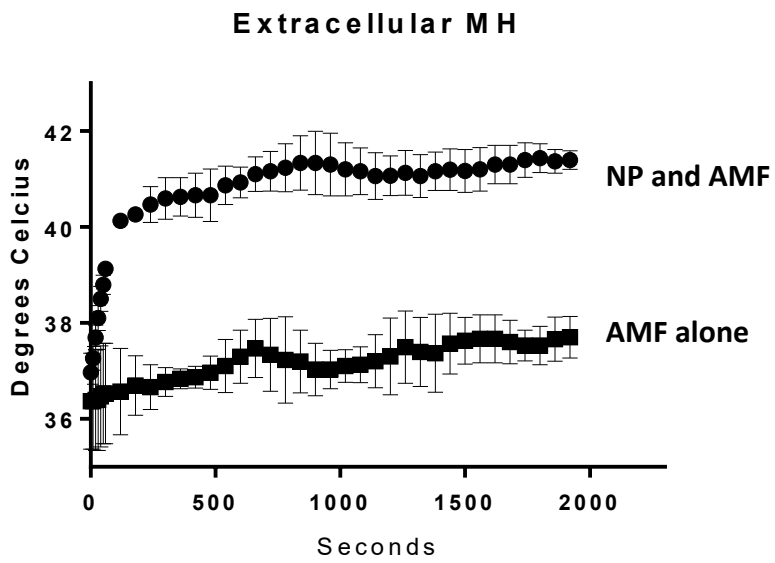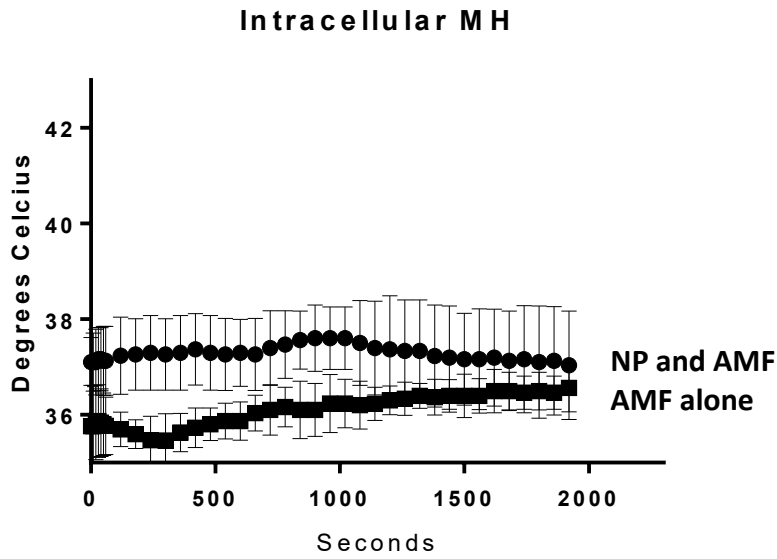
Intracellular MH

Figure 2.5. Temperature graphs of magnetic hyperthermia with BxPC-3 cells.

Intracellular and extracellular nanoparticles (A) and extracellular nanoparticles alone (B) successfully generated temperatures required for mild hyperthermia when stimulated by the AMF. Intracellular exposed to AMF only remained at biologically viable temperatures (C). Graphs show the average temperature at each time-point for 6 experiments. Error bars = standard deviation. Abbreviations: MH, magnetic hyperthermia; AMF, alternating magnetic field; NP, Nanoparticle.

2.5.5.   Apoptosis/ Necrosis detection

Intracellular magnetic hyperthermia displayed no significant effect on the viability of the BxPC-3 cells when compared against the untreated, whereas extracellular magnetic hyperthermia- both alone and in combination with intracellular magnetic hyperthermia – showed significant reductions in cell viability after 30 minutes treatment. Additionally, the presence of the magnetic field alone had no effect on the cells either. This significant reduction in viability with extracellular magnetic hyperthermia is also observed when compared against the nanoparticles alone; therefore, the nanoparticles by themselves are not inducing this effect, but the whole magnetic hyperthermia treatment (Figure 2.6. and Table 3.). Moreover, heating the BxPC-3 cells with an incubator to 42.5 °C for 30 minutes showed no significant effect on viability against untreated cells, confirming that the magnetic hyperthermia treatment as a whole was affecting the cells, and not just the inherent temperature elevation (Supplementary Figure 4).

A.

B.

C. Vital cells

D. Early apoptotic cells
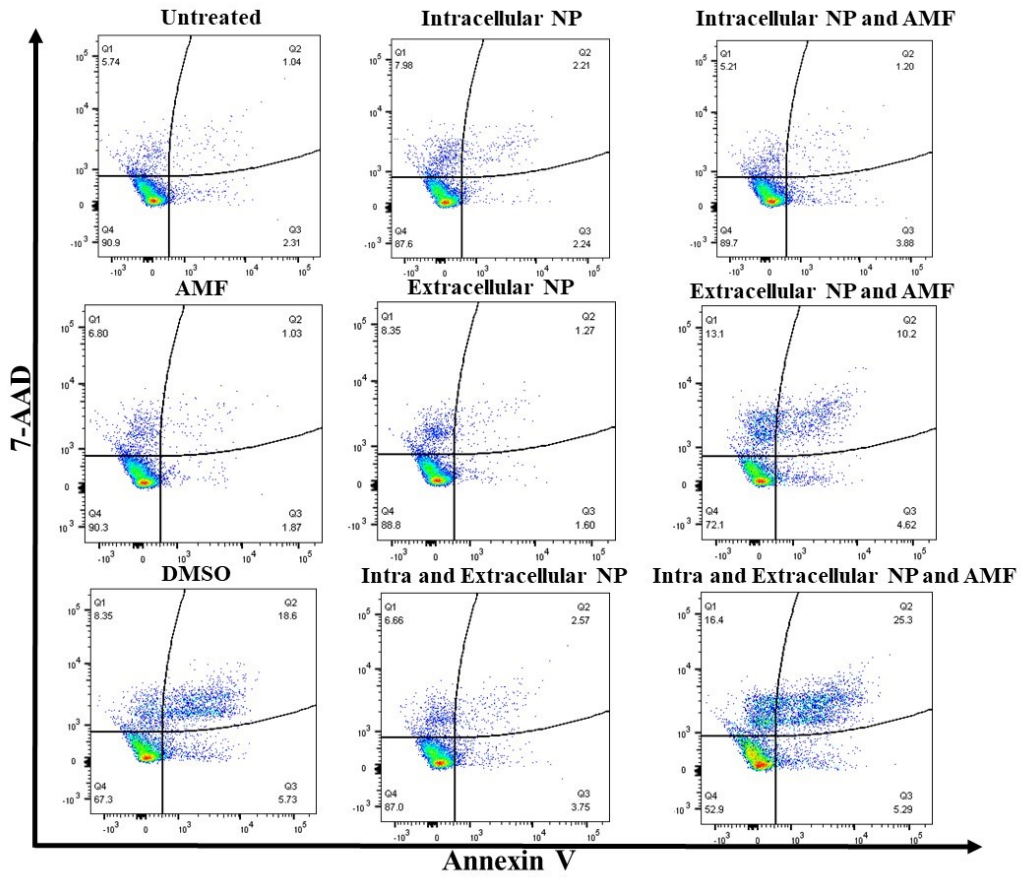
E. Late apoptotic cells
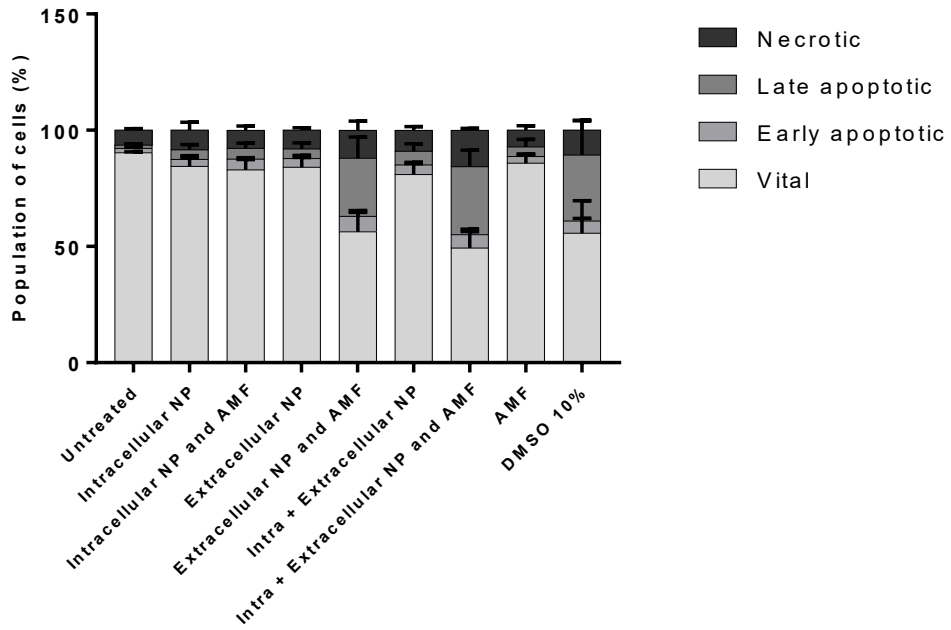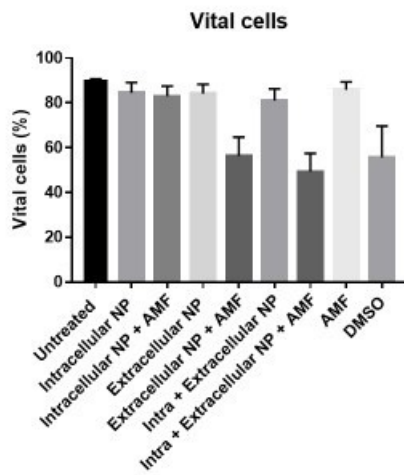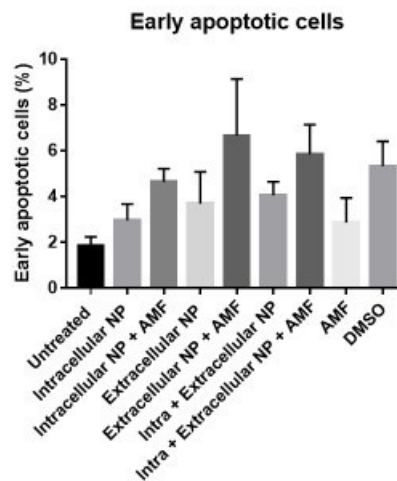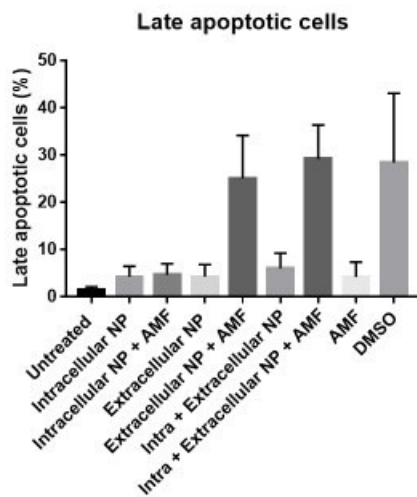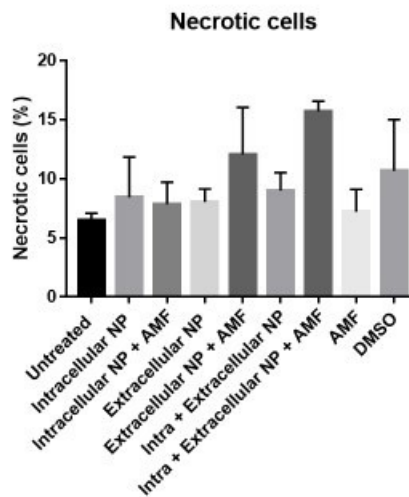
F. Necrotic cells

Figure 2.6. Viability of BxPC-3 cells after *in vitro* magnetic hyperthermia.

A. Representative flow experiment depicting Annexin V$^+$/7- AAD$^-$ (early apoptotic), Annexin V$^+$/7- AAD$^+$ (late apoptotic), 7- AAD$^+$ (necrotic) and Annexin V$^-$/7-AAD$^-$ (vital) cells in each treatment group. B. Graph comparing populations of vital, early apoptotic, late apoptotic, and necrotic cells in each treatment group. C. Annexin V$^-$/7-AAD$^-$ cells for each treatment group. D. Annexin V$^+$/7-AAD$^-$ cells for each treatment group. E. Annexin V$^+$/7-AAD$^+$ cells for each treatment group. F. Annexin V$^-$/7-AAD$^+$ cells for each treatment group. Results are from 6 individual experiments with 10,000 events recorded for each. Error bars = standard deviation. Abbreviations: NP, nanoparticle; Intra, intracellular; Extra, extracellular; AMF, alternating magnetic field.

Table 3. Statistical analysis if *in vitro* magnetic hyperthermia in BxPC-3 cells.

A. Significant differences in vital, early apoptotic, late apoptotic and necrotic cells from each treatment group against untreated cells. B. C. and D. describe the significant differences of these same cellular populations with nanoparticles exposed to AMF versus nanoparticles alone. Results are from 6 individual experiments with 10,000 events recorded for each. Abbreviations: ns, not significant; NP, nanoparticle; Intra, intracellular; Extra, extracellular; AMF, alternating magnetic field. Analysed using two-way ANOVA followed by Tukey's test for multiple comparisons. *P<0.05. **** P<0.0001.

A.

Viability against untreated	Intra NP	Intra NP + AMF	Extra NP	Extra NP + AMF	Intra + Extra NP	Intra + Extra NP + AMF	AMF	DMSO
Vital	ns	ns	ns	****	*	****	ns	****
Early Apoptosis	ns	ns	ns	ns	ns	ns	ns	ns
Late Apoptosis	ns	ns	ns	****	ns	****	ns	****
Necrosis	ns	ns	ns	ns	ns	*	ns	ns

B.

Viability against Extra NP	Extra NP + AMF
Vital	****
Early apoptosis	ns
Late apoptosis	****
Necrosis	ns

C.

Viability against Intra NP	Intra NP + AMF
Vital	ns
Early apoptosis	ns
Late apoptosis	ns
Necrosis	ns

D.

Viability against Intra +extra NP	Intra + extra NP + AMF
Vital	****
Early apoptosis	ns
Late apoptosis	****
Necrosis	ns

2.5.6. Caspase 3 activity

Differences in caspase 3 activity were negligible in all treatment groups except for the positive control (Figure 2.7.). Pairing this with the flow cytometry data suggests that the primary mechanism of cell death in this case was necrosis, as the cells stained positive for both Annexin and 7- AAD, following extracellular magnetic hyperthermia treatment.
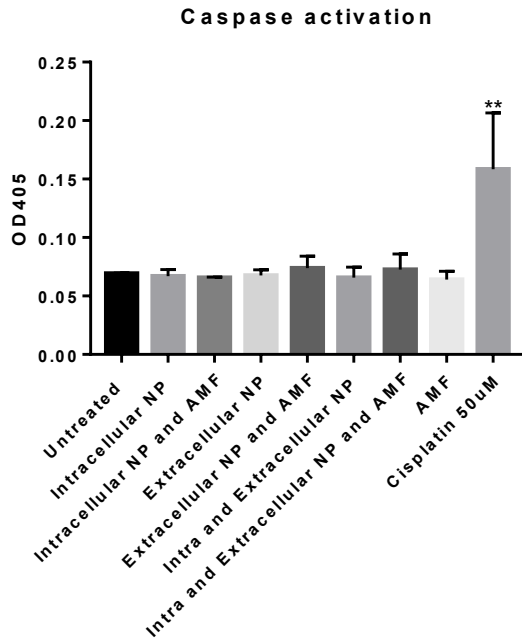
Figure 2.7. Caspase activation in BxPC-3 cells following magnetic hyperthermia.

Results are from four individual experiments, of which two experiments are pooled together to get the desired concentration of protein required for the assay. Values are a result of absorptions at 405 nm. Significance is against the untreated. Significance was assessed using one-way ANOVA followed by Dunnett's test. Abbreviations: NP, nanoparticle; Intra, intracellular; Extra, extracellular; AMF, alternating magnetic field. Error bars = standard deviation. **$P<0.01$.

2.6. Discussion

FluidMAG/C11-D nanoparticles were characterized and assessed for their heating capabilities in response to an AMF of 35 mT at 92 kHz. The nanoparticles were deemed safe at concentrations up to 200 µg/ml *in vitro* using high content screening analysis and so this concentration was used to evaluate their uptake into the cells. ICP- OES demonstrated that an average of 12.8 ± 3.6 pg Fe was internalised into each cell (with 12.8 pg Fe equating to 16,487 nanoparticles) and subsequent Prussian blue staining confirmed this internalisation and identified the nanoparticles propensity to accumulate around the nuclear membrane. This level of iron uptake into cells is similar to the results reported from similar protocols published previously [231-233]. Next, intracellular hyperthermia, extracellular hyperthermia, and intracellular and extracellular hyperthermia were compared in order to define differences in viability through Annexin V/ 7- AAD staining. Intracellular hyperthermia showed no change in viability against the untreated, whereas cells exposed to extracellular nanoparticles and magnetic fields underwent significant apoptosis/necrosis (staining positively for both Annexin V and 7-AAD) against untreated cells and nanoparticle- treated cells alone. This result was similar to that reported in Ludwig *et al* for BxPC-3 cells [85].

Cells that stain positively for 7-AAD have a permeabilised cellular membrane characteristic of cells undergone late apoptosis or necrosis, which allows 7-AAD to become internalised and intercalate to guanine and cytosine regions of DNA [234]. By contrast, Annexin V relies on the extracellular exposure of phosphatidyl serine (PS) from the plasma membrane -which normally faces internally in healthy cells- where it binds to PS in a calcium-dependant manner, acting as a positive early stain for apoptosis [235]. These two mechanisms of cell death can overlap if the cells undergoing apoptosis don't get phagocytosed, and so enter a stage of secondary necrosis which shares many features of primary necrosis [236, 237]. In order to distinguish the primary mechanism of cell death following hyperthermia, caspase 3 activity was evaluated using a colorimetric assay. Caspase-3 activity is essential for efficient apoptosis and so its expression levels against the untreated will indicate if apoptosis is occurring or not [238]. No changes in caspase activity was identified following magnetic hyperthermia and so necrosis was deemed the primary mechanism of cell death in this case. This strong population of necrotic cells was also observed in the above- mentioned Ludwig *et al* [85].

Although no differences in cell viability were established after intracellular hyperthermia, it is yet to be fully elucidated whether intracellular nanoparticles can

contribute to magnetic hyperthermia in alternative ways such as activating the immune system, or inhibiting DNA repair mechanisms, that magnetic hyperthermia is known to induce and so it may contribute to treatment efficacy indirectly. Elaborating on this point further, papers have shown that intracellular magnetic hyperthermia alone requires much longer times to induce significant effects on the viability of cells (up to 2 hours, at 200-400 pg of Fe per cell [230]) , and so the effects that are observed in *in vivo* and clinical studies may be primarily due to extracellular magnetic hyperthermia. Additionally, efforts to improve the internalisation of IONP with targeting peptides before magnetic hyperthermia *in vivo* has shown mixed results and not all cases have proven entirely beneficial to the efficacy of the treatment. For example, treating breast cancer xenographs with bare nanoparticles versus nanoparticles conjugated with the tumour-internalising peptide nucant and/ or doxorubicin showed that there were negligible differences between the two formulations following hyperthermia treatment [86]. On the other hand, BxPC-3 models were shown to be highly sensitive to nanoparticles conjugated with nucant and/ or gemcitabine when compared to bare nanoparticles alone [212]. This response could be cancer dependant, and some cancers are more sensitive to 'free' nucant than others which may enhance the hyperthermic response [239]. Another consideration to this matter is the fact that SAR and ILP values of nanoparticles reduce when they are conjugated with an active pharmaceutical ingredient (API) due to a restriction of motion [86], which means a higher concentration of the nanoparticle would be required to induce the desired heating effect. Therefore, there is a trade- off between improved treatment efficacy versus safety. Finally, there are also considerations derived from the regulatory front; functionalising a nanoparticle with an API would change its regulatory path of a medical device to that of a medicinal product [216], which costs considerably more time and finances. It is also worth noting that MagForce's Nanotherm® treatment that is clinically approved (since 2011) to treat glioblastoma utilising magnetic hyperthermia- and is undergoing clinical trials in other cancers [68]- and has yet to undergo clinical testing with a functionalised version of its nanoparticle.

2.7. Conclusion

The effect of intracellular and extracellular magnetic hyperthermia on the viability of BxPC-3 cells was compared after 30 minutes treatment. It was found that extracellular magnetic hyperthermia (at temperatures of 41.2±0.6 °C) induced significant levels of necrosis in these cells whereas intracellular magnetic hyperthermia showed no effect.

This therefore leads to questions on the overall importance of intracellular IONP to the efficacy of the treatment, and whether it can play indirect functions that could enhance this treatment, such as DNA repair inhibition or immune stimulation in tumours.

3. Chapter 3: Endotoxin Contamination Assessment of fluidMAG/C11-D nanoparticles

3.1. Background

Following *in vitro* efficacy experiments, fluidMAG/C11-D nanoparticles were tested for endotoxin contamination to establish whether they were within regulatory guidelines in this regard. It was established that the nanoparticles had levels of endotoxin above regulatory requirements for a medical device and so an endotoxin screen of superparamagnetic IONP from many industrial partners was undertaken to identify a new suitable candidate nanoparticle to bring into preclinical assessment. In addition to this work, many more nanoparticles were tested for endotoxin as part of collaborations with academia, industry and the EUNCL; this work is also summarized in this chapter.

This work, and work of others in the group (Dr Elena De Calatrava-Pérez), will form a paper that is currently in writing.

3.2. Introduction

Endotoxin – or lipopolysaccharide (LPS) – is a large (200 – 1000 kDa), essential component of the cell membrane of gram- negative bacteria. It consists of a highly conserved, intracellular lipid A anchor, an extracellular polysaccharide antigen termed 'O-antigen', and an interconnected oligosaccharide core (Figure 3.1.). Upon cell death, and during growth and division, endotoxin is released into the local environment. Endotoxin in the circulation triggers TLR-4 signalling, which subsequently mounts an inflammatory response against bacteria [240, 241]. Our bodies are highly sensitive to this toxin, with picogram to nanogram levels known to induce inflammatory cytokine expression *in vitro* [242], while 2-4 ng/ kg levels associated with systemic inflammation and sepsis in humans [243].
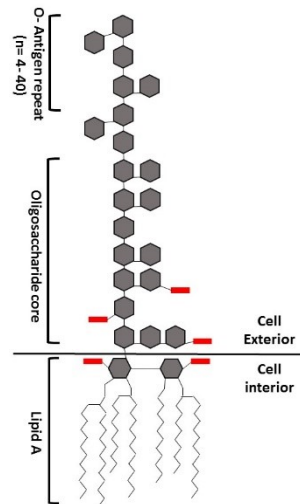
Figure 3.1. Schematic representation of endotoxin derived from E. coli O111:B4.

Endotoxin consists of a highly conserved lipid A region which carries most of the potency of endotoxin. The lipid is embedded in the cell membrane, acting as an anchor for the polysaccharide backbone. The O-antigen region consists of repeating oligosaccharide units which varies in structure between species. Figure adapted from [244].

Endotoxin is notoriously heat- stable and so this molecule is ubiquitously found on surface tops, glassware, lab reagents and in the air [245-247]. Nanomaterials are particularly vulnerable to endotoxin contamination due to its available phosphate groups and hydrophobic lipid sites, and nanoparticles high surface- to- volume ratios (Figure 3.2.). Removing it is also incredibly difficult, with common sterilisation techniques such as autoclaving and ionization radiation proving ineffective [248]. The United States Nanoparticle Characterization Laboratory (USNCL) reported previously that more than a third of the nanomaterials they tested failed early preclinical assessment due to endotoxin levels that do not satisfy regulatory requirements [249].
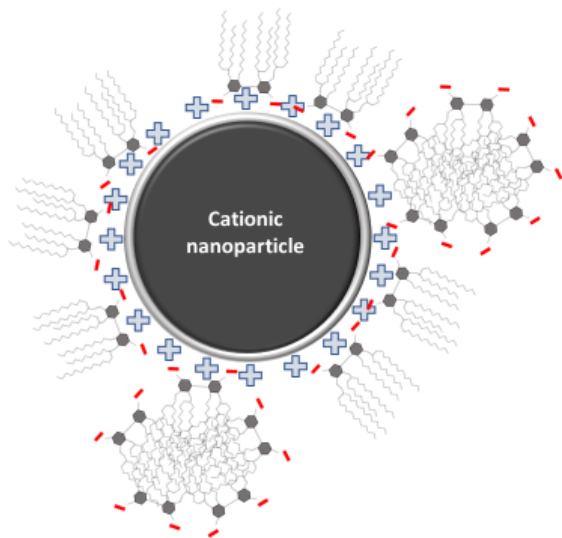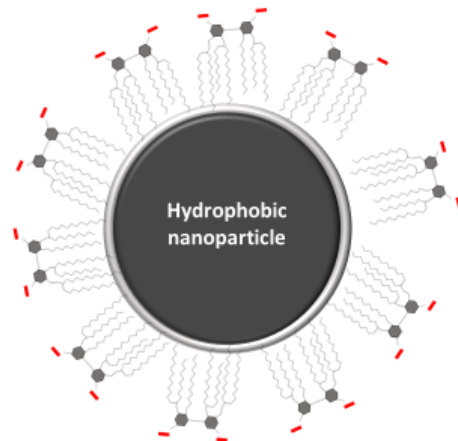
Figure 3.2: Endotoxin binding to cationic and hydrophobic surfaces on nanoparticles.

A. Nanoparticles with cationic surfaces are susceptible to endotoxin binding due to their negatively- charged phosphate groups (illustrated in red). Endotoxin can also form micelles due to their hydrophobic lipids and hydrophilic polysaccharides, which too can interact electrostatically via their available phosphate groups. B. The lipid A structure on endotoxin can hydrophobically bind to lipophilic surfaces on nanoparticles.

Nanoparticles have been approved as both 'Medical Devices' and 'Medicinal products', and the endotoxin requirements vary between each. It is important to note that in the regulatory setting, endotoxin levels are described as endotoxin units, or EU, to account for the varying potencies of endotoxin derived from various bacteria [250, 251]. In the research setting, it is common to approximate 1 EU to 100 picograms of endotoxin [252]. For medical devices that do not come into contact with cerebral spinal fluid (CSF), their limits are 0.5 EU/ ml at no more than 20 EU/ device. If contact with CSF does occur, the limits are 0.06 EU/ ml at no more than 2.15 EU/ device. Medicinal products that avoid the CSF have a limit of 5 EU/ kg per hour, whereas contact with CSF results in a limit of 0.2 EU/ kg per hour [253, 254]

In order to evaluate the levels of endotoxin in a nanoparticle, two methods are commonly used: the *in vitro* limulus amoebocyte lysate (LAL) assay, and the *in vivo* rabbit pyrogen test (RPT). The LAL assay can be further broken down into the chromogenic, turbidimetric and gel clot assays [252, 255]. The lysate used in LAL assays derives from the blood of a horseshoe crab – *Limulus polyphemus* – which clots at a rate dependant on the concentration of endotoxin [256]. Based on this physiological mechanism, three regulatory approved assays have been developed that rely on three different endpoint measurements: turbidity, absorbance and gel clotting [257]. These assays are also accepted under ISO 29701:2010, the international standard for endotoxin contamination assessment of nanomaterials [258] and the United States Pharmacopoeia standards for endotoxin testing [254] .

Nanoparticles are well known for interfering with many different common assays, such as MTT, LDH and ELISA's [259]. They have also been shown to interfere commonly with the LAL assays. Nanoparticles with high absorbance between 400 – 550 nm may interfere with the chromogenic assay, nanoparticles with high turbidity may interfere with the turbidimetric assay, and nanoparticles may interfere with the clotting cascade of the gel clot assay; additionally, the surface chemistry of nanoparticles may lead to the adsorption of endotoxin, or components of the LAL assay itself, which can also lead to interference. For this reason, the inhibition/ enhancement control (IEC) is now included with these assays to identify any potential interference [255, 260].

In this chapter, the fluidMAG/C11-D nanoparticles from chapter 1 are assessed for endotoxin contamination using the chromogenic LAL assay. After overcoming initial interference with the assay, it was discovered that the nanoparticle contained levels of endotoxin above regulatory requirements, making it unsuitable for preclinical testing.

Following this result, the manufacturers of the nanoparticle sent the iron oxide core, the polymer coating and the dispersant to be tested individually for endotoxin to identify the source of the endotoxin. Following this work, many more superparamagnetic IONP from various suppliers were screened for endotoxin to identify a new lead nanoparticle to bring forward to preclinical assessment. In parallel to this study, the lab began testing endotoxin for academic labs, industry and the EU nanoparticle characterization laboratory (EUNCL). A summary of this work is also detailed herein.

3.3. Materials

Nanomaterials tested were obtained from a variety of sources as described above. LAL assays used were the endpoint chromogenic assay and the gel clot assay (Associates of Cape Cod, UK). Tips and tubes were certified endotoxin- free and diluents were certified to have levels of endotoxin lower than 0.001 EU/ml. Each of these were also from Associates of Cape Cod, UK.

3.4. Methods

3.4.1.   Nanoparticles

All nanoparticles were handled in a sterile hood and only opened directly before testing for endotoxin. Manufactures guidelines for handling were followed at all times (i.e. light sensitive nanoparticle, nanoparticles that must be stored frozen etc.). If the nanoparticles were in solid form, they were dispersed in endotoxin-free water before testing; if in solution, they were diluted directly into endotoxin- free water. All materials were pH tested (Fischer Scientific pH indicator paper) to ensure they were between pH 6.0 and 8.0, to prevent assay interference from this regard [261], and if they were outside this range, their pH was adjusted with pyrogen-free 1M NaOH or HCl (Sigma Aldrich, Ireland).

Information on nanoparticle concentrations were obtained from the suppliers and used to determine the maximum valid dilution (MVD). The MVD refers to the maximum dilution a nanomaterial can undergo before it reaches its endotoxin limit and cannot be diluted any further for endotoxin assessment [253, 254]. To calculate MVD, the following equation is used:

$$\text{MVD} = \frac{EL \; x \; Concentration \; of \; material}{Assay \; Sensitivity}$$

where *EL* is the endotoxin limit of the particular nanoparticle, concentration is the undiluted concentration of the nanoparticle (or carried active pharmaceutical ingredient) in mg/ml and assay sensitivity is the lowest concentration of endotoxin recognised by the LAL assay. For determining the EL, the regulatory path of the nanoparticle must be first established. Based on the nanoparticles desired mechanism or action – pharmacological or physical – the nanoparticle was considered a medicinal product or medical device respectively [216]. Therefore, as described above, the endotoxin limits associated with these are used to calculate the MVD. With regards to assay sensitivity, this will vary between LAL assays. For the chromogenic and turbidimetric assays this would be the lowest value on the standard curve, for the gel clot assay this value is provided with the kit [262] [Note: The sensitivity of the gel clot assay was confirmed before undergoing endotoxin testing of materials].

3.4.2. Chromogenic endpoint assay

The USNCL protocol (NCL Method STE-1.1) for endpoint chromogenic assay was followed for this test [261], this is in compliance with ISO 29701:2010 [258], and the US Pharmacopoeia standard for endotoxin testing [254]. In summary, a standard curve was made from the control standard endotoxin (CSE) and endotoxin- free water based on the sensitivity of the LAL reagent. Each nanoparticle to be tested was diluted in endotoxin-free water (not exceeding the MVD) and spiked with a known concentration of CSE. Negative and quality controls were also included which consisted of endotoxin- free water and a known concentration of CSE respectively. Standards, samples and controls were tested in duplicate in 50 µl volumes in a 96 well plate. Each of these wells were incubated with 50 µl LAL reagent for 15 ±5 mins (incubation time varies between LAL reagents) at 37°C. Once this time has passed, 25 µl of acetic acid is added to each well to terminate the reaction (at a final concentration of 10%). The plate is then read at 405 nm with an Epoch microplate reader (BioTek, US). The test was deemed a success if the standards, samples, IEC and quality control have a coefficient of variation (CV) within 25%, the standard curve has a correlation coefficient of at least 0.98 and the spike recovery was within 50%- 200%. A spike recovery of <50% was considered an inhibition of the assay, where the nanoparticle itself gave a false negative result. Likewise, a spike recovery of >200% was considered an enhancement, or false positive result.

In order to get over interference with nanoparticles that absorb highly at 405 nm, a modification is made to the chromogenic assay to shift the absorbance endpoint to 540-

550 nm. In this case, the protocol is followed as before but instead of stopping the reaction with acetic acid, the reaction is stopped with 50 μl of sodium nitrite in HCl, 50 μl ammonium sulfamate and 50 μl N-(1-Naphthyl) ethylenediamine sequentially. The plate can then be read at 540- 550 nm.

3.4.3.   Gel clot assay

The EUNCL (EUNCL-STE-001.3.2) and USNCL (NCL Method STE-1.3) protocols were followed for the gel clot assay [261, 263]. Again, this was in compliance with ISO and the US pharmacopeia standards for endotoxin assessment of nanomaterials. For each gel clot lysate used, a sensitivity test was initially performed to confirm the sensitivity of the lysate. For this, the CSE was diluted in endotoxin- free water at 4X, 2X, X and 0.5X, where X is the 'known' sensitivity of the lysate, provided by the manufacturer. 100 μl of these dilutions was added to gel clot tubes (Associates of Cape Cod, UK) in replicates of four. Additionally, there are four negative controls which were endotoxin- free water alone. Then, 100 μl of LAL reagent is added to each tube, making the final concentrations tested 2X, X, 0.5X and 0.25X the sensitivity of the lysate, along with the negative controls. Each tube is vortexed and then incubated at 37°C for one hour. Following incubation, the tubes are inverted 180 degrees to observe if a clot has been formed. A positive result consisted of a firm clot that is maintained following inversion. Anything other than a firm clot following inversion was considered a negative result. The test was deemed successful if all negative controls failed to clot the gel. From these results, a geometric mean sensitivity for the lysate is calculated by taking the antilog of the sum log endpoints for each concentration divided by the number of replicates (seen in the equation below):

$$\text{Geometric mean sensitivity} = \text{Antilog}\left((\textstyle\sum e) / f\right),$$

where $\sum e$ is the sum of the log endpoints and f is the number of replicates. If the calculated mean sensitivity is between 0.5X – 2X of the stated manufacturer sensitivity, the sensitivity of the lysate is confirmed.

Following this confirmation, an interference/ enhancement control (IEC) is performed. Here, nanoparticles are tested at a concentration that doesn't clot the gel in replicates of four. At this concentration, the nanoparticles are spiked with CSE at a concentration of 4X the sensitivity of the lysate and serial diluted three times so that you test nanoparticles alone, nanoparticles and 4X CSE, nanoparticles and 2X CSE, nanoparticles and X CSE and finally nanoparticles and 0.5X CSE. Again, when 100 μl of

the LAL reagent is added, this equates to a final concentration of nanoparticles and 2X CSE, nanoparticles and X CSE, nanoparticles and 0.5X CSE, nanoparticles and 0.25X CSE, as well as nanoparticles alone. In addition to the IEC, a sensitivity test is run again in duplicate in parallel as a quality control. For this test to be deemed successful, the nanoparticles alone must not clot the gel and the lysate sensitivity must be confirmed again in the parallel test. Additionally, if the lysate retains its sensitivity when the nanoparticles are added to the CSE, the nanoparticles are deemed to not interfere with the assay; however, if the sensitivity is outside the 0.5X- 2X range then the nanoparticles do interfere. Furthermore, if the lysate sensitivity is calculated below 0.5X, the nanoparticles induce an inhibition to the assay; likewise, a sensitivity above 2X is associated with an enhancement. If the nanoparticles pass the IEC, it can then be tested for the quantity of endotoxin it possesses.

For the limit test, the nanoparticles are diluted continuously from their stock with endotoxin-free water (not exceeding the MVD) and tested in duplicate until no clotting of the gel is observed. At this concentration, an additional test is run with nanoparticles alone, nanoparticles spiked with 2X the sensitivity of the lysate, an additional 2X CSE in water, and water alone in duplicate. If the spiked nanoparticle sample and water sample is positive, and nanoparticles alone and water alone is negative, the limit test is successful and endotoxin results at this concentration can be reported (Figure 3.3.).
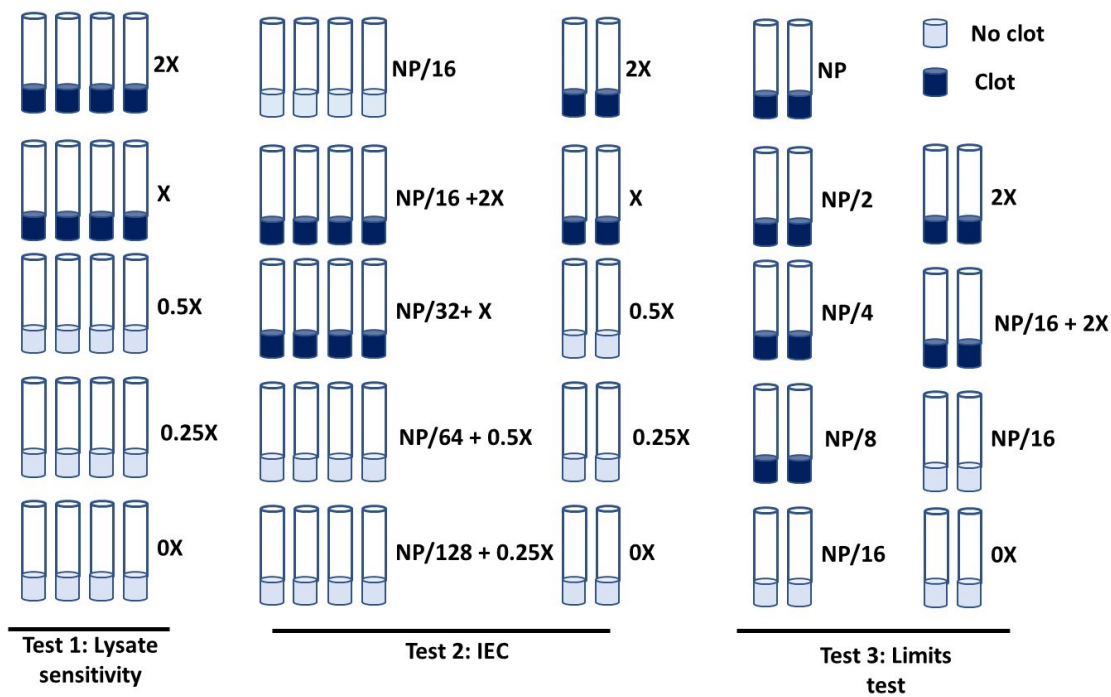
Figure 3.3. The three tests required for endotoxin contamination assessment with nanoparticles and the gel clot assay.

X in this case is the concentration of endotoxin that the gel clot lysate is reportedly sensitive to. The forward slash refers to the dilution of nanoparticle. Dark blue colours refer to a gel clot, whereas light blue is an unclotted gel. If these three tests occur as illustrated above, and the nanoparticle is not diluted further than its calculated MVD, the endotoxin levels of the nanoparticle can be reported.

3.5. Results

3.5.1. FluidMAG/ C11-D endotoxin assessment

The fluidMAG/ C11-D nanoparticles described in chapter 2 were found to interfere with the chromogenic assay, but this interference was overcome using the diazo modification to shift the absorbance endpoint after the nanoparticles were shown to have a high absorbance at 405 nm and a lower absorbance at 550 nm (Varian Cary 500 UV-Vis spectrometer). Results showed an endotoxin concentration of 0.8 EU/mg of nanoparticle which corresponded to 80 EU/ml of stock concentration (100 mg/ml). In order to determine the source of the endotoxin, the nanoparticle core, polymer coating (starch) and diluent (water) were tested for endotoxin. The starch polymer showed high levels of contamination (1.38 EU/mg), whereas the iron core and diluent had lower levels (0.63 EU/mg and <0.125 EU/ml respectfully) (Figure 3.4.).

Nanoparticle	Chromogenic assay results
FluidMAG/C11-D	Interference (inhibition)

FluidMAG/ C11-D UV-Vis absorption

Chromogenic (0.91AU) Diazo (0.23AU)

(Absorbance (AU) vs Wavelenght (nm), 400–800)

Nanoparticle	Diazo Chromogenic assay results
FluidMAG/C11-D	0.8EU/mg NP

Regulated product	Endotoxin requirements
Medical Device	20EU at 0.5EU/ ml
Drug	5EU/ kg/ hour

Material	Chromogenic results	Diazo Chromogenic results
Diluent	N/A	Below detection
Iron oxide core	Interference (inhibition)	Interference (inhibition)
Starch coating	1.25EU/mg	N/A

Material	Gel clot results
Iron oxide core	0.625EU/mg
Starch polymer	1.38EU/mg

Figure 3.4. Endotoxin assessment of fluidMAG/C11-D nanoparticle.

Following interference in the chromogenic assay, the UV-Vis absorbance spectra of fluidMAG/C11-D nanoparticles showed that they absorbed highly at the wavelengths used in the assay (0.91 AU at 405 nm). With wavelengths used in the diazo chromogenic assay, however, it absorbed considerably less (0.23 AU at 550 nm). Based on this, the diazo chromogenic assay was successfully used to get over the interference and determine the endotoxin contamination of the nanoparticle. This concentration was deemed too high to fulfil the requirements of a medical device and so the nanoformulations constituents were tested for endotoxin to find the source of the contamination. The starch polymer coating around the nanoparticle was found to have a considerable amount of endotoxin, whereas the iron oxide core contributed less than half this concentration, and the diluent had levels of endotoxin that were undetected by the assay (i.e. levels below the standard curve).

3.5.2. Summary of all nanoparticles tested for endotoxin assessment

21 nanomaterials from industry, academia, the EUNCL or nanomaterials produced in-house were successfully tested for endotoxin contamination (Table 4. and Figure 3.5.). If the nanomaterial interfered with a particular assay, the assay was changed (chromogenic to gel clot) or modified (diazo reagent) until it could be successfully measured. 9 of the 21 nanomaterials had levels of endotoxin that prevented progress to further testing. These 9 nanomaterials consisted of 7 IONP and 2 gold nanoparticles (GNP) derived from in-house, academia and industry. The liposome and polymeric nanoparticles all passed endotoxin assessment and have proceeded into further testing.

Table 4. Summary of all nanoparticles tested for endotoxin contamination.

Nanoparticle source, potential medical application, predicted regulatory path, assay used for assessment, MVD value calculated, determined EU stock concentration and whether it passes or fails based on these levels are described within. Abbreviations: NM, Nanomaterial; MH, magnetic hyperthermia; Multiple, multiple potential applications; DD, drug delivery; IONP, iron oxide nanoparticle; GNP, gold nanoparticle; Liposome, Lipid-based nanoparticle; Polymer, polymeric-based nanoparticle; MVD, maximum valid dilution, EU conc., endotoxin unit concentration.

NM	Source	Medical application	Expected regulatory path	Assay	MVD	EU conc (EU/ml)	Pass/Fail
IONP1	Industry	MH	Device	Gel clot	633	0.4EU	Pass
IONP2	Industry	MH	Device	Gel clot	671	98.4EU	Fail
IONP3	Industry	Imaging	Device	Diazo	467	0.48EU	Pass
IONP4	Industry	Multiple	Medicinal	Gel clot	1000	15.75EU	Fail
IONP5	Industry	Multiple	Medicinal	Diazo	4167	77.5EU	Fail
IONP6	Industry	Multiple	Medicinal	Gel Clot	1,000	30EU	Fail
IONP7	Industry	Multiple	Device	Diazo	1667	80EU	Fail
IONP8	Industry	Multiple	Medicinal	Gel Clot	1000	43.75EU	Fail
IONP9	Industry	Multiple	Medicinal	Diazo	517	31EU	Fail
GNP1	Academia	DD	Medicinal	Diazo	25	0.26EU	Pass
GNP2	Academia	DD	Medicinal	Diazo	25	0.28EU	Pass
GNP3	Academia	DD	Medicinal	Diazo	25	4.1EU	Fail
GNP4	Academia	DD	Medicinal	Diazo	25	5.64EU	Fail
GNP5	Industry	DD	Medicinal	Gel clot	41667	4.8EU	Pass
GNP6	In-house	DD	Medicinal	Diazo	28.5	0.06EU	Pass
GNP7	In-house	DD	Medicinal	Diazo	27.8	0.43EU	Pass
GNP8	In-house	DD	Medicinal	Gel Clot	5	<0.06EU	Pass
GNP9	In-house	DD	Medicinal	Diazo	27.5	1.49EU	Pass
Liposome1	EUNCL	Imaging	Device	Diazo	8333	0.37EU	Pass
Liposome2	EUNCL	Imaging	Device	Diazo	833	0.28EU	Pass
Polymer1	EUNCL	DD	Medicinal	Diazo	16667	1.7EU	Pass
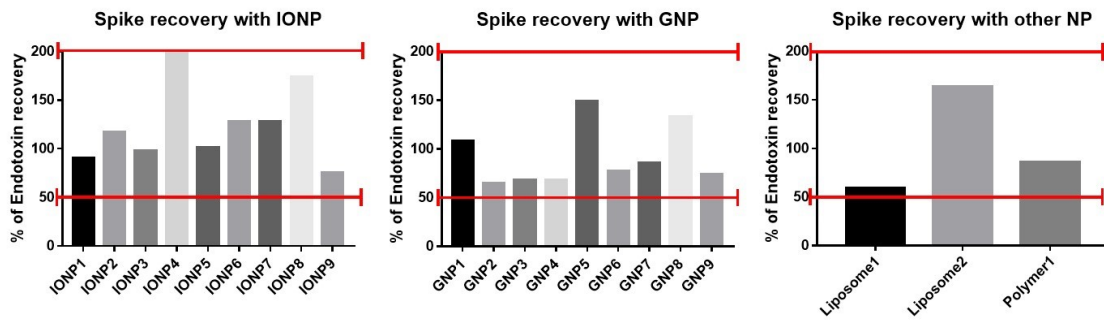
Figure 3.5. Nanoparticles passing the IEC and successfully tested for endotoxin contamination.

Interference with these assays is determined using a spike recovery control (given by the red lines). Spike recovery is given by percentage. Abbreviations: IONP, iron oxide nanoparticle; GNP, gold nanoparticle; NP, nanoparticle; Liposome, Lipid-based nanoparticle; Polymer, polymeric-based nanoparticle.

3.5.3. Overcoming interference

Interference with the chromogenic assay was commonly observed with IONP and GNP. In both cases, this interference was in the form of inhibitions. Interference by IONP can be observed in Figure 3.6 where five IONP were shown to strongly inhibit the chromogenic assay. From Figure 3.4. above, it was shown that fluidMAG/C11-D had high absorbance at 405 nm which could interfere with the assay and shifting the absorbance to 550 nm could overcome this. 4 other IONP showed similar interference, and so they were tested with the diazo chromogenic also. Shifting to 550 nm was effective at removing inhibitions for all but one nanoparticle: IONP4. In order to overcome this interference, the gel clot assay was used in an attempt to change the endpoint measured. The gel clot assay proved successful in overcoming interference and the endotoxin levels for all of these IONP could be reported (Figure 3.6.).
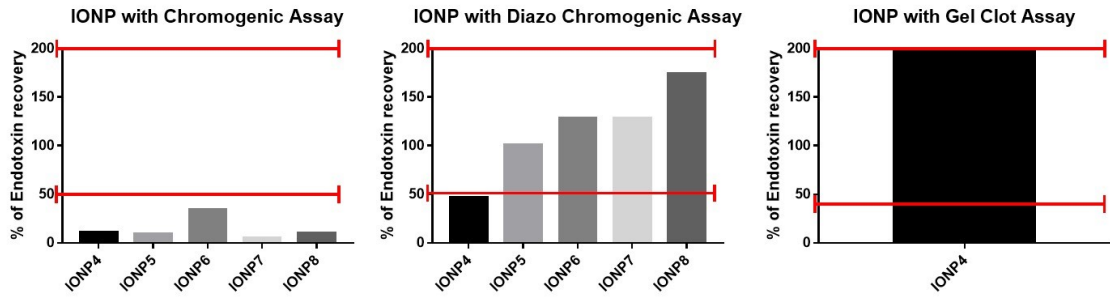
Figure 3.6. Overcoming IONP interference with LAL assays

IONP strongly inhibited the chromogenic assay, with spike recoveries falling far below the 50% concentration. Adding the diazo reagent to shift the absorbance endpoint to 550 nm proved successful at overcoming interference for most IONP, except IONP4. Subsequently, the gel clot assay was used to get over this inhibition and endotoxin contamination for IONP4 was successfully measured.

3.6.Discussion

Nanotherm®, as described in section 1.3.3., is currently the only treatment approved in the clinic to treat cancers through magnetic hyperthermia. Importantly, Nanotherm® is approved as a medical device, as its mechanism of action can be described as 'physical' rather than 'pharmacological'[216]. As such, fluidMAG/ C11-D nanoparticles would be regulated in the same manner and so would have endotoxin limits associated with a medical device: 20EU/device at no more than 0.5 EU/ ml [193, 254]. The median dose used by Nanotherm® in the clinic is 504 mg Fe [216], which, if fluidMAG/C11-D nanoparticles were to be used in that concentration range, would make them non-clinically viable (0.8 EU/mg). Because of this, it was important to determine where exactly this endotoxin originated from in the nanoformulation. Therefore, the iron oxide core, starch polymer coating and nanoparticle diluent were tested individually to establish to what extent each constituent was contaminated. The levels of endotoxin in the diluent were below the levels of detection in the assay, the iron oxide core was found to have 0.625 EU/mg and the starch coating contributed 1.38 EU/mg to the nanoformulation. Based on these results, an important lesson was learned: ensuring that the starting reagents are endotoxin-free is essential to producing a final nanoparticle product within the regulatory guidelines for endotoxin contamination. Other groups have also voiced this as the most important consideration to preventing contamination [248, 264].

Following the detection of high levels of endotoxin in the fluidMAG/C11-D nanoparticles, superparamagnetic IONP from various suppliers were screened to identify a new lead nanoparticle to take into preclinical evaluation. The levels of endotoxin of these nanoparticles were compared against the levels identified with Sienna +®, a clinically approved IONP used to detect lymph node metastasis in breast cancer patients [265] (kindly provided by Endomagnetics, UK). Of these tested, one nanoparticle had levels of endotoxin comparable (in fact lower) to the clinically-approved Sienna +®: RCL-01. RCL-01 had an endotoxin level of 0.006 EU/mg which corresponded to 0.4 EU/ml of stock concentration, whereas Sienna +® had more than double this value with 0.017 EU/mg, corresponding to 0.48 EU/ml of the stock. Moreover, RCL-01 had ILP values 5 times larger than fluidMAG/C11-D (1.1 versus 5.7 nHm^2kg^{-1}; ILP data for RCL-01 was provided by the supplier: Resonance Circuits Limited), meaning less of the nanoparticle would be required to achieve the desired temperature elevations *in vivo*. Notably, other than RCL-01 and Sienna+®, all of the IONP had levels of endotoxin above regulatory requirements.

Interference was commonly encountered with IONP and GNP using the chromogenic and diazo chromogenic assay. Both of these materials are known to absorb highly between 405 nm and 550 nm and so interference can occur if endpoints are measured close to these wavelengths [255, 259, 266, 267]. 5 IONP were shown to interfere strongly through inhibitions when assessed with the chromogenic assay at 405 nm. The spike recovery was lower than 10% in some cases for these nanoparticles. Shifting the absorbance to 550 nm proved effective at removing this interference with 4 of the 5 nanoparticles. Interestingly, the nanoparticle that still interfered -IONP4- was the only cationic nanoparticle tested in this screen, and so it can be surmised that the inhibitions that remained in its case are from direct binding of endotoxin to the nanoparticle via its negatively-charged phosphate groups, resulting in a false negative in the assay [248]. Following this, IONP4 was assessed for endotoxin with the gel clot assay. This test proved successful with the spike recovery at exactly 200% and within requirements for a successful test.

Of the total 21 nanoparticles tested, 9 had contamination that prevented further progress into preclinical studies. What is of additional importance in this regard is the fact that these nanoparticles have been developed specifically for biomedical applications and have now failed due to excessive endotoxin levels. Moreover, these materials originated from many different sources including in-house, academia and industry, and so this is a major issue across-the-board that must be considered at all levels.

3.7. Conclusion

The fluidMAG/C11-D nanoparticles from chapter 2 were assessed for endotoxin contamination following successful efficacy data *in vitro*. The nanoparticles were found to have concentrations of endotoxin that would make them clinically non-viable when compared to Nanotherm®, which is regulated as a medical device. Subsequent endotoxin testing of the nanoparticle components determined that the polymeric coating of the nanoparticle was introducing a significant amount of endotoxin into the final product, with a smaller contribution from the iron oxide core. Following these results, many more IONP were screened to identify a new lead candidate to bring into further testing. Additionally, many nanoparticles synthesised in-house and obtained from academic and industrial institutions were also tested. It was found that 9 of the 21 nanomaterials contained endotoxin levels that would prevent them progressing further into preclinical testing. These results emphasise the extent of this issue at all levels of research.

4. Chapter 4: Complement Activation Assessment with Lead Nanoparticles

4.1. Background

Based on the endotoxin screen, one IONP (RCL-01) was shown to have levels of endotoxin within regulatory requirements for a medical device and so this nanoparticle was taken forward into a blood compatibility assessment. In addition to this lead IONP, an IONP found to be contaminated with high levels of endotoxin (NOC-0001) was included as a contaminated control, and the clinically- approved Sienna+® was also included as a clinical comparison. For this study, human plasma was treated with each nanoparticle at clinically relevant concentrations to determine the concentration a positive complement activation response occurs with each material. Complement activation is a marker for hypersensitive effects *in vivo* that is a concern for IONP in the clinic.

This work will contribute to a paper in collaboration with Dr. Neill Liptrott and his group at the University of Liverpool who are testing these same nanoparticles for their potential to induce coagulopathies, haemolysis and immune stimulation/suppression in human plasma.

4.2. Introduction

The complement system plays an integral role in the opsonization and removal of pathogens form the body. As described in section 1.4, this complex system comprises more than 30 proteins that can be activated through three mechanisms: the classical, lectin and alternative pathways. Each of these pathways is linked by the cleavage of complement 3 (C3) into its active subunits C3a and C3b, the critical step in complement activation [198]. The surface chemistry and large surface area of nanoparticles make them susceptible to complement activation, and efforts to limit their recognition with biocompatible coatings are not always successful [197, 202, 268]. Significant activation can cause hypersensitive reactions than manifest as symptoms such as rash, dyspnea, flushing, hypertension, hypotension, and even fatal cardiopulmonary syndrome in rare cases [269]. One such hypersensitive reaction is complement activation related pseudoallergy (CARPA), which, as the name suggests, is a non- IgE mediated reaction. CARPA can result in harmful haematological alterations such as leukopenia and thrombocytopenia [202]. Nanoparticles have been highly associated with inducing CARPA, and it is thought to have contributed to the withdrawal of several IONP in the clinic [211]. Following these withdrawals, health warnings from the FDA and EMA were

published regarding hypersensitivity reactions associated with IONP and recommended precautions to take [191, 192].

Based on this evidence, complement activation was assessed with the lead nanoparticle identified from the endotoxin contamination screen (RCL-01). Additionally, Sienna +® was used as a clinical comparison along with another IONP (NOC-0001) that was found to have high levels of endotoxin (98.4 EU/mg) as a contaminated comparison. The aim of this chapter was to determine doses of IONP that induce complement activation, providing an indication for potential hypersensitive effects further down the line.

4.3. Materials

Sienna +® was kindly provided by Endomagnetics, UK as a clinical standard for these experiments. NOC-0001 and RCL-01 were also generously provided by BioKeralty and Resonance Circuits Limited respectively. Each of these IONP are coated in a form of dextran and sterilised through gamma irradiation. iC3b ELISA's were purchased from Pathway Diagnostics, UK. Zymosan was purchased from Sigma Aldrich, Ireland, and phosphate buffered saline free from magnesium and calcium ions was purchased from VWR International, UK. Sodium citrate vacutainer tubes were from Fischer Scientific, UK.

4.4. Methods

4.4.1. Characterization

Size distribution (NTA and DLS) and zeta potential (DLS) measurements were performed according to protocols from the EUNCL [223, 224, 270] (See Supplementary Figures 5, 6 and 7).

4.4.2. Dose selection

The dose chosen was based on the median dose used by Nanotherm® in the clinic – 504 mg of iron [216]. Based on this concentration, a 70 kg individual would be treated with 7.2 mg Fe/kg. A 70 kg individual has approximately 5.6 L of blood, and so at this concentration, the levels of iron in the blood would be 90 µg/ml. On top of this concentration, additional concentrations of 2X, 0.5X, 0.25X, 0.125X, 0.06X, 0.03X and 0.015X (where X is the median concentration of Nanotherm®) were tested with the aim of identifying a window at which complement activation occurs and stops. This method of dose calculation is recommended by the EUNCL and USNCL [271, 272].

4.4.3. Blood treatment with nanoparticles and zymosan

The EUNCL and USNCL protocols for complement activation assessment of nanoparticles was followed herein and described below [271, 272]. This test is also in compliance with ISO standards for biological evaluation of medical devices (ISO 10993-4:2017). In short, 3 healthy donors (2 females and 1 male; on no medication) supplied blood that was drawn directly into sodium citrate vacutainer tubes. The first 5 ml of blood was discarded and not used for assessment. The blood is immediately spun at 2500 g for 10 minutes to extract the plasma. Upon completion, the plasma is inspected for signs of haemolysis (reddening of the plasma). In these experiments, no indications of haemolysis were observed with any donors. The plasma is then extracted and ready for treatment. For this, 100 µl of plasma, 100 µl of veronal buffer and 100 µl of test sample (at each concentration described above) is added together in 1.5 ml falcon tubes (each test is run in duplicate). The tubes are vortexed and then heated to 37 °C for 30 minutes. Following heating, the samples are aliquoted and frozen at -80 °C for subsequent analysis by ELISA. The negative control for this experiment was Ca^{2+} and Mg^{2+} -free PBS, while the positive control was activated zymosan (activated by dispersal in 1% 0.15M NaCl, heated to 100 °C for one hour, centrifuge for 30 minutes at 4000 rpm and re-disperse at 15 mg/ml in 0.15M NaCl) at a final plasma concentration of 5 mg/ml, as used in [203, 273].

4.4.4. iC3b ELISA

iC3b was chosen as the component of the complement system to measure as an indicator of activation. Upon cleavage of C3 to C3a and C3b, C3b is quickly broken down further into iC3b through the activity of factor I and H [274, 275]. The level of iC3b in serum is reflective to the level of complement activation [201]. Additionally, iC3b ELISA has previously been shown to have a larger signal-to-noise ratio than C3a [201]. Manufacturers recommendations were followed for this ELISA (Pathway Diagnostics, UK). Serum samples were thawed no more than once. If the sample dilution had to be adjusted to fit the standard curve, a separate unthawed aliquot was used.

4.5. Results

4.5.1. Characterization

Sienna +® were deemed the smallest nanoparticle by NTA and DLS measurements, followed by NOC-0001 and RCL-01 respectively. Both Sienna+® and RCL-01 were anionic while NOC-0001 was considered neutral in charge [276]. With regards to endotoxin contamination, Sienna+® and RCL-01 have low levels within regulatory

requirements for medical devices, whereas NOC-0001 have levels vastly exceeding the other two and not suitable for clinical applications (Table 5).

Table 5. Summary of characterization data from NOC-0001, RCL-01 and Sienna+®.
Values for size distribution, zeta potential and endotoxin contamination are provided for each nanoparticle. pH = 7 for all nanoparticles. Values represent mean± standard deviation. NOC-0001 and RCL-01 were tested for endotoxin contamination using the gel clot assay. Sienna +® was tested for endotoxin contamination using the diazo chromogenic assay. See Supplementary Figures 5,6 and 7 for NTA and DLS graphs. Abbreviations: NTA, nanoparticle tracking analysis; DLS, dynamic light scattering; PDI, polydispersity index; EU, endotoxin unit.

Nanoparticle	Mean size (NTA)	Mean size (DLS)	PDI (DLS)	Zeta potential (DLS)	Endotoxin contamination
NOC-0001	72.5±3.8 nm	106.3 nm	0.224	-2.59± 1.08 mV	98.4 EU/mg
RCL-01	128.1±13.2 nm	115.4 nm	0.25	-5.72± 0.15 mV	0.006 EU/mg
Sienna +®	62.1±8.4 nm	58.7 nm	0.177	-16.2± 0.895 mV	0.017 EU/mg

4.5.2. Complement activation

All nanoparticles activated complement at concentrations 2X, X, 0.5X 0.25X, where X is the median concentration used by Nanotherm® in the clinic (7.2 mg/kg for a 70 kg individual). A positive response in this case is described as at least a two-fold induction of the complement component in question against the negative control [271, 272] (as highlighted by the red line in A. and B. of Figure 4.1.). This positive response stops at concentrations of 0.125X and below for each nanoparticle. Moreover, as described in section 3.1, nanoparticles have been shown to interfere with ELISA's, giving false positive/ negative results, and so nanoparticle interference was evaluated with the assay. At the highest concentration used in the assay (2X median Nanotherm® dose), the nanoparticles are spiked with 0.6 µg/ml of iC3b standard with the aim of assessing their spike recovery against the standard alone. The nanoparticles were shown to have negligible effects on the assay (Graph C of Figure 4.1.). Finally, as NOC-0001 was shown to have high levels of endotoxin from chapter 3 (98.4 EU/mg), endotoxin (US Pharmacopeia endotoxin standard; Sigma Aldrich, Ireland) alone was assessed for its ability to activate complement also. No concentration of endotoxin (up to 5 ng/ml) induced a positive response, however a slight increase in iC3b against the negative control was observed (Graph D of Figure 4.1.).
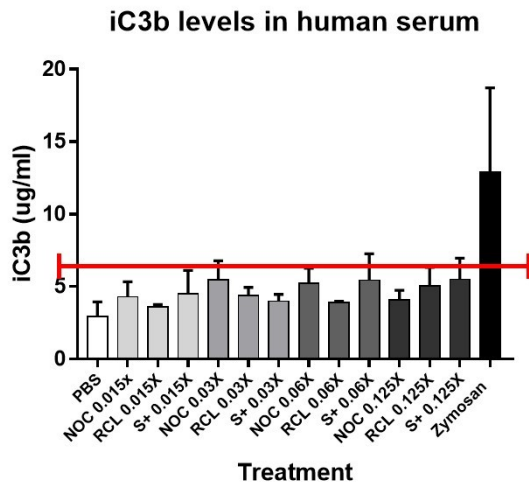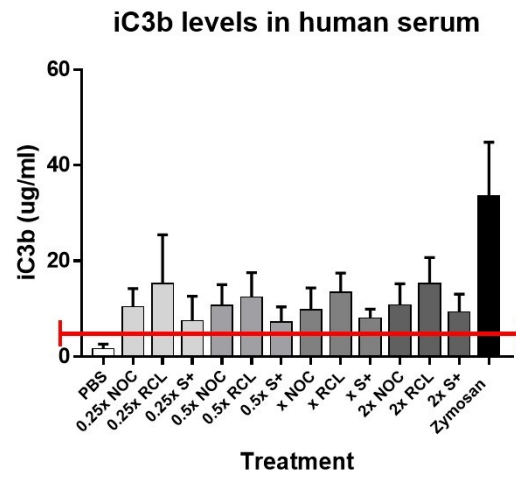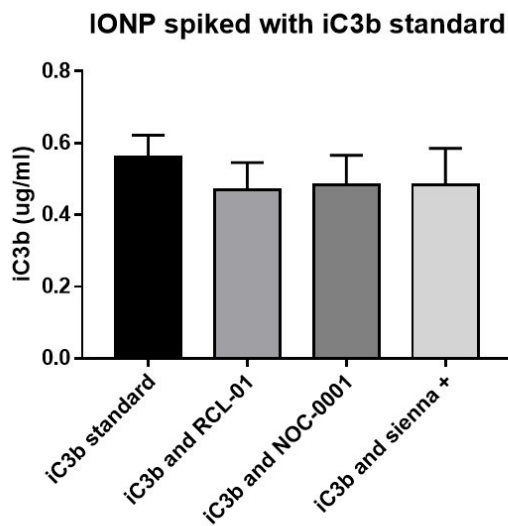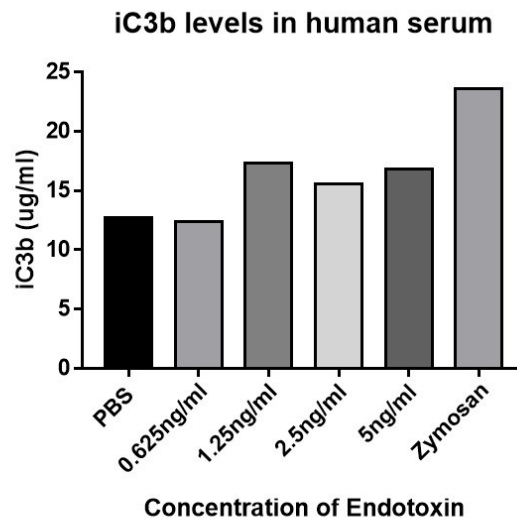
Figure 4.1. Summary of complement activation results.

A. Complement activation with nanoparticles up to 0.125X the median dose of Nanotherm®. B. Complement activation with nanoparticles up to 2X the median dose of Nanotherm®. C. Interference test for highest concentration of nanoparticles used in the assay (2X). D. Complement activation with endotoxin alone. Red line in A. and B. indicates what is considered as a positive complement response by the EUNCL and USNCL. Error bars = standard deviation. X = median dose used by Nanotherm® in the clinic (504 mg of iron). A. and B. shows results for N=3 independent donors in duplicate. C. shows results for 3 independent donors in duplicate. D. shows results from 3 independent donors pooled plasma in duplicate. Abbreviations: NOC, NOC-0001 nanoparticles; RCL, RCL-01 nanoparticles; S+, Sienna +® nanoparticles.

4.6.Discussion

A dose could be determined where each nanoparticle stopped inducing a positive complement response (Figure 4.1.). This was found to be between 0.125X and 0.25X the median dose of Nanotherm® used in the clinic for all three nanoparticles. This corresponds to 1.8 – 3.6 mg/kg for a 70 kg individual. Interestingly, the maximum dose used by Sienna +® in the clinic is 56 mg of iron or 0.8 mg/kg for a 70 kg individual [216], and so this matches up well to what is currently being used in the clinic. To ensure that this response is not a result of interference from the nanoparticles with absorbance readings or through interactions with the constituents of the assay, a spike recovery test was performed with the highest concentration of each nanoparticle used in the assay. The nanoparticles were shown to have negligible effects on the assay (Graph C of Figure 4.1.). Moreover, as NOC-0001 nanoparticles were shown to be highly contaminated with endotoxin, an endotoxin assessment was performed with increasing concentrations tested to observe if the endotoxin alone could induce a complement response at these concentrations. Although a positive response didn't occur, a slight increase in iC3b was observed following endotoxin treatment, and so it cannot be ruled out that endotoxin contributed to the increased iC3b levels observed at the higher concentrations of NOC-0001 used (2X concentration corresponds to 1.8 ng/ml of endotoxin), even though similar complement responses were observed with Sienna+® and RCL-01, and they have negligible endotoxin levels in their formulations.

As each of these nanoparticles are coated in dextran, it is possible that basal levels of C3b in serum is directly binding to the nanoparticles through nucleophilic attack of the hydroxyl groups on dextran to the thioester sites on C3b, forming stable covalent bonds [277, 278]. From here, the C3b could be brought into close proximity to convertases on the surface of the nanoparticles which cleave C3b, and initiate the complement cascade [279]. Efforts to shield or modify these alcohol groups have had mixed results: modifying hydroxyl groups on dextran beads could inhibit their capacity to activate complement [280], whereas crosslinking of the hydroxyls on IONW mentioned previously showed no similar damping effect [208]. Additionally, a study published in Nature in 2019 found that complement activation could be dependent on the protein corona formed on nanoparticles, which can facilitate immunoglobulin deposition and in-turn C3b binding [210]. Therefore, there could be many potential mechanisms involved in the complement activation observed in this case.

Importantly, although EUNCL and USNCL guidelines for complement activation recommend the use of sodium citrate anticoagulant in their protocols, citrate is known to chelate Ca^{2+} and Mg^{2+} ions, thus inhibiting complement activation [281]. Moreover, these protocols approximate the test drugs final blood concentration with the final plasma concentration tested, which may not be truly reflective. Based on this, it is possible that these results underestimate the true complement activation associated with these nanoparticles.

4.7.Conclusion

Three nanoparticles were assessed for their ability to activate complement and potentially induce hypersensitive affects if introduced intravenously. RCL-01 (lead nanoparticle), NOC-0001 (endotoxin contaminated nanoparticle) and Sienna +® (clinically approved nanoparticle) were tested at multiple concentrations relevant to the doses used by Nanotherm® in the clinic. It was discovered that all nanoparticles activated complement strongly up to a certain point, but this response stopped at concentrations of 1.8 mg/kg (for a 70 kg individual). Additionally, these nanoparticles were shown not to interfere with the assay via a spike recovery control. A further test with endotoxin alone suggested that it may have contributed to the complement activation observed with NOC-0001, but the similar results for complement activation observed with the low-endotoxin RCL-01 and Sienna+® make this questionable. These results, although potentially underestimating the true complement activation, provide an important insight into the potential acute effects to expect during *in vivo* safety assessments.

5. Chapter 5: *In vivo* safety Assessment with Lead Nanoparticles

5.1. Background

The lead IONP identified from the endotoxin screen was evaluated here for acute toxicities and organ damage *in vivo*. Single, high doses of RCL-01 were administered intravenously into rats with the aim of determining the concentration at which acute effects occur, their manifestation, and their level of severity. The rats are scored and weighed continuously to monitor the severity of these effects and the recovery time. Seven days post injection, the animals are euthanized, and their organs are harvested for ICP-MS and histological analysis. A dose at which acute effects begin occurring with RCL-01 was identified, and all animals went on to make a full recovery from these initial effects.

This chapter will form a paper when combined with the histological data currently being generated within our group by Anna Bogdanska and Dr Olivero Gobbo.

5.2. Introduction

IONP have been shown to display multiple haemotoxic effects both *in vivo* and in the clinic. These effects range from clinical reports of hypersensitive reactions, to many *in vivo* studies reporting haemolysis, coagulation dysfunction and immune stimulation/ suppression [193, 211, 282]. Therefore, predicting the toxic effects of these nanoparticles can be complicated as the literature contradicts itself quite regularly; for example, there are reports of IONP both prolonging and shortening thrombin time *in vivo* [283, 284], while there are an abundance of studies showing the immunosuppressive and immunostimulatory effects of these materials [285, 286]. Resovist®, for example, has been shown to induce an M1-like phenotype in THP-1's *in vitro*, while also showing reductions in levels of IL-6 and TNF-α at site of injection *in vivo* [144, 287]. Additionally, liver damage and chronic kidney disease has been reported for clinically approved IONP that were subsequently discontinued [211].

Based on this, an *in vivo* study with Wistar rats was undertaken to determine any potential acute systemic toxicities associated with the lead nanoparticle RCL-01 in accordance with ISO 10993-11:2018 (biological evaluation of medical devices). In this study, RCL-01 were injected intravenously as a single, high dose based on the highest doses of IONP used in rats in the literature [288] (30 mg/kg, 45 mg/kg and 60 mg/kg) to determine the point at which acute affects occur and identify the dose-limiting effects associated with the lead nanoparticle. Additionally, the study aimed to identify organ

accumulation and damage through inductively coupled plasma mass spectrometry (ICP-MS) and histological analysis.

5.3. Materials

5.3.1.   Nanoparticles

The nanoparticles used for this study were RCL-01 IONP supplied by Resonance Circuits Limited, UK. These nanoparticles are coated in dextran and sterilised through gamma irradiation, which was confirmed by microorganism contamination analysis by the supplier. Characterization was performed in Chapter 4 but summarized again in Table 6 below (also see Supplementary Figure 5). Additionally, endotoxin contamination assessment and complement activation was also assessed in previous chapters (Chapter 3 and 4 respectively). The nanoparticles displayed lower levels of endotoxin than the clinically approved Sienna +® (0.006 EU/mg versus 0.017 EU/mg respectively).

5.3.2.   Animal ethics

This work was carried out following ethical approval from the Animal Research Ethics Committee at Trinity College Dublin and Health Project Regulatory Authority (HPRA) under the project license number AE19136 /P0890.

5.3.3.   Animal husbandry

Female Wistar rats weighing 239±20 g were bred in-house and kept at Trinity College's Institute for Neuroscience where they were provided food and water *ad libitum.* They were kept under 12 hr light/dark cycles at temperatures of 20±3 °C. Acclimatisation to the facility was allowed for two weeks prior to experimentation.

5.4. Methods

5.4.1.   Nanoparticle characterization

EUNCL protocols for characterization by NTA and DLS was followed for analysing these nanoparticles [223, 224, 270] (Supplementary Figure 5).

5.4.2.   Study procedure

The animals were randomised into two blocks of 12 where they were treated in triplicate with either saline, 30 mg/kg, 45 mg/kg or 60 mg/kg of RCL-01 in 1 ml total volume (Figure 5.1.). Treatments were administered through tail vein injections with 26-gauge 1ml syringes (BD PlastiPak, Ireland). For this, the animals were placed under anaesthetic with 3% isoflurane for no more than 5 minutes and injected with treatments or controls.

As the injection time of IONP can be critical to the development of any potential hypersensitive affects [289], this was kept consistent as best as possible to between 90 – 120 seconds for each injection. Following injection, each animal was monitored for two hours or until full recovery. The animals were housed randomly post injection in groups of four with weight and severity scores taken 0.5, 1 and 2 hours post injection and then every day until study completion (7 days), where they are euthanised via anaesthetic and cardiac perfusion. The severity score system used was approved by HPRA and described in Supplementary Figure 8. Finally, the liver, spleen, lungs and kidney were harvested, weighed and sampled for both ICP-MS and histological analysis.
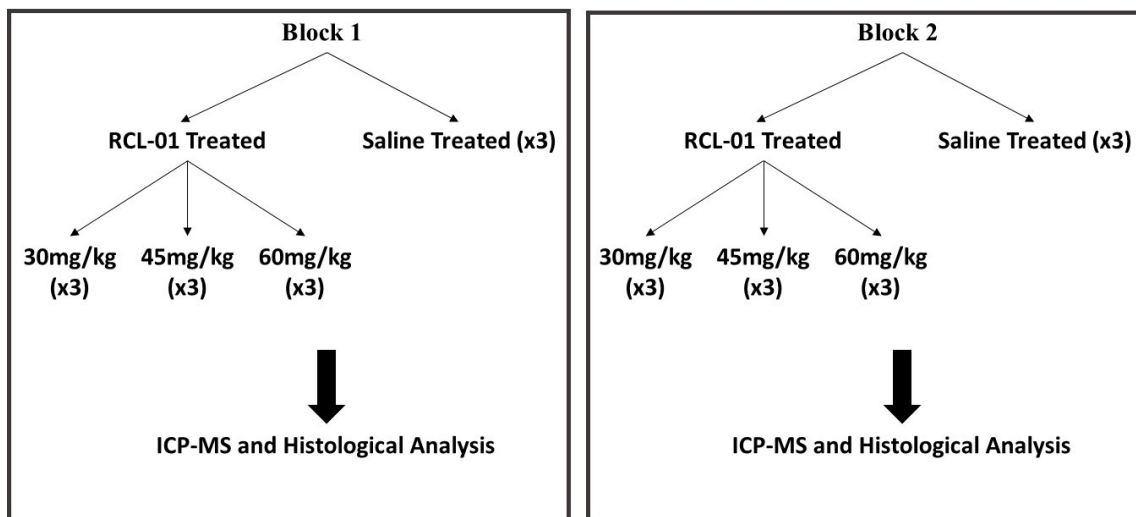
Figure 5.1. *In vivo* study summary.

This study was divided into two identical blocks. In each block, animals are treated in triplicate with either saline, 30 mg/kg, 45 mg/kg or 60 mg/kg of RCL-01. After 7 days, the animals are euthanized, and their organs are processed to determine iron accumulation (ICP-MS) and organ damage (histological analysis).

5.4.3. Organ processing

Following organ sampling, each tissue is dissolved in 67-69 % trace-element nitric acid (Fischer Scientific, UK) at a concentration that is ten times the weight of the sample (i.e. 1 g of tissue would be dissolved in 10 ml nitric acid) in 15 ml tubes with colourless caps (Eppendorf, UK). [Note: Caps with colours contain metals including iron that can dissolve in acid and interfere with the analysis]. The tubes are then heated to 60 °C and left overnight to dissolve. The dissolved samples are then diluted into trace-element water (Fischer Scientific, UK) to a total volume of 5 ml for subsequent ICP-MS analysis.

5.4.4. ICP-MS

Following organ processing, all samples were sent to the London Metallomics Facility at Kings College London for ICP-MS analysis using the NexION 350D. The procedure involved a seven standard calibration curve between 1 µg/L and 10,000 µg/L and negative controls every twenty samples as an internal quality control.

5.4.5. Statistics

All statistical analysis was done using GraphPad 7. Data presented with error bars describes the mean ± standard deviation. All results represent n=6 per treatment group. Severity score is analysed using a two-way ANOVA followed by a Dunnett's test.

5.5. Results

5.5.1. Nanoparticle characterization

RCL-01 characterisation data has been described previously in chapter 4. In addition to the previous data, the suppliers also provided data for ILP and microorganism contamination which is included in the table below (Table 6).

Table 6. Summary of RCL-01 characterization.

Values for size distribution, zeta potential (pH = 7), endotoxin and microorganism contamination and ILP are provided within (see Supplementary Figure 5 for NTA and DLS graphs). Endotoxin contamination was assessed using the gel clot assay. Microorganism contamination and intrinsic loss power was provided by the supplier: Resonance Circuits Limited. Values represent mean± standard deviation. Abbreviations: NTA, nanoparticle tracking analysis; DLS, dynamic light scattering; EU, endotoxin unit; CFU, colony forming units.

Measured Parameter	Value
Mean size (NTA)	128.1 ± 13.2 nm
Mean size (DLS)	115.4 nm
Polydispersity index (DLS)	0.250
Endotoxin level (Gel clot)	0.006 EU/mg
Zeta potential (DLS)	-5.72 ± 0.152 mV
Microorganism contamination	<1 CFU
Intrinsic loss power	5.7 nHm^2kg^{-1}

5.5.2. Body weight

Negligible changes in body weight were observed for all treatments up to 7 days post injection (Figure 5.2.).
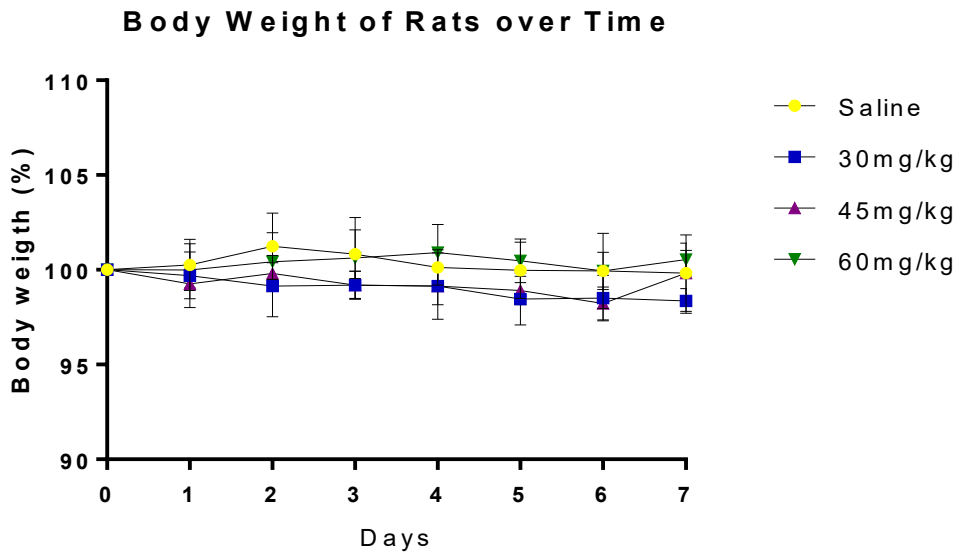
Figure 5.2. Body weight of rats each day post injection.

Changes in body weight of rats is given as a percentage of weight recorded at time zero. Each data point represents the mean with error bars indicating standard deviation. n=6 for each treatment.

5.5.3. Severity score

All animals injected with saline or 30 mg/kg recovered swiftly after the anaesthetic and showed no signs of suffering. Following injections with concentrations of 45 mg/kg and 60 mg/kg, however, the rats were slower to recover from the anaesthetic and displayed a considerable drop in mobility. Additionally, these same animals underwent a dramatic drop in body temperature up to 1 hour post injection, and also produced soft stools throughout this time. Piloerection and arching of the back could also be observed with these animals. Of particular note, one animal treated at the highest dose (60 mg/kg) showed delayed, heavy breathing and was completely unresponsive for 30 minutes post injection. Importantly, all animals went on to make a full recovery within 2 hours (Figure 5.3. and Table 7).

Severity Score Post Injection

Legend:
- Saline
- 30mg/kg
- 45mg/kg
- 60mg/kg
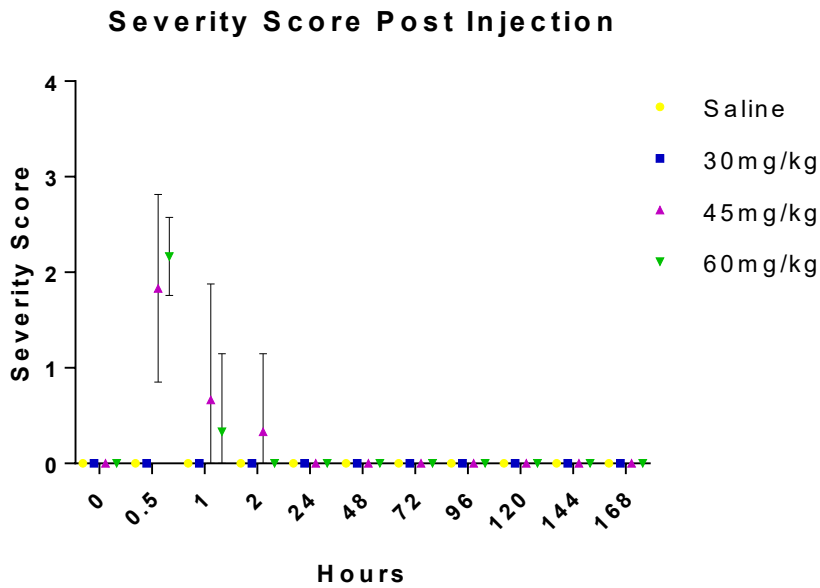
Figure 5.3. Severity score of rats post injection.

Changes in rat severity scores over time. Each coloured dot represents the mean severity score of a treatment group at a particular time point. Error bars represent standard deviation. Severity scores were taken regularly post-injection (0.5, 1 and 2 hours post injection), and then daily after 24 hours. n=6 for each treatment.

Table 7: Statistical analysis of severity scores in rats.

Summary of significance in severity scores of nanoparticle-treated rats against saline-treated controls. n=6 for each treatment. Analysed with two-way ANOVA followed by Dunnett's test for multiple comparisons. P*** < 0.001; P**** < 0.0001. Abbreviations: NS, not significant.

Hours post injection	30mg/kg	45mg/kg	60mg/kg
0	NS	NS	NS
0.5	NS	****	****
1	NS	***	NS
2	NS	NS	NS
24	NS	NS	NS
48	NS	NS	NS
72	NS	NS	NS
96	NS	NS	NS
120	NS	NS	NS
144	NS	NS	NS
168	NS	NS	NS

5.5.4. Levels of iron in organs

A dose dependant increase in iron concentrations in the liver and spleen was observed in treated animals after 7 days. This was not observed in the kidneys or lungs (Figure 5.4.).
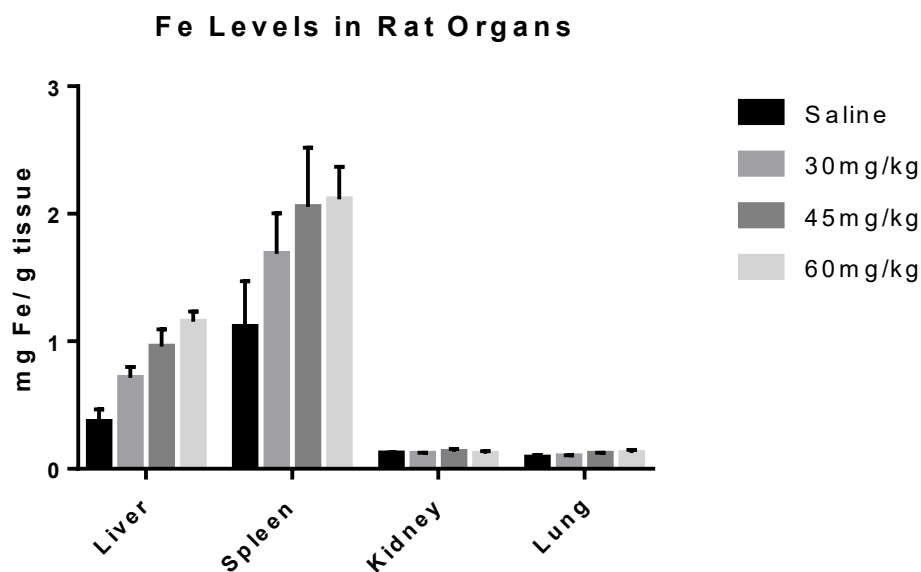
Figure 5.4. Levels of iron in rat organs 7 days post injection.

Levels of iron in organs of rats displayed as mean± standard deviation. n=6 for each treatment.

5.6. Discussion

RCL-01 nanoparticles were characterized in previous chapters and shown to have low levels of endotoxin and microorganism contamination making them suitable for clinical applications in this regard. Noteworthy, these nanoparticles also have a considerably higher ILP value than the fluidMAG/C11-D nanoparticles described in Chapter 2 (1.4 versus 5.7 nHm^2kg^{-1}), meaning a smaller concentration of these nanoparticles would be needed to achieve the desired temperature elevations *in vivo*.

Following injection, the animals exposed to concentrations of 45 mg/kg and 60 mg/kg experienced a slower recovery after anaesthetic than the saline treated and 30 mg/kg treated animals, although all rats eventually recovered fully. Most of the 45 mg/kg and 60 mg/kg treated groups had a significant reduction in mobility, a noticeable drop in temperature and soft stools up to 30 minutes post injection. Additionally, up to 1 hour post injection the rats also showed signs of discomfort through arching of the back and piloerection. In one notable case, one rat treated with 60 mg/kg was completely unresponsive for 30 minutes post injection and showed signs of acute dyspnea, but then went on to make a full recovery (Figure 5.3.). Additionally, body weight measurements confirmed this full recovery with all animals displaying negligible changes at each day of the study (Figure 5.2.). Based on these results, it would suggest that hypersensitive effects occur at doses starting from 45 mg/kg in rats. Interestingly, the concentrations of IONP injected intravenously here are one the highest reported in the literature. To the best of our knowledge, *in vivo* studies in the literature similar to this have tested a maximum concentration of 30 mg/kg in rats and 50-60 mg/kg in mice [286, 288, 290].

Organ accumulation was measured through ICP-MS and both spleen and liver were shown to have dose-dependent increases in iron levels after seven days (Figure 5.4.). Accumulation at these sites is commonly observed with nanoparticles as they are in the same size range of viruses and other nanoparticles naturally present in the air, water and food that living organisms have always been exposed to. Therefore, our immune system has evolved ways of overcoming potential toxic effects associated with their exposure, and so nanoparticles inherently face this hurdle [291, 292]. As mentioned in section 1.4., nanoparticles become immediately covered with serum-derived proteins when they reach the circulation. Of these proteins, opsonins (including complement proteins) bind to nanoparticles and act as signals for phagocytosis and clearance by the mononuclear phagocyte system. Once internalised, the nanoparticles are then directed to organs of the reticuloendothelial system (liver, spleen, lymph nodes and bone marrow) which

macrophages readily localise to [293]. It can therefore be suggested that when the RCL-01 nanoparticles were injected intravenously they become covered in opsonins, internalised by the MPS and cleared from the blood over time into the liver and spleen. In addition to these ICP-MS measurements, histological analysis is ongoing within our group to determine whether this accumulation subsequently results in organ damage.

Furthermore, to fully investigate the manifestation of hypersensitive effects with these nanoparticles - and the doses at which they occur- further haematological and biochemical evaluation is required. Pigs have been shown to be the most relevant animal model for assessing hypersensitive effects [203]. This study would provide information on changes to blood pressure, blood cell count and inflammatory and allergy markers that would be the most relevant predictor of potential acute effects in humans [294].

5.7. Conclusion

The lead IONP with low levels of endotoxin and microorganism contamination and high ILP values was assessed for its acute systemic effects in Wistar rats. As IONP are known for inducing hypersensitive effects in the clinic, it is imperative to assess acute infusion reactions as part of their preclinical assessment. A single, high dose of these IONP were injected intravenously with the aim of determining doses at which hypersensitive reactions occur. Symptoms of hypersensitive reactions were observed in the majority of rats injected with concentrations of 45 mg/kg and 60 mg/kg. Moreover, iron levels in organs were measured after the study and a dose-dependent increase in iron was observed in both the liver and spleen of treated animals. Histological analysis by our group will reveal whether this accumulation coincides with any associative organ damage. Additionally, assessing these acute toxicities further in pigs would provide the most reflective data to the expected hypersensitive effects in humans.

6. Overall Conclusion

FluidMAG/C11-D IONP were characterized and assessed for their ability to treat BxPC-3 cells with magnetic hyperthermia. In this chapter, it was discovered that extracellular hyperthermia was shown to effectively kill cells through necrosis, whereas intracellular hyperthermia was shown to have no role in treatment efficacy.

Following successful efficacy data *in vitro*, these nanoparticles were tested for endotoxin contamination. The nanoparticles were found to have high levels of endotoxin which would make them unsuitable for clinical applications as they did not satisfy regulatory requirements for a medical device. Following this result, a large amount of superparamagnetic IONP were screened for endotoxin contamination in an effort to find a lead nanoparticle to take into preclinical assessment. Subsequently, new lead IONP was identified and found to have lower levels of endotoxin than a clinical approved IONP control. In parallel to this, the laboratory began doing endotoxin assessment of nanoparticles from a variety of sources included academia, industry, in-house and nanoparticles submitted for evaluation with the EUNCL. During this work, a total of 21 nanoparticles were tested for endotoxin contamination, with 9 having unsatisfactory levels, emphasising the significance of this issue across-the-board.

As IONP are well known to induce hypersensitive effects related to complement activation, the lead nanoparticle was tested for complement activation in human serum and compared against a clinically approved and contaminated IONP control. A dose was identified for the lead nanoparticle where complement activation stops occurring.

Finally, an *in vivo* safety assessment was undertaken to determine any potential hypersensitive effects that are observed *in vivo* with these nanoparticles, and at what doses these effects occur. Rats were injected intravenously with high doses of the lead nanoparticle and, once again, a window was identified where their hypersensitive effects stop occurring.

The characterization data generated with the lead IONP, along with the endotoxin, complement activation and *in vivo* assessments, will contribute to the clinical trial dossier for this lead nanoparticle (figure 6.1.).

Translational Considerations for Nanomedicines
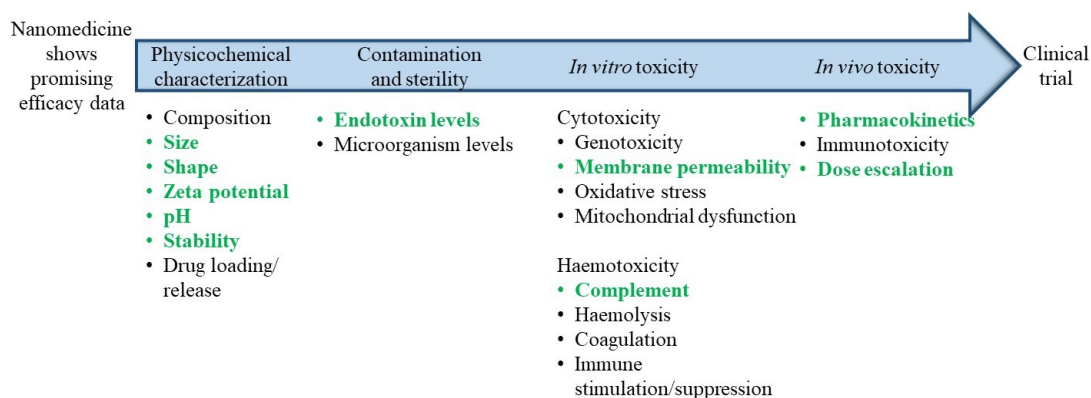
Figure 6.1. Contribution to the translation of a nanomedicine to the clinic.

Reproduced from figure 1.13. in the introduction is the work this thesis has contributed to in relation to the translation of an IONP to a clinical trial (highlighted in green). Size, shape, zeta potential, pH and stability were assessed for multiple nanoparticles during the initial characterization step. Magnetic hyperthermia proved efficient at inducing membrane permeability *in vitro*. An endotoxin screen was performed on many nanoparticles to identify a new lead that would satisfy regulatory requirements. This lead IONP was assessed for complement activation, along with clinical and positive controls. Finally, the nanoparticle was tested for safety *in vivo*.

7. Future Work

Following this work, further *in vivo* safety and efficacy studies are necessary to generate the clinical data required for a clinical trial. These studies are ongoing with our collaborators of the NoCanTher project and aim to answer questions related to the right temperatures to use, their duration and how they can be best incorporated into the conventional treatment regime for PDAC to ensure maximum overall efficacy.

An *in vivo* safety study that would shed light on the true hypersensitive effects associated with the lead IONP would involve assessment in pigs. Pigs have been shown to be the most sensitive and relevant model for evaluation of hypersensitive effects with nanomedicines and other pharmaceuticals [203]. This model can provide haematological (pulmonary arterial pressure, systemic arterial pressure, O_2 saturation and blood cell count), biochemical (inflammatory and allergy marker analysis) and skin rash analysis which enables a relevant dose to be established at which hypersensitive effects can occur [294].

One important efficacy experiment would be to assess the inhibition of DNA repair mechanisms in PDAC tumours following magnetic hyperthermia and how combination treatments can be used to take full advantage of this effect. As discussed in section 1.2.2.3., magnetic hyperthermia can inhibit DNA repair mechanisms in cells, and this response may vary depending on treatment temperatures, durations and the cells involved. Mutations to DNA repair genes occur in 10-33% of metastatic PDAC cases, with alterations to BRCA1 and BRCA2 genes being the most prevalent and occurring in both germline and sporadic forms of PDAC [295, 296]. Interestingly, clinical trials have shown encouraging results with BRCA-mutated PDAC treated with platinum drugs in combination with PARP inhibitors [297]. As previously discussed, hyperthermia and PARP inhibition could induce synthetic lethality *in vivo*, prolonging survival in both cancer models [121]. If magnetic hyperthermia is optimised to inhibit BRCA1 or BRCA2 signalling in PDAC (through a screen of different temperatures and durations), it could be combined with PARP inhibitors and chemotherapies that generate double stranded breaks (platinum drugs) with the hopes inducing synthetic lethality in DNA repair and active, irreparable DNA damage in the cancer. Likewise, if PDAC harbours BRCA mutations, magnetic hyperthermia alone may induce synthetic lethality on this pathway, and so combination with chemotherapy may induce the same effect in this case.

Another avenue yet to be fully exploited is the potential of magnetic hyperthermia to induce an anti-tumour immune response. As mentioned in section 1.2.2.5., most *in vivo* efficacy studies with magnetic hyperthermia use immunocompromised mice which may undervalue the immunostimulatory effects of this treatment. Available literature lends weight to a potential anti-tumour immune response following magnetic hyperthermia which needs to be explored further in relevant models [81, 132]. *In vivo* cancer models with immunocompetent mice are required to shed light on this effect, with immunophenotyping of tumours necessary to decipher the immune infiltrate following treatment. Additionally, once the mechanism by which the immune response is understood, this could provide indications to potential immunotherapies that could be combined with this treatment.

Finally, establishing the parameters necessary to improve vascular perfusion and reduce tumour stiffness simultaneously will give combination therapies the best chance of success following magnetic hyperthermia treatment. Important factors to consider in this case is the fact that achieving both effects at the same temperature and duration will take considerable optimisation and mathematical modelling may be required. Additionally, as both effects are transient, treatment timepoints will be an essential consideration to fully capitalise on these effects within a narrow time window.

8. Supplementary Data

Supplementary Figure 1: Nanoparticle tracking analysis, dynamic light scattering and transmission electron microscopy graphs for fluidMAG/C11-D.

A.

B.

C.

D.
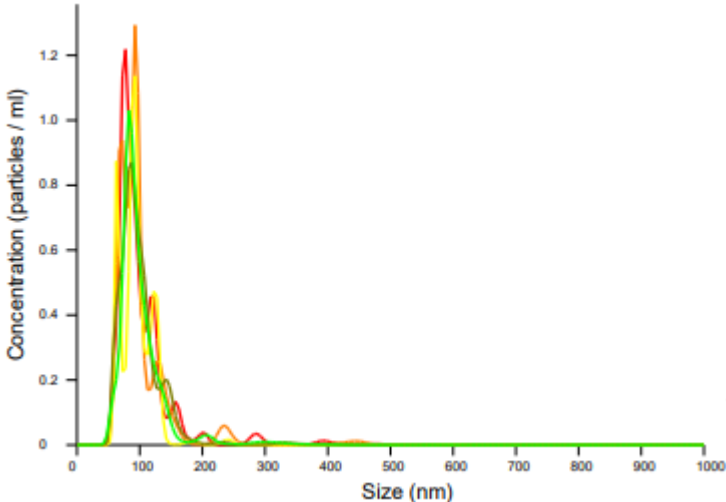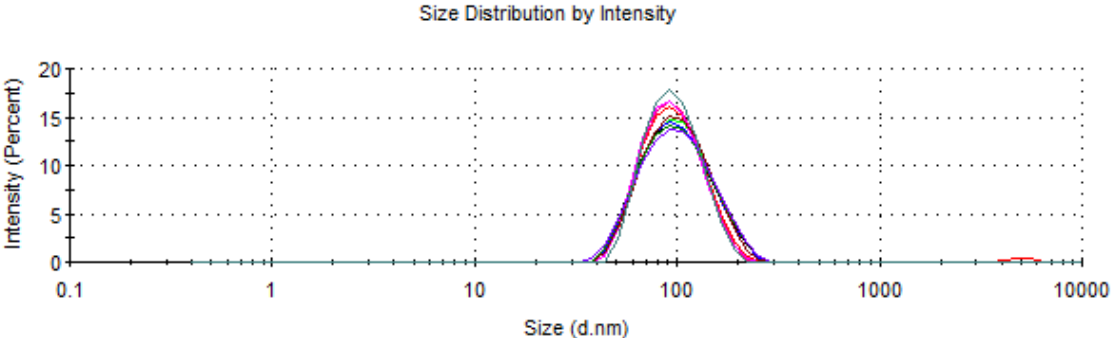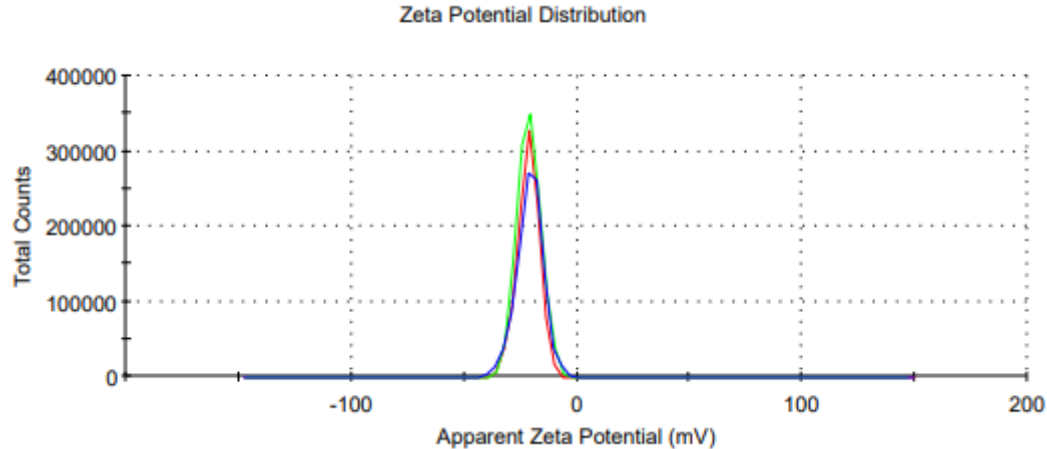
Size distribution of FluidMAG C11-D

A. Nanoparticle tracking analysis size versus concentration graph. Here, the nanoparticles were diluted to 10 µg/ml in particle- free water (Sigma Aldrich, Ireland) and analysed through 5, 60 second recordings. B. Dynamic light scattering graphs depicting size distribution and apparent zeta potential at pH 7. Zeta potential data was provided by the suppliers, Chemicell (C). For size measurements with DLS, the nanoparticles were diluted to 50 µg/ml in particle-free water. The nanoparticles are then analysed with 10 measurements of 12 runs. D. Size distribution graph of 200 individual nanoparticles imaged via transmission electron microscopy and analysed through ImageJ software.

Supplementary Figure 2: Nanoparticle shows little interference with APC or PerCP-Cy5.5 channels.
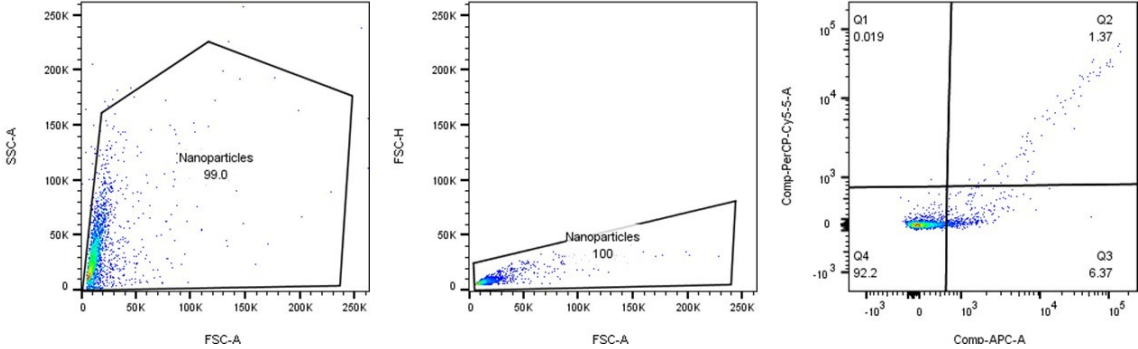
After gating for 99% of nanoparticles, less than 10% of the population were shown to interfere with APC and PerCP- Cy5.5 channels. It is also important to note that care was taken to avoid any nanoparticles when gating BxPC-3 cells in these experiments.

Supplementary Figure 3: Gating strategy for BxPC-3 cells
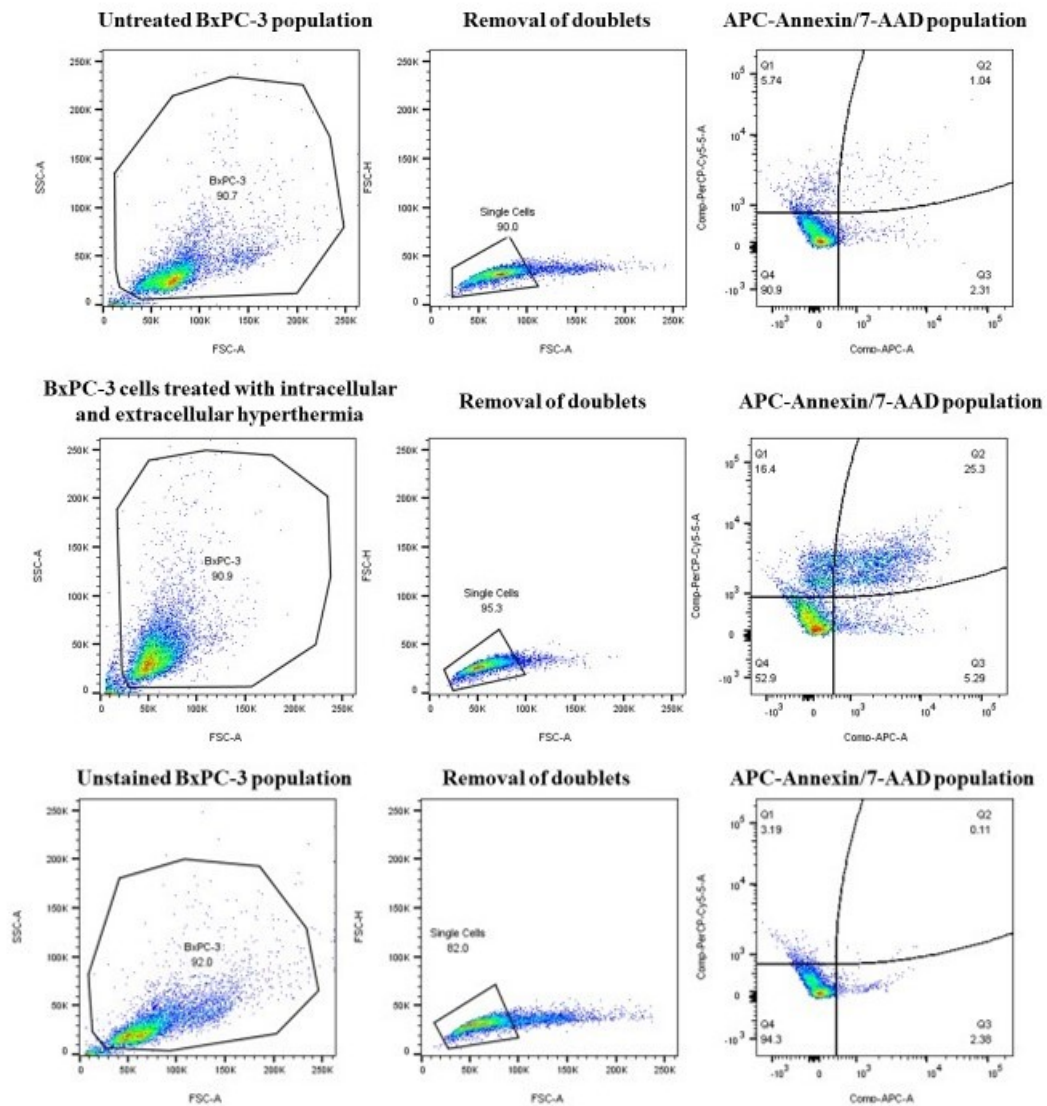
BxPC-3 treated with nanoparticles were gated to ensure nanoparticle avoidance. Doublets are removed through forward scatter height versus forward scatter area. BxPC-3 cells APC⁻/PerCP-Cy5-5⁻ were considered vital, APC⁺/PerCP-Cy5-5⁻ were considered early apoptotic, APC⁺/PerCP-Cy5-5⁺ were considered late apoptotic and APC⁻/PerCP-Cy5⁻5+ were considered necrotic.

Supplementary Figure 4: Annexin V/ 7- AAD staining of cells treated with incubator hyperthermia (42.5 °C for 30 minutes) versus untreated.
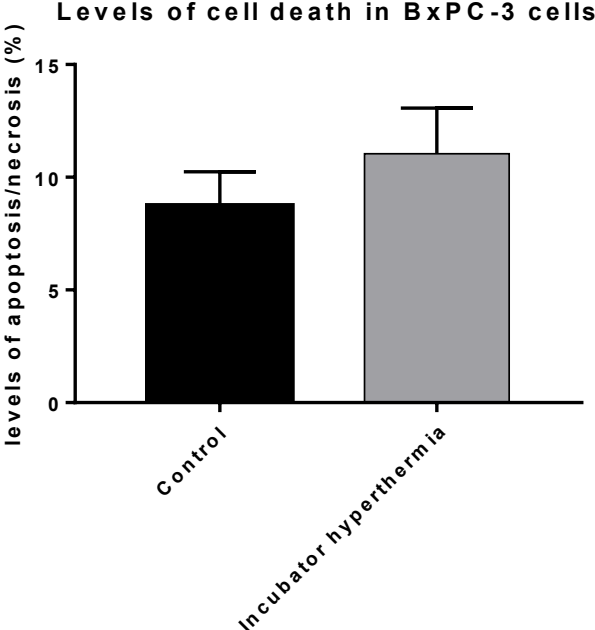
The levels of apoptosis and necrosis in incubator heated cells were not significantly different to untreated cells. n=5 (triplicate). Analysed with unpaired t-test.

Supplementary Figure 5: Nanoparticle tracking analysis and dynamic light scattering measurements for RCL-01.

A.
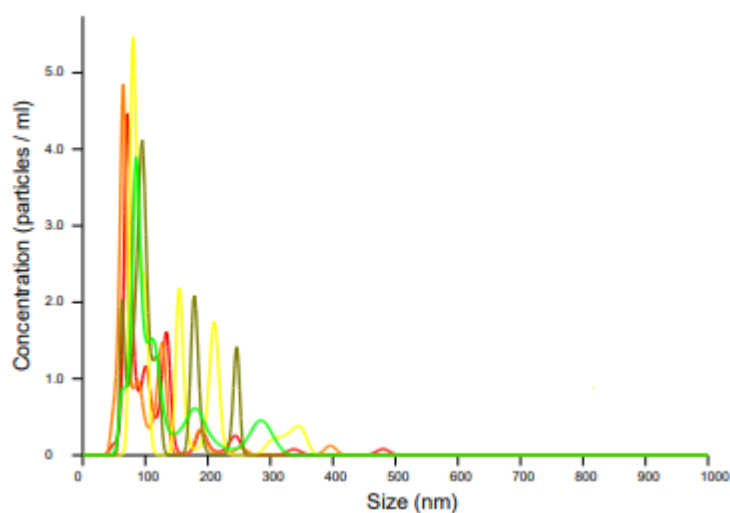
B.
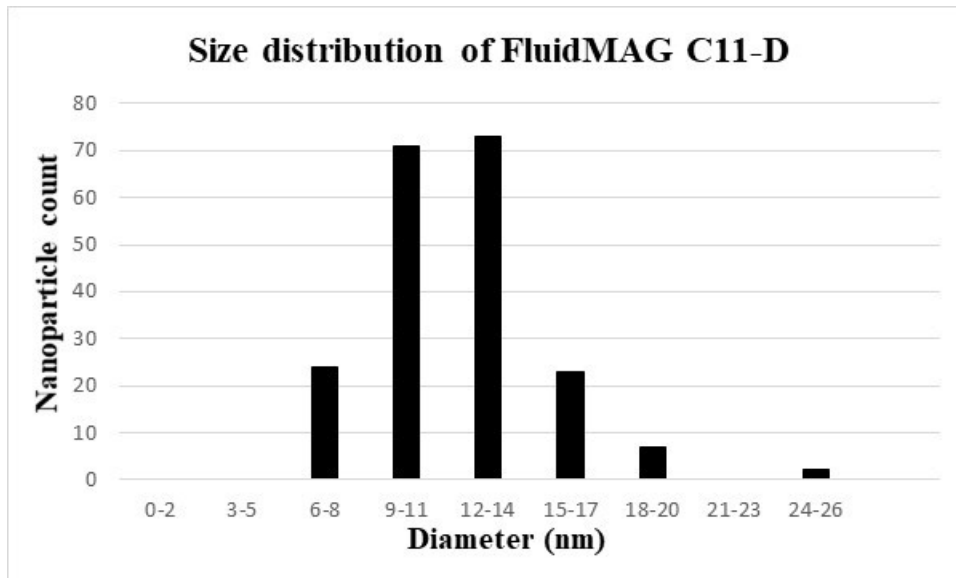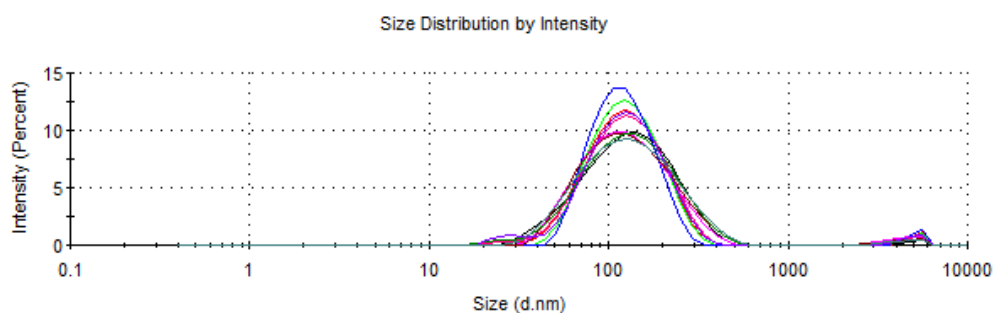

C.
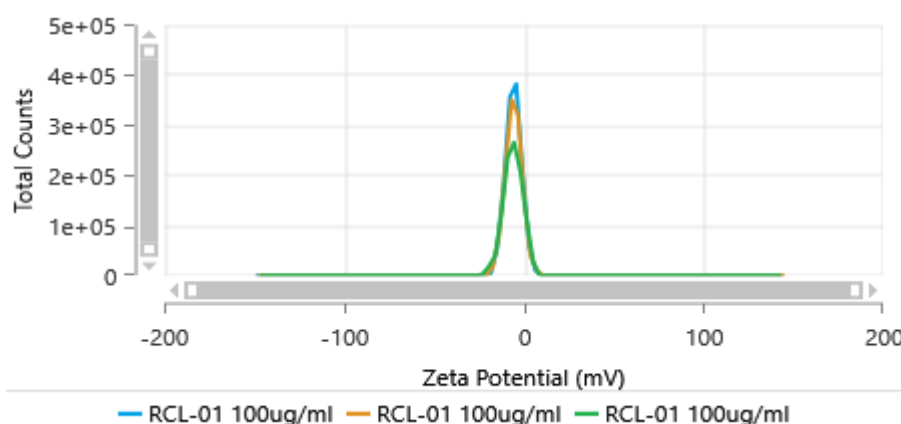

A. Nanoparticle tracking analysis size versus concentration graph. The nanoparticles were diluted to 0.0076 µg/ml in particle-free water and analysed with 5, 60 second recordings. B. Dynamic light scattering size versus intensity graph. The nanoparticles were diluted to 30 µg/ml and analysed with 10 measurements of 12 runs. C. Dynamic light scattering counts versus apparent zeta potential graph (sample pH = 7). The nanoparticles are diluted to 100 µg/ml in particle-free water and analysed with 3 measurements of 100 runs.

Supplementary Figure 6: Nanoparticle tracking analysis and dynamic light scattering measurements for Sienna+®.

A.
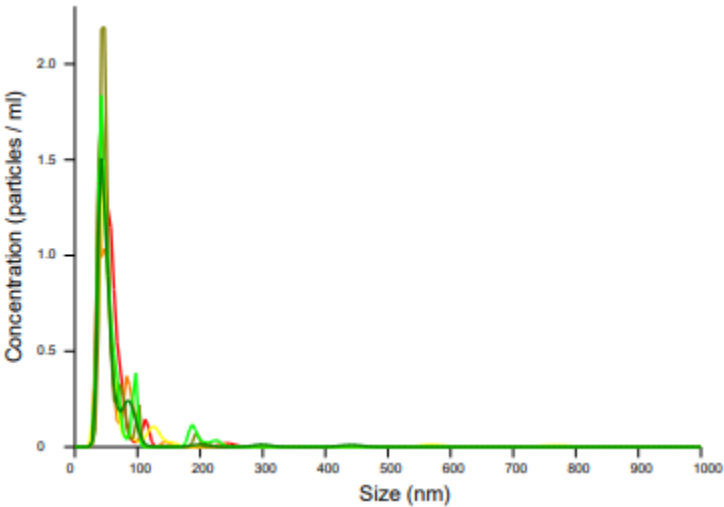
B.
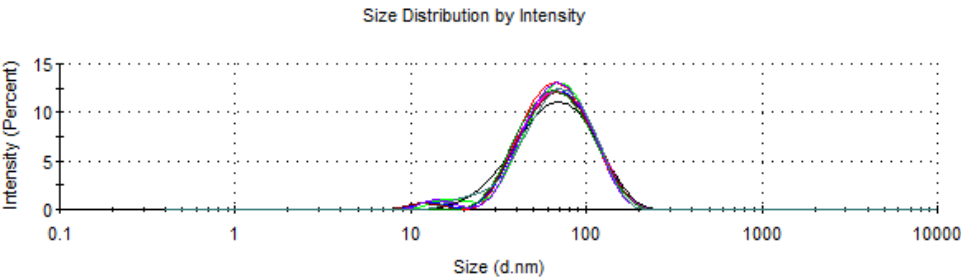
C.
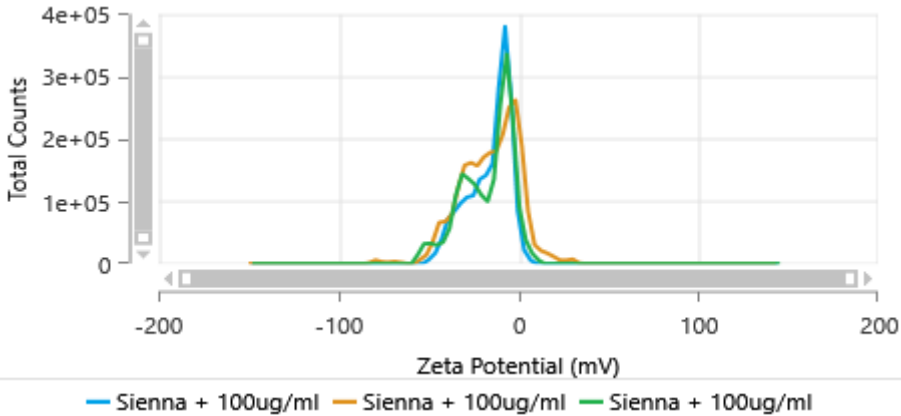
A. Nanoparticle tracking analysis size versus concentration graph. The nanoparticles were diluted to 0.06 µg/ml in particle-free water and analysed with 6, 60 second recordings. B. Dynamic light scattering size versus intensity graph. The nanoparticles were diluted to 30 µg/ml and analysed with 10 measurements of 12 runs. C. Dynamic light scattering counts versus apparent zeta potential graph (sample pH = 7). The nanoparticles are diluted to 100 µg/ml in particle-free water and analysed with 3 measurements of 100 runs.

Supplementary Figure 7: Nanoparticle tracking analysis and dynamic light scattering measurements of NOC-0001.

A.
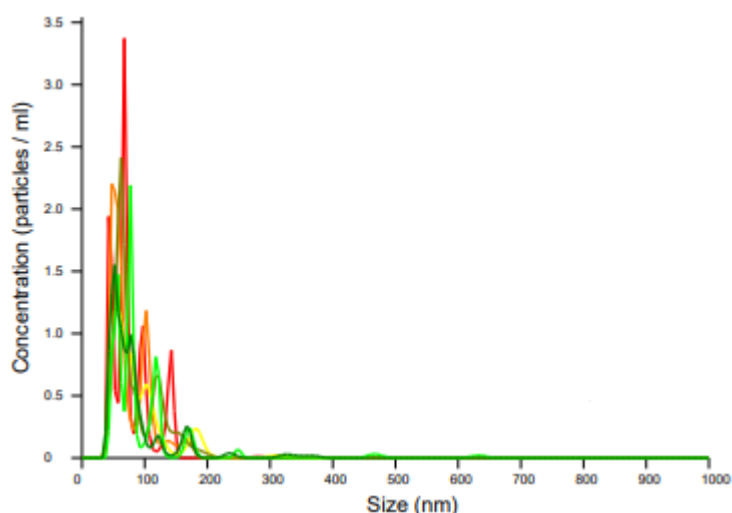
B.
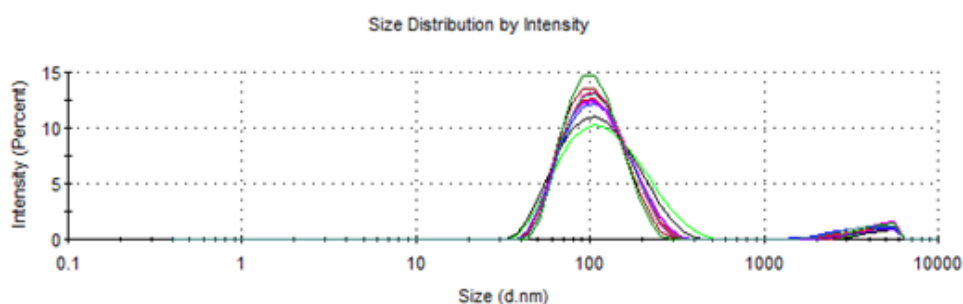
C.
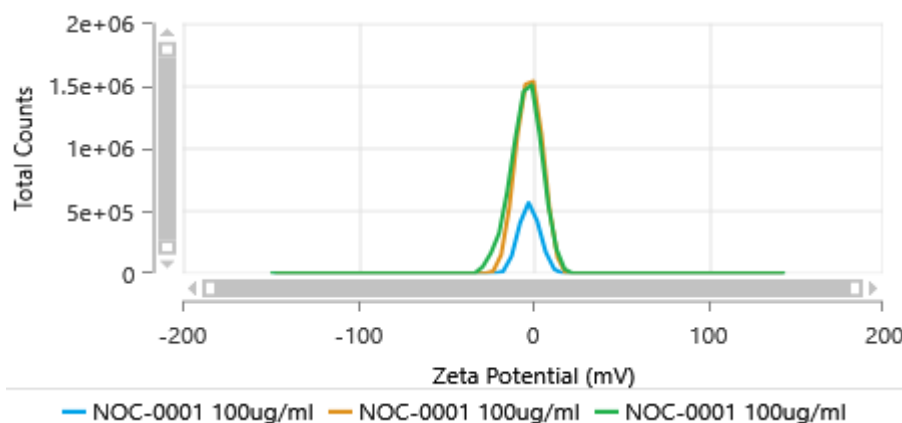
A. Nanoparticle tracking analysis size versus concentration graph. The nanoparticles were diluted to 0.08 µg/ml in particle-free water and analysed with 6, 60 second recordings. B. Dynamic light scattering size versus intensity graph. The nanoparticles were diluted to 50 µg/ml and analysed with 10 measurements of 12 runs. C. Dynamic light scattering counts versus apparent zeta potential graph (sample pH = 7). The nanoparticles are diluted to 100 µg/ml in particle-free water and analysed with 3 measurements of 100 runs.

Supplementary Figure 8: Severity score system for *in vivo* study.

Score	Variables measured	Clinical signs of sickness	Care to be provided
0	1. Body weight 2. Activity 3. Appearance	All clinically normal	Not applicable
1	1. Body weight 2. Activity 3. Appearance/ behaviour	1. Weight loss <10% 2. Decreased 3. Normal, Oculo-nasal discharge	Monitor animal twice daily.
2	1. Body weight 2. Activity 3. Appearance/ behaviour	1. Weight loss >10% 2. Reduced activity 3. Normal, Dehydration, Pilo-erection, Reduced peer interaction, Subdued behaviour	Provide moistened food pellets on floor of the cage. Check body temperature regularly. If suffering persists, the animal will be rehydrated daily with injections of saline. If there are observable signs of pain, 0.05-0.1 mg/kg of buprenorphine will be administered subcutaneously.
3	1. Body weight 2. Activity 3. Temperature 4. Appearance/ behaviour	1. Weight loss >15% 2. Reduced activity 3. Cold when handled 4. Hunched posture, Decrease in grooming behaviour, Diarrhoea	Separate weak rat from stronger animals. Monitor and weigh animal twice a day. Provide water and food by oral gavage to compensate the dehydration and weight loss. A hypothermic animal will be placed in an individual cage under an infrared lamp or a heating pad. If there are observable signs of pain, 0.05-0.1 mg/kg of buprenorphine will be administered subcutaneously.

| 4 | 1. Body weight
2. Activity
3. Temperature
4. Appearance/ behaviour
5. Appetite | 1. Weight loss >20%
2. Reduced activity
3. Persistent hypothermia
4. Hunched posture, Hind-limb paralysis or weakness, visible signs of anaemia
5. Inability to obtain food & water | This animal must be euthanized immediately.
It will be humanely sacrificed with CO_2 followed by post mortem analysis. |

This table describes a scoring system of 0 to 4 based on weight changes and observable signs of suffering or discomfort in the animals. Depending on the score of the animal, appropriate action was taken which is described in the far-right column. The animals were weighed prior to injection and this formed the baseline for subsequent scoring daily, on top of visible behavioural/appearance changes. Following injection, the animals were observed closely for two hours (or until full recovery). At no point in this study did any animal have a score of four. Three animals scored had a score of three after injection, however all animals completely recovered within three hours.

9. Bibliography

1.   Adamska, A., A. Domenichini, and M. Falasca, *Pancreatic Ductal Adenocarcinoma: Current and Evolving Therapies.* International journal of molecular sciences, 2017. **18**(7): p. 1338.
2.   Becker, A.E., et al., *Pancreatic ductal adenocarcinoma: risk factors, screening, and early detection.* World journal of gastroenterology, 2014. **20**(32): p. 11182-11198.
3.   Ying, H., et al., *Genetics and biology of pancreatic ductal adenocarcinoma.* Genes & development, 2016. **30**(4): p. 355-385.
4.   Páez, D., et al., *Pancreatic cancer: medical management (novel chemotherapeutics).* Gastroenterology clinics of North America, 2012. **41**(1): p. 189-209.
5.   Sun, H., et al., *Survival improvement in patients with pancreatic cancer by decade: a period analysis of the SEER database, 1981-2010.* Scientific reports, 2014. **4**: p. 6747-6747.
6.   Ilic, M. and I. Ilic, *Epidemiology of pancreatic cancer.* World journal of gastroenterology, 2016. **22**(44): p. 9694-9705.
7.   Oberstein, P.E. and K.P. Olive, *Pancreatic cancer: why is it so hard to treat?* Therapeutic advances in gastroenterology, 2013. **6**(4): p. 321-337.
8.   Rahib, L., et al., *Projecting Cancer Incidence and Deaths to 2030: The Unexpected Burden of Thyroid, Liver, and Pancreas Cancers in the United States.* Cancer Research, 2014. **74**(11): p. 2913-2921.
9.   Liang, C., et al., *Complex roles of the stroma in the intrinsic resistance to gemcitabine in pancreatic cancer: where we are and where we are going.* Experimental &Amp; Molecular Medicine, 2017. **49**: p. e406.
10.   Ansari, D., et al., *Pancreatic cancer stroma: controversies and current insights.* Scandinavian Journal of Gastroenterology, 2017. **52**(6-7): p. 641-646.
11.   Whatcott, C.J., et al., *Desmoplasia and chemoresistance in pancreatic cancer.* 2012.
12.   Ferdek, P.E. and M.A. Jakubowska, *Biology of pancreatic stellate cells-more than just pancreatic cancer.* Pflugers Archiv : European journal of physiology, 2017. **469**(9): p. 1039-1050.
13.   Moffitt, R.A., et al., *Virtual microdissection identifies distinct tumor- and stroma-specific subtypes of pancreatic ductal adenocarcinoma.* Nature genetics, 2015. **47**(10): p. 1168-1178.
14.   Weniger, M., K.C. Honselmann, and A.S. Liss, *The Extracellular Matrix and Pancreatic Cancer: A Complex Relationship.* Cancers, 2018. **10**(9): p. 316.
15.   Gouirand, V. and S. Vasseur, *Fountain of youth of pancreatic cancer cells: the extracellular matrix.* Cell Death Discovery, 2018. **4**(1): p. 1.
16.   Cannon, A., et al., *Desmoplasia in pancreatic ductal adenocarcinoma: insight into pathological function and therapeutic potential.* Genes & cancer, 2018. **9**(3-4): p. 78-86.
17.   Koong, A.C., et al., *Pancreatic tumors show high levels of hypoxia.* International Journal of Radiation Oncology*Biology*Physics, 2000. **48**(4): p. 919-922.
18.   Michalski, C.W., et al., *Tumor metabolism to blood flow ratio in pancreatic cancer: helpful in patient stratification?* Future Oncology, 2010. **6**(1): p. 13-15.
19.   Lee, H.S. and S.W. Park, *Systemic Chemotherapy in Advanced Pancreatic Cancer.* Gut and liver, 2016. **10**(3): p. 340-347.

20. Hazard, L., *The role of radiation therapy in pancreas cancer.* Gastrointestinal cancer research : GCR, 2009. **3**(1): p. 20-28.

21. Wolfgang, C.L., et al., *Recent progress in pancreatic cancer.* CA: a cancer journal for clinicians, 2013. **63**(5): p. 318-348.

22. Roy, R. and A. Maraveyas, *Chemoradiation in Pancreatic Adenocarcinoma: A Literature Review.* The Oncologist, 2010. **15**(3): p. 259-269.

23. Samandari, M., et al., *Liquid Biopsies for Management of Pancreatic Cancer.* Translational Research, 2018. **201**: p. 98-127.

24. Zhang, Y., et al., *Novel agents for pancreatic ductal adenocarcinoma: emerging therapeutics and future directions.* Journal of hematology & oncology, 2018. **11**(1): p. 14-14.

25. Ahn, D.H. and R.K. Ramanathan, *Targeting the stroma in pancreatic cancer.* Chinese Clinical Oncology, 2017. **6**(6).

26. Feig, C., et al., *The pancreas cancer microenvironment.* Clinical cancer research : an official journal of the American Association for Cancer Research, 2012. **18**(16): p. 4266-4276.

27. Xiong, H.Q. and J.L. Abbruzzese, *Chapter 35 - Molecular Pathogenesis of Pancreatic Adenocarcinoma*, in *The Molecular Basis of Cancer (Third Edition)*, J. Mendelsohn, et al., Editors. 2008, W.B. Saunders: Philadelphia. p. 455-461.

28. Walter, K., et al., *Overexpression of smoothened activates the sonic hedgehog signaling pathway in pancreatic cancer-associated fibroblasts.* Clinical cancer research : an official journal of the American Association for Cancer Research, 2010. **16**(6): p. 1781-1789.

29. Bai, Y., et al., *Hedgehog Signaling in Pancreatic Fibrosis and Cancer.* Medicine, 2016. **95**(10): p. e2996-e2996.

30. Pasca di Magliano, M. and M. Hebrok, *Hedgehog Signaling Pathways in Pancreatic Cancer Pathogenesis*, in *Pancreatic Cancer*. 2010, Springer New York: New York, NY. p. 403-418.

31. Mpekris, F., et al., *Sonic-hedgehog pathway inhibition normalizes desmoplastic tumor microenvironment to improve chemo- and nanotherapy.* Journal of controlled release : official journal of the Controlled Release Society, 2017. **261**: p. 105-112.

32. Olive, K.P., et al., *Inhibition of Hedgehog signaling enhances delivery of chemotherapy in a mouse model of pancreatic cancer.* Science (New York, N.Y.), 2009. **324**(5933): p. 1457-1461.

33. Roy Chaudhuri, T., et al., *Tumor-Priming Smoothened Inhibitor Enhances Deposition and Efficacy of Cytotoxic Nanoparticles in a Pancreatic Cancer Model.* Molecular cancer therapeutics, 2016. **15**(1): p. 84-93.

34. Catenacci, D.V.T., et al., *Randomized Phase Ib/II Study of Gemcitabine Plus Placebo or Vismodegib, a Hedgehog Pathway Inhibitor, in Patients With Metastatic Pancreatic Cancer.* Journal of clinical oncology : official journal of the American Society of Clinical Oncology, 2015. **33**(36): p. 4284-4292.

35. Theocharis, A.D., et al., *Pancreatic carcinoma is characterized by elevated content of hyaluronan and chondroitin sulfate with altered disaccharide composition.* Biochimica et Biophysica Acta (BBA) - Molecular Basis of Disease, 2000. **1502**(2): p. 201-206.

36. Kultti, A., et al., *Accumulation of Extracellular Hyaluronan by Hyaluronan Synthase 3 Promotes Tumor Growth and Modulates the Pancreatic Cancer Microenvironment.* BioMed Research International, 2014. **2014**: p. 15.

37. Cheng, X.-B., et al., *Hyaluronan stimulates pancreatic cancer cell motility.* Oncotarget, 2015. **7**(4): p. 4829-4840.

38. Provenzano, P.P., et al., *Enzymatic targeting of the stroma ablates physical barriers to treatment of pancreatic ductal adenocarcinoma.* Cancer cell, 2012. **21**(3): p. 418-429.

39. Doherty, G.J., M. Tempero, and P.G. Corrie, *HALO-109–301: a Phase III trial of PEGPH20 (with gemcitabine and nab-paclitaxel) in hyaluronic acid-high stage IV pancreatic cancer.* Future Oncology, 2018. **14**(1): p. 13-22.

40. Clark, C.E., et al., *Dynamics of the Immune Reaction to Pancreatic Cancer from Inception to Invasion.* Cancer Research, 2007. **67**(19): p. 9518-9527.

41. Daniela, B., *Pancreatic Cancer Fostered Immunosuppression Privileges Tumor Growth and Progression.* Journal of Clinical & Cellular Immunology, 2014. **5**(6): p. 1-16.

42. Ikemoto, T., et al., *Clinical Roles of Increased Populations of Foxp3+CD4+ T Cells in Peripheral Blood from Advanced Pancreatic Cancer Patients.* Pancreas, 2006. **33**(4): p. 386-390.

43. Hiraoka, N., et al., *Prevalence of FOXP3+ Regulatory T Cells Increases During the Progression of Pancreatic Ductal Adenocarcinoma and Its Premalignant Lesions.* Clinical Cancer Research, 2006. **12**(18): p. 5423-5434.

44. Nomi, T., et al., *Clinical Significance and Therapeutic Potential of the Programmed Death-1 Ligand/Programmed Death-1 Pathway in Human Pancreatic Cancer.* Clinical Cancer Research, 2007. **13**(7): p. 2151-2157.

45. Gao, H.-L., et al., *The clinicopathological and prognostic significance of PD-L1 expression in pancreatic cancer: A meta-analysis.* Hepatobiliary & Pancreatic Diseases International, 2018. **17**(2): p. 95-100.

46. Wu, A.A., E. Jaffee, and V. Lee, *Current Status of Immunotherapies for Treating Pancreatic Cancer.* Current Oncology Reports, 2019. **21**(7): p. 60.

47. Hilmi, M., L. Bartholin, and C. Neuzillet, *Immune therapies in pancreatic ductal adenocarcinoma: Where are we now?* World journal of gastroenterology, 2018. **24**(20): p. 2137-2151.

48. Seidel, J.A., A. Otsuka, and K. Kabashima, *Anti-PD-1 and Anti-CTLA-4 Therapies in Cancer: Mechanisms of Action, Efficacy, and Limitations.* Frontiers in oncology, 2018. **8**: p. 86-86.

49. Granier, C., et al., *Mechanisms of action and rationale for the use of checkpoint inhibitors in cancer.* ESMO Open, 2017. **2**(2): p. e000213.

50. Manzur, A., et al., *Nanotechnologies in Pancreatic Cancer Therapy.* Pharmaceutics, 2017. **9**(4): p. 39.

51. Desai, P., et al., *Pancreatic Cancer: Recent Advances in Nanoformulation-Based Therapies.* 2019. **36**(1): p. 59-91.

52. Golombek, S.K., et al., *Tumor targeting via EPR: Strategies to enhance patient responses.* Advanced drug delivery reviews, 2018. **130**: p. 17-38.

53. Au, M., et al., *Emerging Therapeutic Potential of Nanoparticles in Pancreatic Cancer: A Systematic Review of Clinical Trials.* Biomedicines, 2016. **4**(3): p. 20.

54. Adiseshaiah, P.P., et al., *Nanomedicine strategies to overcome the pathophysiological barriers of pancreatic cancer.* Nature Reviews Clinical Oncology, 2016. **13**: p. 750.

55. Saung, M.T. and L. Zheng, *Current Standards of Chemotherapy for Pancreatic Cancer.* Clinical therapeutics, 2017. **39**(11): p. 2125-2134.

56. De Luca, R., et al., *Clinical efficacy of nab-paclitaxel in patients with metastatic pancreatic cancer.* Drug design, development and therapy, 2018. **12**: p. 1769-1775.

57. Kalra, A.V., et al., *Preclinical Activity of Nanoliposomal Irinotecan Is Governed by Tumor Deposition and Intratumor Prodrug Conversion.* Cancer Research, 2014. **74**(23): p. 7003-7013.

58. Chang, T.C., et al., *Phase I study of nanoliposomal irinotecan (PEP02) in advanced solid tumor patients.* Cancer chemotherapy and pharmacology, 2015. **75**(3): p. 579-586.

59. Yardley, D.A., *nab-Paclitaxel mechanisms of action and delivery.* Journal of Controlled Release, 2013. **170**(3): p. 365-372.

60. Drummond, D.C., et al., *Development of a Highly Active Nanoliposomal Irinotecan Using a Novel Intraliposomal Stabilization Strategy.* Cancer Research, 2006. **66**(6): p. 3271-3277.

61. Rebelo, A. and C. Reis, *Emerging therapeutic nanotechnologies in pancreatic cancer: advances, risks and challenges.* Therapeutic Delivery, 2018. **9**(10): p. 691-694.

62. DeNardo, G.L. and S.J. DeNardo, *Update: Turning the heat on cancer.* Cancer biotherapy & radiopharmaceuticals, 2008. **23**(6): p. 671-680.

63. Zhang, P., et al., *Recent Progress in Light-Triggered Nanotheranostics for Cancer Treatment.* Theranostics, 2016. **6**(7): p. 948-968.

64. Beik, J., et al., *Nanotechnology in hyperthermia cancer therapy: From fundamental principles to advanced applications.* Journal of Controlled Release, 2016. **235**: p. 205-221.

65. Chen, F. and W. Cai, *Nanomedicine for targeted photothermal cancer therapy: where are we now?* Nanomedicine (London, England), 2015. **10**(1): p. 1-3.

66. Sohail, A., et al., *A review on hyperthermia via nanoparticle-mediated therapy.* Bulletin du Cancer, 2017. **104**(5): p. 452-461.

67. van der Horst, A., et al., *The clinical benefit of hyperthermia in pancreatic cancer: a systematic review.* International Journal of Hyperthermia, 2018. **34**(7): p. 969-979.

68. MagForce. *https://www.magforce.com/home/.* [cited 2019.

69. Luo S, et al., *Clinical trials of magnetic induction hyperthermia for treatment of tumours.* OA Cancer, 2014. **2**(1): p. 1-6.

70. Glazer, E.S. and S.A. Curley, *The ongoing history of thermal therapy for cancer.* Surgical oncology clinics of North America, 2011. **20**(2): p. 229-vii.

71. Kienle, G.S., *Fever in Cancer Treatment: Coley's Therapy and Epidemiologic Observations.* Global advances in health and medicine, 2012. **1**(1): p. 92-100.

72. Coley, W.B., *End results in hodgkins disease and lymphosarcoma treated by the mixed toxins of erysipelas and bacilllus prodigiosus, alone or combined with radiation* Annals of surgery, 1928. **88**(4): p. 641-667.

73. Kalamida, D., et al., *Fever-range hyperthermia vs. hypothermia effect on cancer cell viability, proliferation and HSP90 expression.* PloS one, 2015. **10**(1): p. e0116021-e0116021.

74. Gilchrist, R.K., et al., *Selective inductive heating of lymph nodes.* Annals of surgery, 1957. **146**(4): p. 596-606.

75. Ito, A., et al., *Magnetite nanoparticle-loaded anti-HER2 immunoliposomes for combination of antibody therapy with hyperthermia.* Cancer Letters, 2004. **212**(2): p. 167-175.

76.   DeNardo, S.J., et al., *Development of Tumor Targeting Bioprobes (^{111}In-Chimeric L6 Monoclonal Antibody Nanoparticles) for Alternating Magnetic Field Cancer Therapy.* Clinical Cancer Research, 2005. **11**(19): p. 7087s-7092s.

77.   Shinkai, M., et al., *Targeting hyperthermia for renal cell carcinoma using human MN antigen-specific magnetoliposomes.* Japanese journal of cancer research : Gann, 2001. **92**(10): p. 1138-1145.

78.   Hilger, I., R. Hergt, and W.A. Kaiser, *Use of magnetic nanoparticle heating in the treatment of breast cancer.* IEE proceedings. Nanobiotechnology, 2005. **152**: p. 33-9.

79.   Hilger, I., et al., *Thermal Ablation of Tumors Using Magnetic Nanoparticles: An In Vivo Feasibility Study.* Investigative Radiology, 2002. **37**(10): p. 580-586.

80.   Hilger, I., et al., *Electromagnetic Heating of Breast Tumors in Interventional Radiology: In Vitro and in Vivo Studies in Human Cadavers and Mice.* Radiology, 2001. **218**(2): p. 570-575.

81.   Yanase, M., et al., *Intracellular hyperthermia for cancer using magnetite cationic liposomes: an in vivo study.* Japanese journal of cancer research : Gann, 1998. **89**(4): p. 463-469.

82.   Dennis, C.L., et al., *Nearly complete regression of tumors via collective behavior of magnetic nanoparticles in hyperthermia.* Nanotechnology, 2009. **20**(39): p. 395103-395103.

83.   Paula, I.P.S., et al., *Application of Hyperthermia for Cancer Treatment: Recent Patents Review.* Recent Patents on Anti-Cancer Drug Discovery, 2012. **7**(1): p. 64-73.

84.   Kettering, M., et al., *Means to increase the therapeutic efficiency of magnetic heating of tumors*, in *Biomedical Engineering / Biomedizinische Technik*. 2015. p. 505.

85.   Ludwig, R., et al., *Nanoparticle-based hyperthermia distinctly impacts production of ROS, expression of Ki-67, TOP2A, and TPX2, and induction of apoptosis in pancreatic cancer.* International journal of nanomedicine, 2017. **12**: p. 1009-1018.

86.   Kossatz, S., et al., *Efficient treatment of breast cancer xenografts with multifunctionalized iron oxide nanoparticles combining magnetic hyperthermia and anti-cancer drug delivery.* Breast cancer research : BCR, 2015. **17**(1): p. 66-66.

87.   Cavaliere, R., et al., *Selective heat sensitivity of cancer cells. Biochemical and clinical studies.* Cancer, 1967. **20**(9): p. 1351-1381.

88.   Strom, R., et al., *Biochemical Aspects of Heat Sensitivity of Tumour Cells*, in *Selective Heat Sensitivity of Cancer Cells*, A. Rossi-Fanelli, et al., Editors. 1977, Springer Berlin Heidelberg: Berlin, Heidelberg. p. 7-35.

89.   Auersperg, N., *Differential heat sensitivity of cells in tissue culture.* Nature, 1966. **209**(5021): p. 415-416.

90.   Endrich, B., *Hyperthermia and Microcirculatory Effects of Heat in Animal Tumors* Vol. 109. 1988: Recent Results Cancer Res.

91.   Liu, D.L., et al., *Tumour vessel damage resulting from laser-induced hyperthermia alone and in combination with photodynamic therapy.* Cancer Letters, 1997. **111**(1): p. 157-165.

92.   Vaupel, P., et al. *Microcirculatory and pH Alterations in Isotransplanted Rat and Xenotransplanted Human Tumors Associated with Hyperthermia.* 1988. Berlin, Heidelberg: Springer Berlin Heidelberg.

93.   Song, C.W., et al., *Implications of increased tumor blood flow and oxygenation caused by mild temperature hyperthermia in tumor treatment.* International Journal of Hyperthermia, 2005. **21**(8): p. 761-767.

94.   Song, C.W., *Effect of Local Hyperthermia on Blood Flow and Microenvironment: A Review.* Cancer Research, 1984. **44**(10 Supplement): p. 4721s-4730s.

95.   Graham, K. and E. Unger, *Overcoming tumor hypoxia as a barrier to radiotherapy, chemotherapy and immunotherapy in cancer treatment.* International journal of nanomedicine, 2018. **13**: p. 6049-6058.

96.   Teicher, B.A., J.S. Lazo, and A.C. Sartorelli, *Classification of Antineoplastic Agents by their Selective Toxicities toward Oxygenated and Hypoxic Tumor Cells.* Cancer Research, 1981. **41**(1): p. 73-81.

97.   Graeber, T.G., et al., *Hypoxia-mediated selection of cells with diminished apoptotic potential in solid tumours.* Nature, 1996. **379**(6560): p. 88-91.

98.   Rohwer, N. and T. Cramer, *Hypoxia-mediated drug resistance: Novel insights on the functional interaction of HIFs and cell death pathways.* Drug Resistance Updates, 2011. **14**(3): p. 191-201.

99.   Wang, H., et al., *Hypoxic Radioresistance: Can ROS Be the Key to Overcome It?* Cancers, 2019. **11**(1): p. 112.

100.   Spirou, S.V., et al., *Magnetic Hyperthermia and Radiation Therapy: Radiobiological Principles and Current Practice (†).* Nanomaterials (Basel, Switzerland), 2018. **8**(6): p. 401.

101.   Hilger, I., *In vivo applications of magnetic nanoparticle hyperthermia.* International Journal of Hyperthermia, 2013. **29**(8): p. 828-834.

102.   Katschinski, D.M., et al., *Pivotal Role of Reactive Oxygen Species as Intracellular Mediators of Hyperthermia-induced Apoptosis.* Journal of Biological Chemistry, 2000. **275**(28): p. 21094-21098.

103.   Petters, C., et al., *Uptake and Metabolism of Iron Oxide Nanoparticles in Brain Cells.* Neurochemical Research, 2014. **39**(9): p. 1648-1660.

104.   Yunok, O., et al., *In vitro study on apoptotic cell death by effective magnetic hyperthermia with chitosan-coated MnFe2O4.* Nanotechnology, 2016. **27**: p. 115101.

105.   O'Neill, K.L., et al., *Critical parameters influencing hyperthermia-induced apoptosis in human lymphoid cell lines.* Apoptosis, 1998. **3**(5): p. 369-375.

106.   Harmon, B.V., et al., *Cell Death Induced in a Murine Mastocytoma by 42–47°C Heating in Vitro: Evidence that the Form of Death Changes from Apoptosis to Necrosis Above a Critical Heat Load.* International Journal of Radiation Biology, 1990. **58**(5): p. 845-858.

107.   Oei, A.L., et al., *Effects of hyperthermia on DNA repair pathways: one treatment to inhibit them all.* Radiation oncology (London, England), 2015. **10**: p. 165-165.

108.   Kampinga, H.H., J.R. Dynlacht, and E. Dikomey, *Mechanism of radiosensitization by hyperthermia (43°C) as derived from studies with DNA repair defective mutant cell lines.* International Journal of Hyperthermia, 2004. **20**(2): p. 131-139.

109.   Dewey, W.C., S.A. Sapareto, and D.A. Betten, *Hyperthermic Radiosensitization of Synchronous Chinese Hamster Cells: Relationship between Lethality and Chromosomal Aberrations.* Radiation Research, 1978. **76**(1): p. 48-59.

110. Bergs, J., et al., *Effect of 41°C and 43°C on cisplatin radiosensitization in two human carcinoma cell lines with different sensitivies for cisplatin.* Oncology reports, 2007. **18**: p. 219-26.

111. Fantini, D., et al., *Rapid inactivation and proteasome-mediated degradation of OGG1 contribute to the synergistic effect of hyperthermia on genotoxic treatments.* DNA Repair, 2013. **12**(3): p. 227-237.

112. Krokan, H.E. and M. Bjørås, *Base excision repair.* Cold Spring Harbor perspectives in biology, 2013. **5**(4): p. a012583-a012583.

113. Raaphorst, G.P., et al., *A Comparison of the Enhancement of Radiation Sensitivity and DNA Polymerase Inactivation by Hyperthermia in Human Glioma Cells.* Radiation Research, 1993. **134**(3): p. 331-336.

114. Dikomey, E. and H. Jung, *Correlation between Thermal Radiosensitization and Heat-induced Loss of DNA Polymerase β Activity in CHO Cells.* International Journal of Radiation Biology, 1993. **63**(2): p. 215-221.

115. Issels, R., et al., *Hallmarks of hyperthermia in driving the future of clinical hyperthermia as targeted therapy: translation into clinical application.* International Journal of Hyperthermia, 2016. **32**(1): p. 89-95.

116. Matsumoto, Y., et al., *A Possible Mechanism for Hyperthermic Radiosensitization Mediated through Hyperthermic Lability of Ku Subunits in DNA-Dependent Protein Kinase.* Biochemical and Biophysical Research Communications, 1997. **234**(3): p. 568-572.

117. Beck, B.D. and J.R. Dynlacht, *Heat-Induced Aggregation of XRCC5 (Ku80) in Nontolerant and Thermotolerant Cells.* Radiation Research, 2001. **156**(6): p. 767-774.

118. Okumura, Y., et al., *Heat Inactivation of DNA-Dependent Protein Kinase: Possible Mechanism of Hyperthermic Radiosensitization*, in *Thermotherapy for Neoplasia, Inflammation, and Pain*, M. Kosaka, et al., Editors. 2001, Springer Japan: Tokyo. p. 420-423.

119. Ihara, M., et al., *Heat exposure enhances radiosensitivity by depressing DNA-PK kinase activity during double strand break repair.* International Journal of Hyperthermia, 2014. **30**(2): p. 102-109.

120. Powell, S.N. and L.A. Kachnic, *Homologous recombination research is heating up and ready for therapy.* Proceedings of the National Academy of Sciences, 2011. **108**(24): p. 9731.

121. Krawczyk, P.M., et al., *Mild hyperthermia inhibits homologous recombination, induces BRCA2 degradation, and sensitizes cancer cells to poly (ADP-ribose) polymerase-1 inhibition.* Proceedings of the National Academy of Sciences of the United States of America, 2011. **108**(24): p. 9851-9856.

122. Eppink, B., et al., *Hyperthermia-induced DNA repair deficiency suggests novel therapeutic anti-cancer strategies.* International Journal of Hyperthermia, 2012. **28**(6): p. 509-517.

123. Bergs, J., et al., *Inhibition of homologous recombination by mild hyperthermia shunts early double strand break repair to non-homologous end-joining in G2 phase cells.* DNA repair, 2012. **12**.

124. Hilger, I., et al., *Assessment of DNA Damage in Target Tumor Cells after Thermoablation in Mice.* Radiology, 2005. **237**(2): p. 500-506.

125. Marangon, I., et al., *Tumor Stiffening, a Key Determinant of Tumor Progression, is Reversed by Nanomaterial-Induced Photothermal Therapy.* Theranostics, 2017. **7**: p. 329-343.

126. Kolosnjaj-Tabi, J., et al., *Heat-Generating Iron Oxide Nanocubes: Subtle "Destructurators" of the Tumoral Microenvironment.* ACS Nano, 2014. **8**(5): p. 4268-4283.

127. Kolosnjaj-Tabi, J., et al., *Nanoparticle-based hyperthermia, a local treatment modulating the tumor extracellular matrix.* Pharmacological Research, 2017. **126**: p. 123-137.

128. Farr, N., et al., *Hyperthermia-enhanced targeted drug delivery using magnetic resonance-guided focussed ultrasound: a pre-clinical study in a genetic model of pancreatic cancer.* International journal of hyperthermia : the official journal of European Society for Hyperthermic Oncology, North American Hyperthermia Group, 2018. **34**(3): p. 284-291.

129. Matteucci, M.L., et al., *Hyperthermia Increases Accumulation of Technetium-99m-labeled Liposomes in Feline Sarcomas.* Clinical Cancer Research, 2000. **6**(9): p. 3748-3755.

130. Peer, A.J., et al., *Diverse immune mechanisms may contribute to the survival benefit seen in cancer patients receiving hyperthermia.* Immunologic research, 2010. **46**(1-3): p. 137-154.

131. Terunuma, H., *Potentiating Immune System by Hyperthermia*, in *Hyperthermic Oncology from Bench to Bedside*, S. Kokura, T. Yoshikawa, and T. Ohnishi, Editors. 2016, Springer Singapore: Singapore. p. 127-135.

132. Yanase, M., et al., *Antitumor immunity induction by intracellular hyperthermia using magnetite cationic liposomes.* Japanese journal of cancer research : Gann, 1998. **89**(7): p. 775-782.

133. Lin, F.-C., C.-H. Hsu, and Y.-Y. Lin, *Nano-therapeutic cancer immunotherapy using hyperthermia-induced heat shock proteins: insights from mathematical modeling.* International journal of nanomedicine, 2018. **13**: p. 3529-3539.

134. Li, Z. and P. Srivastava, *Heat-Shock Proteins.* Current Protocols in Immunology, 2003. **58**(1): p. A.1T.1-A.1T.6.

135. Kobayashi, T., A. Ito, and H. Honda, *Magnetic Nanoparticle-Mediated Hyperthermia and Induction of Anti-Tumor Immune Responses*, in *Hyperthermic Oncology from Bench to Bedside*, S. Kokura, T. Yoshikawa, and T. Ohnishi, Editors. 2016, Springer Singapore: Singapore. p. 137-150.

136. Ito, A., et al., *Heat shock protein 70 expression induces antitumor immunity during intracellular hyperthermia using magnetite nanoparticles.* Cancer Immunology, Immunotherapy, 2003. **52**(2): p. 80-88.

137. Sekihara, K., et al., *Pifithrin-μ, an Inhibitor of Heat-Shock Protein 70, Can Increase the Antitumor Effects of Hyperthermia Against Human Prostate Cancer Cells.* PLOS ONE, 2013. **8**(11): p. e78772.

138. Court, K., et al., *HSP70 Inhibition Synergistically Enhances the Effects of Magnetic Fluid Hyperthermia in Ovarian Cancer.* Molecular cancer therapeutics, 2017. **16**.

139. Zanganeh, S., et al., *Iron oxide nanoparticles inhibit tumour growth by inducing pro-inflammatory macrophage polarization in tumour tissues.* Nature Nanotechnology, 2016. **11**(11): p. 986-994.

140. Curley, S.A., et al., *The effects of non-invasive radiofrequency treatment and hyperthermia on malignant and nonmalignant cells.* International journal of environmental research and public health, 2014. **11**(9): p. 9142-9153.

141. Mitov, M.I., et al., *Temperature induces significant changes in both glycolytic reserve and mitochondrial spare respiratory capacity in colorectal cancer cell lines.* Experimental cell research, 2017. **354**(2): p. 112-121.

142. Streffer, C. *Aspects of Metabolic Change After Hyperthermia.* 1988. Berlin, Heidelberg: Springer Berlin Heidelberg.

143. Streffer, C., *Review: Metabolic changes during and after hyperthermia.* International Journal of Hyperthermia, 1985. **1**(4): p. 305-319.

144. Jin, H., et al., *Hyperthermia inhibits the proliferation and invasive ability of mouse malignant melanoma through TGF-β1.* Oncology reports, 2012. **29**.

145. Xie, X., et al., *Effect of hyperthermia on invasion ability and TGF-β1 expression of breast carcinoma MCF-7 cells.* Oncology reports, 2011. **25**: p. 1573-9.

146. Paholak, H.J., et al., *Elimination of epithelial-like and mesenchymal-like breast cancer stem cells to inhibit metastasis following nanoparticle-mediated photothermal therapy.* Biomaterials, 2016. **104**: p. 145-157.

147. Burke, A.R., et al., *The resistance of breast cancer stem cells to conventional hyperthermia and their sensitivity to nanoparticle-mediated photothermal therapy.* Biomaterials, 2012. **33**(10): p. 2961-2970.

148. Sadhukha, T., et al., *Effective Elimination of Cancer Stem Cells by Magnetic Hyperthermia.* Molecular Pharmaceutics, 2013. **10**(4): p. 1432-1441.

149. Wang, C.-H., et al., *Photothermolysis of glioblastoma stem-like cells targeted by carbon nanotubes conjugated with CD133 monoclonal antibody.* Nanomedicine: Nanotechnology, Biology and Medicine, 2011. **7**(1): p. 69-79.

150. Jia, D., et al., *Inhibition of B16 murine melanoma metastasis and enhancement of immunity by fever-range whole body hyperthermia.* International journal of hyperthermia : the official journal of European Society for Hyperthermic Oncology, North American Hyperthermia Group, 2011. **27**: p. 275-85.

151. Wang, C., et al., *Immunological Responses Triggered by Photothermal Therapy with Carbon Nanotubes in Combination with Anti-CTLA-4 Therapy to Inhibit Cancer Metastasis.* Advanced Materials, 2014. **26**(48): p. 8154-8162.

152. Bear, A.S., et al., *Elimination of metastatic melanoma using gold nanoshell-enabled photothermal therapy and adoptive T cell transfer.* PloS one, 2013. **8**(7): p. e69073-e69073.

153. Christophi, C. and V. Muralidharan, *Accelerated tumour recurrence following percutaneous laser hyperthermia of colorectal liver metastases.* HPB, 2000. **2**(4): p. 383-388.

154. Mantso, T., et al., *Effects of hyperthermia as a mitigation strategy in DNA damage-based cancer therapies.* Seminars in Cancer Biology, 2016. **37-38**: p. 96-105.

155. Kantidze, O.L., et al., *Heat Stress-Induced DNA Damage.* Acta naturae, 2016. **8**(2): p. 75-78.

156. Yarjanli, Z., et al., *Iron oxide nanoparticles may damage to the neural tissue through iron accumulation, oxidative stress, and protein aggregation.* BMC neuroscience, 2017. **18**(1): p. 51-51.

157. Wydra, R.J., et al., *The role of ROS generation from magnetic nanoparticles in an alternating magnetic field on cytotoxicity.* Acta biomaterialia, 2015. **25**: p. 284-290.

158. Ansari, M.O., et al., *Evaluation of DNA interaction, genotoxicity and oxidative stress induced by iron oxide nanoparticles both in vitro and in vivo: attenuation by thymoquinone.* Scientific Reports, 2019. **9**(1): p. 6912.

159. Takahashi, A., et al., *Evidence for the Involvement of Double-Strand Breaks in Heat-Induced Cell Killing.* Cancer Research, 2004. **64**(24): p. 8839-8845.

160. Kaneko, H., et al., *Heat shock induces phosphorylation of histone H2AX in mammalian cells.* Biochemical and Biophysical Research Communications, 2005. **328**(4): p. 1101-1106.

161. Podhorecka, M., A. Skladanowski, and P. Bozko, *H2AX Phosphorylation: Its Role in DNA Damage Response and Cancer Therapy.* Journal of Nucleic Acids, 2010. **2010**: p. 9.

162. Hunt, C.R., et al., *Hyperthermia Activates a Subset of Ataxia-Telangiectasia Mutated Effectors Independent of DNA Strand Breaks and Heat Shock Protein 70 Status.* Cancer Research, 2007. **67**(7): p. 3010-3017.

163. Nueda, A., et al., *DNA-dependent Protein Kinase Protects against Heat-induced Apoptosis.* Journal of Biological Chemistry, 1999. **274**(21): p. 14988-14996.

164. Velichko, A.K., et al., *Dual effect of heat shock on DNA replication and genome integrity.* Molecular biology of the cell, 2012. **23**(17): p. 3450-3460.

165. Petrova, N.V., et al., *Early S-phase cell hypersensitivity to heat stress.* Cell cycle (Georgetown, Tex.), 2016. **15**(3): p. 337-344.

166. Bhuyan, B.K., *Kinetics of Cell Kill by Hyperthermia.* Cancer Research, 1979. **39**(6 Part 2): p. 2277-2284.

167. Malyapa, R.S. and S. Sawada, *Cell-Cycle Dependence of Heat-Induced Interphase Death in Mouse L5178Y Cells.* Radiation Research, 1991. **125**(2): p. 134-140.

168. Velichko, A.K., et al., *Mechanism of heat stress-induced cellular senescence elucidates the exclusive vulnerability of early S-phase cells to mild genotoxic stress.* Nucleic acids research, 2015. **43**(13): p. 6309-6320.

169. Bewicke-Copley, F., et al., *Extracellular vesicles released following heat stress induce bystander effect in unstressed populations.* Journal of Extracellular Vesicles, 2017. **6**(1): p. 1340746.

170. Hanahan, D. and Robert A. Weinberg, *Hallmarks of Cancer: The Next Generation.* Cell, 2011. **144**(5): p. 646-674.

171. Campos, E.A., et al., *Synthesis, Characterization and Applications of Iron Oxide Nanoparticles - a Short Review.* Journal of Aerospace Technology and Management, 2015. **7**: p. 267-276.

172. Cotin, G., et al., *Chapter 2 - Iron Oxide Nanoparticles for Biomedical Applications: Synthesis, Functionalization, and Application*, in *Iron Oxide Nanoparticles for Biomedical Applications*, M. Mahmoudi and S. Laurent, Editors. 2018, Elsevier. p. 43-88.

173. Anselmo, A.C. and S. Mitragotri, *Nanoparticles in the clinic.* Bioengineering & translational medicine, 2016. **1**(1): p. 10-29.

174. Anselmo, A.C. and S. Mitragotri, *A Review of Clinical Translation of Inorganic Nanoparticles.* The AAPS journal, 2015. **17**(5): p. 1041-1054.

175. Dennis, C.L. and R. Ivkov, *Physics of heat generation using magnetic nanoparticles for hyperthermia.* International Journal of Hyperthermia, 2013. **29**(8): p. 715-729.

176. Ortega, D. and Q. Pankhurst, *Magnetic Hyperthermia.* 2013. p. 60-88.

177. Kolhatkar, A.G., et al., *Tuning the magnetic properties of nanoparticles.* International journal of molecular sciences, 2013. **14**(8): p. 15977-16009.

178. Hedayatnasab, Z., F. Abnisa, and W.M.A. Wan Daud, *Investigation properties of superparamagnetic nanoparticles and magnetic field-dependent hyperthermia therapy.* IOP Conference Series: Materials Science and Engineering, 2018. **334**: p. 012042.

179. Chang, D., et al., *Biologically Targeted Magnetic Hyperthermia: Potential and Limitations.* Frontiers in Pharmacology, 2018. **9**(831).

180. Alexander, M.T., et al., *Developing Antitumor Magnetic Hyperthermia: Principles, Materials and Devices.* Recent Patents on Anti-Cancer Drug Discovery, 2016. **11**(4): p. 360-375.

181. Miaskowski, A. and M. Subramanian, *Specific absorption rate parameter model in magnetic hyperthermia.* 2017. 1-4.

182. Teran, F., et al., *Accurate determination of the specific absorption rate in superparamagnetic nanoparticles under non-adiabatic conditions.* Vol. 101. 2012.

183. Kossatz, S., et al., *High therapeutic efficiency of magnetic hyperthermia in xenograft models achieved with moderate temperature dosages in the tumor area.* Pharmaceutical research, 2014. **31**(12): p. 3274-3288.

184. Kallumadil, M., et al., *Suitability of commercial colloids for magnetic hyperthermia.* Vol. 321. 2009. 1509-13.

185. Maier-Hauff, K., et al., *Intracranial Thermotherapy using Magnetic Nanoparticles Combined with External Beam Radiotherapy: Results of a Feasibility Study on Patients with Glioblastoma Multiforme.* Journal of Neuro-Oncology, 2007. **81**(1): p. 53-60.

186. Maier-Hauff, K., et al., *Efficacy and safety of intratumoral thermotherapy using magnetic iron-oxide nanoparticles combined with external beam radiotherapy on patients with recurrent glioblastoma multiforme.* Journal of neuro-oncology, 2011. **103**(2): p. 317-324.

187. Luo, S., et al., *Clinical trials of magnetic induction hyperthermia for treatment of tumours.* OA Cancer, 2014. **2**.

188. Fernández, J.G., et al., *Quantitative assessment of the metabolic products of iron oxide nanoparticles to be used as iron supplements in cell cultures.* Analytica Chimica Acta, 2018. **1039**: p. 24-30.

189. Silva, L.H.A., et al., *Labeling mesenchymal cells with DMSA-coated gold and iron oxide nanoparticles: assessment of biocompatibility and potential applications.* Journal of Nanobiotechnology, 2016. **14**(1): p. 59.

190. Poller, W.C., et al., *Very small superparamagnetic iron oxide nanoparticles: Long-term fate and metabolic processing in atherosclerotic mice.* Nanomedicine: Nanotechnology, Biology and Medicine, 2018. **14**(8): p. 2575-2586.

191. EMA. *New recommendations to manage risk of allergic reactions with intravenous iron-containing medicines.* 2013 [cited 2019; Available from: https://www.ema.europa.eu/en/news/new-recommendations-manage-risk-allergic-reactions-intravenous-iron-containing-medicines.

192. FDA. *FDA Drug Safety Communication: FDA strengthens warnings and changes prescribing instructions to decrease the risk of serious allergic reactions with anemia drug Feraheme (ferumoxytol).* 2015 [cited 2019; Available from: https://www.fda.gov/drugs/drug-safety-and-availability/fda-drug-safety-communication-fda-strengthens-warnings-and-changes-prescribing-instructions-decrease.

193. Hannon, G., et al., *Immunotoxicity Considerations for Next Generation Cancer Nanomedicines.* Advanced Science, 2019(0): p. 1900133.

194. Vroman, L., et al., *Interaction of high molecular weight kininogen, factor XII, and fibrinogen in plasma at interfaces.* Blood, 1980. **55**(1): p. 156-159.

195. Nie, S., *Understanding and overcoming major barriers in cancer nanomedicine.* Nanomedicine (London, England), 2010. **5**(4): p. 523-528.

196. Dobrovolskaia, M.A., et al., *Preclinical studies to understand nanoparticle interaction with the immune system and its potential effects on nanoparticle biodistribution.* Molecular pharmaceutics, 2008. **5**(4): p. 487-495.

197. Szebeni, J., *Complement activation-related pseudoallergy: A stress reaction in blood triggered by nanomedicines and biologicals.* Molecular Immunology, 2014. **61**(2): p. 163-173.

198. Sarma, J.V. and P.A. Ward, *The complement system.* Cell and tissue research, 2011. **343**(1): p. 227-235.

199. Nesargikar, P.N., B. Spiller, and R. Chavez, *The complement system: history, pathways, cascade and inhibitors.* European journal of microbiology & immunology, 2012. **2**(2): p. 103-111.

200. Cook, H.T. and M. Botto, *Mechanisms of Disease: the complement system and the pathogenesis of systemic lupus erythematosus.* Nature Clinical Practice Rheumatology, 2006. **2**(6): p. 330-337.

201. Neun, B.W., A.N. Ilinskaya, and M.A. Dobrovolskaia, *Analysis of Complement Activation by Nanoparticles*, in *Characterization of Nanoparticles Intended for Drug Delivery*, S.E. McNeil, Editor. 2018, Springer New York: New York, NY. p. 149-160.

202. Patkó, Z. and J. Szebeni, *Blood cell changes in complement activation-related pseudoallergy*, in *European Journal of Nanomedicine*. 2015. p. 233.

203. Jackman, J.A., et al., *Comparison of complement activation-related pseudoallergy in miniature and domestic pigs: foundation of a validatable immune toxicity model.* Nanomedicine: Nanotechnology, Biology and Medicine, 2016. **12**(4): p. 933-943.

204. Szebeni, J., et al., *Roadmap and strategy for overcoming infusion reactions to nanomedicines.* Nature Nanotechnology, 2018. **13**(12): p. 1100-1108.

205. Wolf-Grosse, S., et al., *Iron oxide nanoparticles induce cytokine secretion in a complement-dependent manner in a human whole blood model.* International Journal of Nanomedicine, 2017. **Volume 12**: p. 3927-3940.

206. Banda, N., et al., *Mechanisms of complement activation by dextran-coated superparamagnetic iron oxide (SPIO) nanoworms in mouse versus human serum.* Particle and Fibre Toxicology, 2014. **11**.

207. Escamilla-Rivera, V., et al., *Plasma protein adsorption on Fe(3)O(4)-PEG nanoparticles activates the complement system and induces an inflammatory response.* International journal of nanomedicine, 2019. **14**: p. 2055-2067.

208. Wang, G., et al., *Activation of Human Complement System by Dextran-Coated Iron Oxide Nanoparticles Is Not Affected by Dextran/Fe Ratio, Hydroxyl Modifications, and Crosslinking.* Frontiers in immunology, 2016. **7**: p. 418-418.

209. Inturi, S., et al., *Modulatory Role of Surface Coating of Superparamagnetic Iron Oxide Nanoworms in Complement Opsonization and Leukocyte Uptake.* ACS Nano, 2015. **9**(11): p. 10758-10768.

210. Vu, V.P., et al., *Immunoglobulin deposition on biomolecule corona determines complement opsonization efficiency of preclinical and clinical nanoparticles.* Nature nanotechnology, 2019. **14**(3): p. 260-268.

211. Shah, A. and M.A. Dobrovolskaia, *Immunological effects of iron oxide nanoparticles and iron-based complex drug formulations: Therapeutic benefits, toxicity, mechanistic insights, and translational considerations.* Nanomedicine : nanotechnology, biology, and medicine, 2018. **14**(3): p. 977-990.

212. Sanhaji, M., et al., *The phenotype of target pancreatic cancer cells influences cell death by magnetic hyperthermia with nanoparticles carrying gemcitabine and the pseudo-peptide NucAnt.* Nanomedicine: Nanotechnology, Biology and Medicine, 2019. **20**: p. 101983.

213. Edge, D., et al., *Pharmacokinetics and bio-distribution of novel super paramagnetic iron oxide nanoparticles (SPIONs) in the anaesthetized pig.* Clinical and Experimental Pharmacology and Physiology, 2016. **43**(3): p. 319-326.

214. Silva, A.K., et al., *Overcoming the tumor microenvironment: the role of nanohyperthermia.* Nanomedicine, 2017. **12**(11): p. 1213-1215.

215. Hallasch, S., et al. *How gastrin-releasing peptide receptor (GRPR) and αvβ3 integrin expression reflect reorganization features of tumors after hyperthermia treatments*. Scientific reports, 2017. **7**, 6916 DOI: 10.1038/s41598-017-06100-7.

216. Southern, P. and Q.A. Pankhurst, *Commentary on the clinical and preclinical dosage limits of interstitially administered magnetic fluids for therapeutic hyperthermia based on current practice and efficacy models.* International Journal of Hyperthermia, 2018. **34**(6): p. 671-686.

217. Southern, P. and Q.A. Pankhurst, *Using the 'dispersion-retention-formulation method' to estimate clinical and preclinical dosage limits for interstitial nanomedicines or agents.* Journal of Magnetism and Magnetic Materials, 2019. **473**: p. 74-78.

218. Blanco-Andujar, C., F.J. Teran, and D. Ortega, *Chapter 8 - Current Outlook and Perspectives on Nanoparticle-Mediated Magnetic Hyperthermia*, in *Iron Oxide Nanoparticles for Biomedical Applications*, M. Mahmoudi and S. Laurent, Editors. 2018, Elsevier. p. 197-245.

219. EUNCL. [cited 2019; Available from: http://www.euncl.eu/about-us/overview/.

220. Hare, J.I., et al., *Challenges and strategies in anti-cancer nanomedicine development: An industry perspective.* Advanced Drug Delivery Reviews, 2017. **108**: p. 25-38.

221. Maguire, C., et al., *Benchmark of Nanoparticle Tracking Analysis on Measuring Nanoparticle Sizing and Concentration.* Journal of Micro and Nano-Manufacturing, 2017. **5**.

222. Hole, P., et al., *Interlaboratory comparison of size measurements on nanoparticles using nanoparticle tracking analysis (NTA).* Journal of nanoparticle research : an interdisciplinary forum for nanoscale science and technology, 2013. **15**: p. 2101.

223. Maguire, C. *Particle Tracking Analysis*. 2018 [cited 2019; Available from: http://www.euncl.eu/about-us/assay-cascade/PDFs/PCC/EUNCL_PCC_023.pdf?m=1526712237&.

224. Calzolai, L. *Measuring the size of nanoparticles using batch mode dynamic light scattering*. 2015 [cited 2019; Available from: http://www.euncl.eu/about-us/assay-cascade/PDFs/Prescreening/EUNCL-PCC-001.pdf?m=1468937875&.

225. Gao, C., et al., *Tacrine induces apoptosis through lysosome- and mitochondria-dependent pathway in HepG2 cells.* Toxicology in Vitro, 2014. **28**(4): p. 667-674.

226. Dise, C.A. and D.B. Goodman, *The relationship between valinomycin-induced alterations in membrane phospholipid fatty acid turnover, membrane potential, and cell volume in the human erythrocyte.* Journal of Biological Chemistry, 1985. **260**(5): p. 2869-2874.

227. Klein, B., et al., *Perturbation of intracellular K+ homeostasis with valinomycin promotes cell death by mitochondrial swelling and autophagic processes.* Apoptosis, 2011. **16**(11): p. 1101.

228. Calero, M., et al., *Characterization of interaction of magnetic nanoparticles with breast cancer cells.* Journal of Nanobiotechnology, 2015. **13**(1): p. 16.

229. Miyamoto, R., et al., *Cetuximab delivery and antitumor effects are enhanced by mild hyperthermia in a xenograft mouse model of pancreatic cancer.* Cancer science, 2016. **107**(4): p. 514-520.

230. Blanco-Andujar, C., et al., *Real-time tracking of delayed-onset cellular apoptosis induced by intracellular magnetic hyperthermia.* Nanomedicine, 2016. **11**(2): p. 121-136.

231. Poller, J.M., et al., *Selection of potential iron oxide nanoparticles for breast cancer treatment based on in vitro cytotoxicity and cellular uptake.* International journal of nanomedicine, 2017. **12**: p. 3207-3220.

232. Ma, W., et al., *Neural Induction Potential and MRI of ADSCs Labeled Cationic Superparamagnetic Iron Oxide Nanoparticle In Vitro.* Contrast Media & Molecular Imaging, 2018. **2018**: p. 11.

233. Su, L., et al., *Enhanced cellular uptake of iron oxide nanoparticles modified with 1,2-dimyristoyl-sn-glycero-3-phosphocholine.* RSC Advances, 2017. **7**(60): p. 38001-38007.

234. Zembruski, N.C.L., et al., *7-Aminoactinomycin D for apoptosis staining in flow cytometry.* Analytical Biochemistry, 2012. **429**(1): p. 79-81.

235. Fadok, V.A., et al., *The role of phosphatidylserine in recognition of apoptotic cells by phagocytes.* Cell Death & Differentiation, 1998. **5**(7): p. 551-562.

236. Berghe, T.V., et al., *Necroptosis, necrosis and secondary necrosis converge on similar cellular disintegration features.* Cell Death And Differentiation, 2009. **17**: p. 922.

237. Krysko, D.V., et al., *Apoptosis and necrosis: Detection, discrimination and phagocytosis.* Methods, 2008. **44**(3): p. 205-221.

238. Porter, A.G. and R.U. Jänicke, *Emerging roles of caspase-3 in apoptosis.* Cell Death & Differentiation, 1999. **6**(2): p. 99-104.

239. Krust, B., et al., *Targeting surface nucleolin with multivalent HB-19 and related Nucant pseudopeptides results in distinct inhibitory mechanisms depending on the malignant tumor cell type.* BMC cancer, 2011. **11**: p. 333-333.

240. Ding, J., et al., *Endotoxins: Structure, Function and Recognition.* 2010. 187.

241. Heine, H., E.T. Rietschel, and A.J. Ulmer, *The biology of endotoxin.* Molecular Biotechnology, 2001. **19**(3): p. 279-296.

242. Meng, F. and C.A. Lowell, *Lipopolysaccharide (LPS)-induced macrophage activation and signal transduction in the absence of Src-family kinases Hck, Fgr, and Lyn.* The Journal of experimental medicine, 1997. **185**(9): p. 1661-1670.

243. Fullerton, J.N., et al., *Intravenous Endotoxin Challenge in Healthy Humans: An Experimental Platform to Investigate and Modulate Systemic Inflammation.* Journal of visualized experiments : JoVE, 2016(111): p. 53913.

244. Magalhães P.O., L.A.M., Mazzola P. G., Rangel-Yagui C, Penna T. C. V., Pessoa A., *Methods of Endotoxin Removal from Biological Preparations: a Review* J Pharm Pharmaceut Sci, 2007. **10**(3): p. 388-404.

245. Gorbet, M.B. and M.V. Sefton, *Endotoxin: The uninvited guest.* Biomaterials, 2005. **26**(34): p. 6811-6817.

246. Jones, C.F. and D.W. Grainger, *In vitro assessments of nanomaterial toxicity.* Advanced drug delivery reviews, 2009. **61**(6): p. 438-456.

247. Raetz, C.R.H. and C. Whitfield, *Lipopolysaccharide endotoxins.* Annual review of biochemistry, 2002. **71**: p. 635-700.

248. Li, Y., M. Fujita, and D. Boraschi, *Endotoxin Contamination in Nanomaterials Leads to the Misinterpretation of Immunosafety Results.* Frontiers in Immunology, 2017. **8**(472).

249. Crist, R.M., et al., *Common pitfalls in nanotechnology: lessons learned from NCI's Nanotechnology Characterization Laboratory.* Integrative biology : quantitative biosciences from nano to macro, 2013. **5**(1): p. 66-73.

250. Morrison, D.C., *Bacterial Endotoxins and Pathogenesis.* Reviews of Infectious Diseases, 1983. **5**: p. S733-S747.

251. Pearson, F.C., et al., *Comparison of several control standard endotoxins to the National Reference Standard Endotoxin--an HIMA collaborative study.* Applied and environmental microbiology, 1985. **50**(1): p. 91-93.

252. Dobrovolskaia, M.A., et al., *Choice of method for endotoxin detection depends on nanoformulation.* Nanomedicine, 2014. **9**(12): p. 1847-1856.

253. FDA. *Guidance for Industry. Pyrogen and Endotoxins testing: Questions and Answers*. 2010; Available from: https://www.fda.gov/media/83477/download.

254. USP. *<85> Bacterial Endotoxins Test*. 2011 [cited 2019; Available from: https://www.usp.org/sites/default/files/usp/document/harmonization/gen-method/q06_current_webpage_stage_6_monograph_23_nov_2011.pdf.

255. Dobrovolskaia, M.A., et al., *Ambiguities in applying traditional Limulus amebocyte lysate tests to quantify endotoxin in nanoparticle formulations.* Nanomedicine (London, England), 2010. **5**(4): p. 555-562.

256. Young, N.S., J. Levin, and R.A. Prendergast, *An invertebrate coagulation system activated by endotoxin: evidence for enzymatic mediation.* The Journal of Clinical Investigation, 1972. **51**(7): p. 1790-1797.

257. Neun, B. and M. Dobrovolskaia, *Detection and Quantitative Evaluation of Endotoxin Contamination in Nanoparticle Formulations by LAL-Based Assays.* Methods in molecular biology (Clifton, N.J.), 2011. **697**: p. 121-30.

258. ISO. *Nanotechnologies - Endotoxin test on nanomaterial samples for in vitro systems - Limulus amebocyte lysate (LAL) test.* 2010 [cited 2019; Available from: https://www.iso.org/standard/45640.html.

259. Kroll, A., et al., *Interference of engineered nanoparticles with in vitro toxicity assays.* Archives of Toxicology, 2012. **86**(7): p. 1123-1136.

260. Dobrovolskaia, M.A., D.R. Germolec, and J.L. Weaver, *Evaluation of nanoparticle immunotoxicity.* Nature Nanotechnology, 2009. **4**: p. 411.

261. Neun B. W., I.A.N., Dobrovolskaia A. M. *Detection and Quantification of Gram Negative Bacterial Endotoxin Contamination in Nanoparticle Formulations by End Point Chromogenic LAL Assay*. 2015 [cited 2019; Available from: https://ncl.cancer.gov/sites/default/files/protocols/NCL_Method_STE-1.1.pdf.

262. Neun, B.W. and M.A. Dobrovolskaia, *Considerations and Some Practical Solutions to Overcome Nanoparticle Interference with LAL Assays and to Avoid Endotoxin Contamination in Nanoformulations*, in *Characterization of Nanoparticles Intended for Drug Delivery*, S.E. McNeil, Editor. 2018, Springer New York: New York, NY. p. 23-33.

263. Ossig R., R.M. *Detection and Quantification of Gram Negative Bacterial Endotoxin Contamination in Nanoparticle Formulations by Gel-Clot LAL Assay.*

2016 [cited 2019; Available from: http://www.euncl.eu/about-us/assay-cascade/PDFs/Prescreening/EUNCL-STE-001_3_2.pdf?m=1476164532&.

264. Li, Y. and D. Boraschi, *Endotoxin contamination: a key element in the interpretation of nanosafety studies.* Nanomedicine, 2016. **11**(3): p. 269-287.

265. Magtrace. [cited 2019; Available from: https://www.endomag.com/products/magtrace/.

266. Amendola, V. and M. Meneghetti, *Size Evaluation of Gold Nanoparticles by UV−vis Spectroscopy.* The Journal of Physical Chemistry C, 2009. **113**(11): p. 4277-4285.

267. Schwaminger, S.P., et al., *Formation of iron oxide nanoparticles for the photooxidation of water: Alteration of finite size effects from ferrihydrite to hematite.* Scientific Reports, 2017. **7**(1): p. 12609.

268. Salvador-Morales Carolina, S.R.B., *Complement activation.* Vol. 12. 2012.

269. Moghimi, S.M., et al., *Material properties in complement activation.* Advanced Drug Delivery Reviews, 2011. **63**(12): p. 1000-1007.

270. Caputo, F. *Measuring Zeta Potential* 2015 [cited 2019; Available from: http://www.euncl.eu/about-us/assay-cascade/PDFs/Prescreening/EUNCL-PCC-002.pdf?m=1468937877&.

271. Liptrott, N.J. *Analysis of complement activation by EIA*. 2016 [cited 2019; Available from: http://www.euncl.eu/about-us/assay-cascade/PDFs/Haematology/EUNCL-ITA-005_2.pdf?m=1526624464&.

272. Neun B. W., I.A.N., Dobrovolskaia A. M. *Analysis of Complement Activation by EIA*. 2015 [cited 2019; Available from: https://ncl.cancer.gov/sites/default/files/protocols/NCL_Method_ITA-5.2.pdf.

273. Moghimi, S.M., et al., *Methylation of the phosphate oxygen moiety of phospholipid-methoxy(polyethylene glycol) conjugate prevents PEGylated liposome-mediated complement activation and anaphylatoxin production.* The FASEB Journal, 2006. **20**(14): p. 2591-2593.

274. Sim, R.B., *Complement, Classical Pathway*, in *Encyclopedia of Immunology (Second Edition)*, P.J. Delves, Editor. 1998, Elsevier: Oxford. p. 604-612.

275. Frank, M.M., *103 - Complement in Control of Infectious Agents*, in *Principles and Practice of Pediatric Infectious Diseases (Fifth Edition)*, S.S. Long, C.G. Prober, and M. Fischer, Editors. 2018, Elsevier. p. 624-628.e1.

276. Clogston, J.D. and A.K. Patri, *Zeta Potential Measurement*, in *Characterization of Nanoparticles Intended for Drug Delivery*, S.E. McNeil, Editor. 2011, Humana Press: Totowa, NJ. p. 63-70.

277. Law, S.K. and A.W. Dodds, *The internal thioester and the covalent binding properties of the complement proteins C3 and C4.* Protein science : a publication of the Protein Society, 1997. **6**(2): p. 263-274.

278. Arima, Y., et al., *Complement Activation by Polymers Carrying Hydroxyl Groups.* ACS applied materials & interfaces, 2009. **1**: p. 2400-7.

279. Moghimi, S.M. and D. Simberg, *Complement activation turnover on surfaces of nanoparticles.* Nano today, 2017. **15**: p. 8-10.

280. Carreno, M.-P., et al., *The ability of sephadex to activate human complement is suppressed in specifically substituted functional sephadex derivatives.* Molecular Immunology, 1988. **25**(2): p. 165-171.

281. Huang, S., et al., *Low concentrations of citrate reduce complement and granulocyte activation in vitro in human blood.* Clinical kidney journal, 2015. **8**(1): p. 31-37.

282. Hannon, G.T., Melissa; Prina-Mello, Adriele, *Immuntoxicity and Safety Considerations for Iron Oxide Nanoparticles*. 2018.

283. Zhu, M.-T., et al., *Comparative study of pulmonary responses to nano- and submicron-sized ferric oxide in rats.* Toxicology, 2008. **247**(2): p. 102-111.

284. Nemmar, A., et al., *Ultrasmall superparamagnetic iron oxide nanoparticles acutely promote thrombosis and cardiac oxidative stress and DNA damage in mice.* Particle and Fibre Toxicology, 2016. **13**(1): p. 22.

285. Blank, F., et al., *Biomedical nanoparticles modulate specific CD4+ T cell stimulation by inhibition of antigen processing in dendritic cells.* Nanotoxicology, 2011. **5**(4): p. 606-621.

286. Couto, D., et al., *Biodistribution of polyacrylic acid-coated iron oxide nanoparticles is associated with proinflammatory activation and liver toxicity.* Journal of Applied Toxicology, 2016. **36**(10): p. 1321-1331.

287. Laskar, A., et al., *SPION primes THP1 derived M2 macrophages towards M1-like macrophages.* Biochemical and Biophysical Research Communications, 2013. **441**(4): p. 737-742.

288. Singh Gaharwar, U. and P. Rajamani, *Iron Oxide Nanoparticles Induced Oxidative Damage in Peripheral Blood Cells of Rat.* Journal of Biomedical Science and Engineering, 2015. **08**: p. 274-286.

289. Rampton, D., et al., *Hypersensitivity reactions to intravenous iron: guidance for risk minimization and management.* Haematologica, 2014. **99**(11): p. 1671-1676.

290. Shen, c.-c., et al., *A single exposure to iron oxide nanoparticles attenuates antigen-specific antibody production and T-cell reactivity in ovalbumin-sensitized BALB/c mice.* International journal of nanomedicine, 2011. **6**: p. 1229-35.

291. Gustafson, H.H., et al., *Nanoparticle Uptake: The Phagocyte Problem.* Nano today, 2015. **10**(4): p. 487-510.

292. Prasad, B.V.V. and M.F. Schmid, *Principles of Virus Structural Organization*, in *Viral Molecular Machines*, M.G. Rossmann and V.B. Rao, Editors. 2012, Springer US: Boston, MA. p. 17-47.

293. Almeida, J.P.M., et al., *In vivo biodistribution of nanoparticles.* Nanomedicine, 2011. **6**(5): p. 815-835.

294. Urbanics, R., P. Bedőcs, and J. Szebeni, *Lessons learned from the porcine CARPA model: constant and variable responses to different nanomedicines and administration protocols*, in *European Journal of Nanomedicine*. 2015. p. 219.

295. Sehdev, A., et al., *Germline and Somatic DNA Damage Repair Gene Mutations and Overall Survival in Metastatic Pancreatic Adenocarcinoma Patients Treated with FOLFIRINOX.* Clinical Cancer Research, 2018. **24**(24): p. 6204-6211.

296. Golan, T. and M. Javle, *DNA Repair Dysfunction in Pancreatic Cancer: A Clinically Relevant Subtype for Drug Development.* JNCCN Journal of the National Comprehensive Cancer Network, 2017. **15**: p. 1063-1069.

297. Pant, S., A. Maitra, and T.A. Yap, *PARP inhibition — opportunities in pancreatic cancer.* Nature Reviews Clinical Oncology, 2019. **16**(10): p. 595-596.